Directly diode-laser-pumped Titanium-doped Sapphire Lasers

Peter Roth

2012

A thesis presented in fulfilment of the requirements
for the degree of Doctor of Philosophy

University of Strathclyde, Department of Physics

Declaration of Authenticity and Author's Rights

This thesis is the result of the author's original research. It has been composed by the author and has not been previously submitted for examination which has led to the award of a degree.

Signed: Date:

Für meine Eltern

Christa & Herbert

Contents

Abstract

Titanium-doped sapphire is one of the most versatile laser gain materials. Tunable between 0.7 μm and 1.1 μm and capable of generating femtosecond pulses, the Ti:sapphire laser has become an important tool for many applications. Its ubiquitous use across many scientific disciplines is increasingly complemented by commercial applications including imaging, spectroscopy, micro-processing of materials and the generation of terahertz radiation.

However, today's Ti:sapphire lasers are complex, bulky and expensive, leaving many applications unaddressed, particularly where lower costs and smaller footprints are vital. The biggest hurdle to smaller and cheaper Ti:sapphire lasers is the pump light source – typically a frequency-doubled, multi-watt neodymium or optically pumped semiconductor laser. Ideally, such intricate and expensive pump lasers would be replaced by compact, robust and cheap diode lasers. Two factors have prevented this: first, Ti:sapphire has a broad but relatively weak absorption in the blue-green region of the spectrum where high-power diode lasers are not currently available; and second, the very short upper laser level lifetime of Ti:sapphire and relatively large parasitic losses result in a high intrinsic laser threshold. Combined, these factors strongly favour high-brightness pump sources.

The recent progress in diode lasers based on gallium nitride materials now opens the way to challenge the perceived wisdom that Ti:sapphire cannot be diode-pumped. In this work diode-laser pumping of Ti:sapphire lasers has been shown to be possible.

The world's first diode-laser-pumped Ti:sapphire laser has been developed, enabling drastic reductions in cost and size over current systems. Using innovative approaches to exploit gallium nitride diode lasers as the pump source, both continuous-wave operation and generation of femtosecond pulses have been demonstrated. As a result, some of the unrivalled performance of today's high-cost, lab-bound Ti:sapphire lasers may soon be available at a fraction of the current cost and footprint.

Acknowledgements

This dissertation would not have been possible without the guidance and the help I received in the course of my PhD from several individuals. First, my utmost gratitude goes to my supervisor Dr. Alan Kemp whose encouragement, guidance and support was invaluable for the accomplishment of this work. His scientific and personal guidance along the way is something I will never forget.

Furthermore, my special thanks to Dr. David Burns for all the lab tricks and knacks I learned from him and all the fruitful discussions we had. I would also like to thank Dr. John-Mark Hopkins and Dr. Alex Maclean for all their help and witty banter.

Dr. Rolf Birch for being the best lab-mate one can wish for deserves credit as well as the rest of the solid-state laser group (past and present) for being a pleasure to work with. These are: Dr. Gareth Valentine, Dr. Walter Lubeight, Dr. Patsy Millar, Dr. Peter Schlosser, Dr. Nils Hempler, Gerald Bonner and Sean Reid.

In addition, I would like to thank Dr. Martin Dawson, Dr. Stephane Calvez, Simon Andrews and Tim Holt for their advice along the way. Paul and Lisa, our technicians, for all always being particularly fast with manufacturing all those little bits I required as well as Lisa, Sharon and Lynda for their administrative support.

Last but not least, I would like to express particular gratitude to my parents who always supported me throughout the years and who were the backbone for the success of this work.

Cheers,
Peter

1 Introduction

1 Introduction

1.1 Titanium-doped sapphire lasers

Titanium-doped sapphire (Ti:sapphire) is one of the most versatile laser gain materials – with an emission wavelength tunable between 670 nm and 1070 nm [1-3] and the capability of generating femtosecond (fs) pulses, Ti:sapphire lasers have become an important tool for many applications. Since its first demonstration in 1982 [4], the Ti:sapphire laser has become the most widely-used broadly tunable laser, replacing the often cumbersome dye laser [5, 6]. Its superior performance enables the generation of pulses with only a few femtoseconds duration [7, 8], driving many scientific fields. As a laboratory tool its utility has been underlined most prominently by its contribution to the Nobel prize winning research on transition states of chemical reactions (Zewail, 1999) and precision spectroscopy (Hänsch, Hall, 2005). However, its ubiquitous use across many scientific disciplines is increasingly rivalled by commercial applications which include imaging, spectroscopy, micro-processing of materials and the generation of terahertz radiation.

Nonetheless, today's Ti:sapphire lasers are complex, bulky and expensive, leaving many applications unaddressed, particularly where lower costs and smaller footprints are vital. The biggest hurdle to smaller and cheaper Ti:sapphire lasers is the pump light source – typically a multi-watt argon-ion [1, 9] or frequency-doubled neodymium laser [1], which is bulky, expensive and complex in itself, see Fig. 1.1. Ideally, such pump lasers would be replaced by compact, robust and cheap diode lasers. Two factors have prevented this: first, Ti:sapphire has a broad but relatively weak pump absorption around 490 nm in the blue-green region of the spectrum where high-power diode lasers are not yet available; and second, the very short upper laser level lifetime of Ti:sapphire and relatively large parasitic losses result in a high intrinsic laser threshold. Both factors combine to make a high brightness pump necessary.

The recent progress in diode lasers based on gallium nitride (GaN) materials now opens the way to challenge the received wisdom that Ti:sapphire cannot be diode-

laser-pumped. Since their first demonstration in 1996 [10], GaN diode lasers have rapidly improved and have had considerable impact on applications requiring blue to ultraviolet wavelengths. Their rapidly expanding production volume reduces costs whilst driving up power density and efficiency [11-15]. Thus, the opportunity arises to replace the argon-ion lasers and the frequency-doubled solid-state lasers currently used as pump sources with GaN diode lasers. However, these diode lasers have a far lower brightness and their emission wavelengths are not at the peak of Ti:sapphire's pump absorption spectrum. A detailed discussion of Ti:sapphire's material properties and the optical characteristics of GaN diode lasers along with the challenges for direct diode-laser pumping of Ti:sapphire lasers are presented in sections 1.2 and 1.3 respectively.

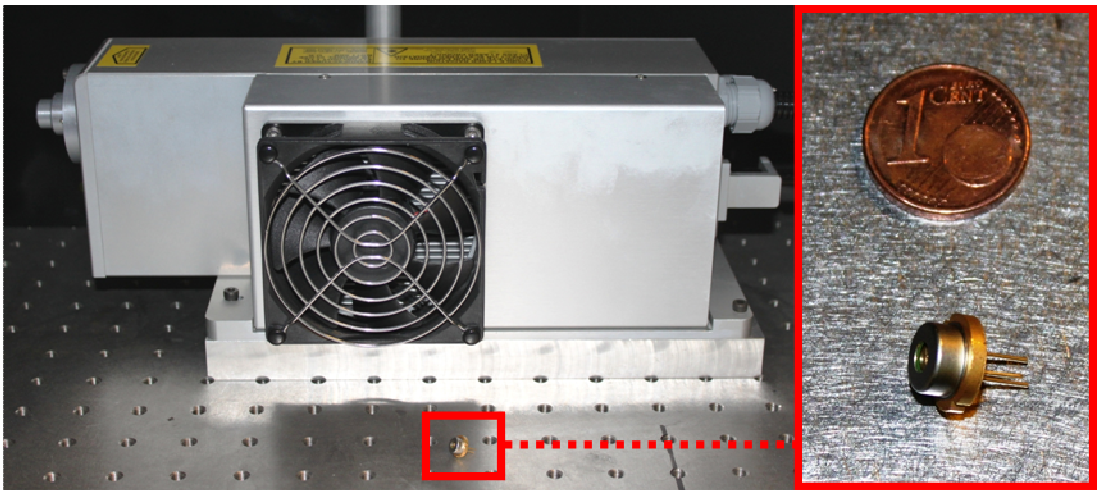

Fig. 1.1. Size comparison of a frequency-doubled neodymium laser head (5 W at 532 nm, Elforlight HPG5000), top left, with a gallium nitride diode laser (1 W at 452 nm, Nichia NDB7352E [11]), bottom right.

1.2 Vibronic laser gain materials

The broad gain spectrum of vibronic lasers stands out among solid-state lasers. In vibronic laser gain materials the absorption and emission of photons is coupled to the absorption and emission of phonons. This electron-phonon coupling allows the discrete transition energy between the electronic states of the laser-active atom/ion to

be split between photons and phonons in a continuous fashion [3]. Hence, vibronic lasers have a broad gain spectrum which allows the laser emission wavelength to be tuned over tens of nanometres or exploited for the generation of femtosecond pulses.

There are a multitude of vibronic laser gain materials but only a few of them are commonly used in applications. Titanium-doped sapphire (Ti:sapphire) is the most widely-used laser gain material for broadly tunable and ultra-short pulse lasers [3, 16]. A detailed discussion of Ti:sapphire's material properties is presented in the next section followed by a brief discussion of alternative laser gain materials to Ti:sapphire.

1.2.1 Ti:sapphire material properties

Titanium-doped consists of a sapphire host (Al_2O_3) in which trivalent Titanium ions (Ti^{3+}) substitute for some of the Al^{3+} ions. The doping concentration is usually expressed as weight percentage of Ti_2O_3 in the crystal melt with typical values of 0.02 – 0.5 wt. % [17-22]. The most important material properties of Ti:Al_2O_3 are listed in Table 1.1.

Table 1.1. Spectroscopic and lasing properties of Ti:Al_2O_3 [1-3, 17-22].

Laser type	4-level vibronic
Upper state lifetime τ	3.2 µs
Fluorescent linewidth (FWHM)	230 nm
Peak stimulated emission wavelength	795 nm
Peak stimulated emission cross-section σ	
- parallel to c-axis (π-polarized)	$4.1 \cdot 10^{-19}$ cm^2
- perpendicular to c-axis (σ-polarized)	$2.0 \cdot 10^{-19}$ cm^2
Peak pump absorption wavelength	490 nm
Index of refraction	
- at 800 nm	1.76
- at 532 nm	1.77
Thermal conductivity	46 Wm^{-1}K^{-1}

The broad fluorescence linewidth of Ti:sapphire, shown in Fig. 1.2, is due to strong interactions between the Ti^{3+} ions and the sapphire host crystal plus a large difference in electron distribution between the two energy levels of the laser transition [3]. As a unique feature among the transition-metal laser ions, the Ti^{3+} ion has no d-state energy levels above the upper laser level eliminating the possibility of excited state absorption which in turn would restrict the tuning range [3]. Hence, laser output can be tuned over 400 nm and can also be used to generate femtosecond pulses. Other advantages are a large stimulated emission cross-section (σ) and the favourable properties of the sapphire host crystal, namely high thermal conductivity, mechanical rigidity and exceptional chemical inertness [3].

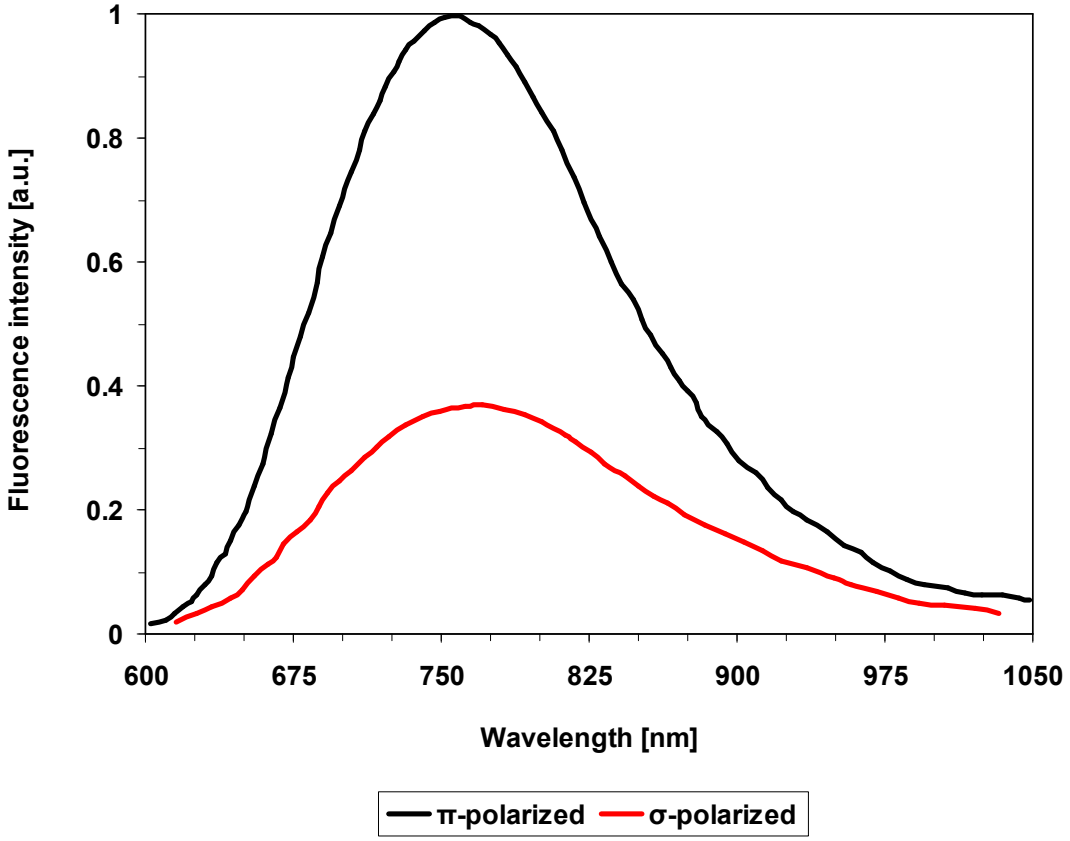

Fig. 1.2. Polarized fluorescence spectra of Ti:sapphire [1].

A drawback is the very short upper state lifetime (τ) of 3.2 μs. Since the population inversion required to reach lasing threshold is inversely proportional to the product

of upper state lifetime and stimulated emission cross-section ($\sigma\tau$), a very high pump flux is required [3, 23]. The small pump absorption cross section of Ti:sapphire (see Fig. 1.3) demands that this pump flux is maintained over a long crystal length. Ti:sapphire crystals of the sort that are typically used in commercial lasers have doping concentrations of around 0.15 wt. % resulting in a pump absorption coefficient of 2.1 cm^{-1} at 532 nm [17, 19] which mandates a crystal length of 11 mm to absorb 90% of the incident pump power in a single pass.

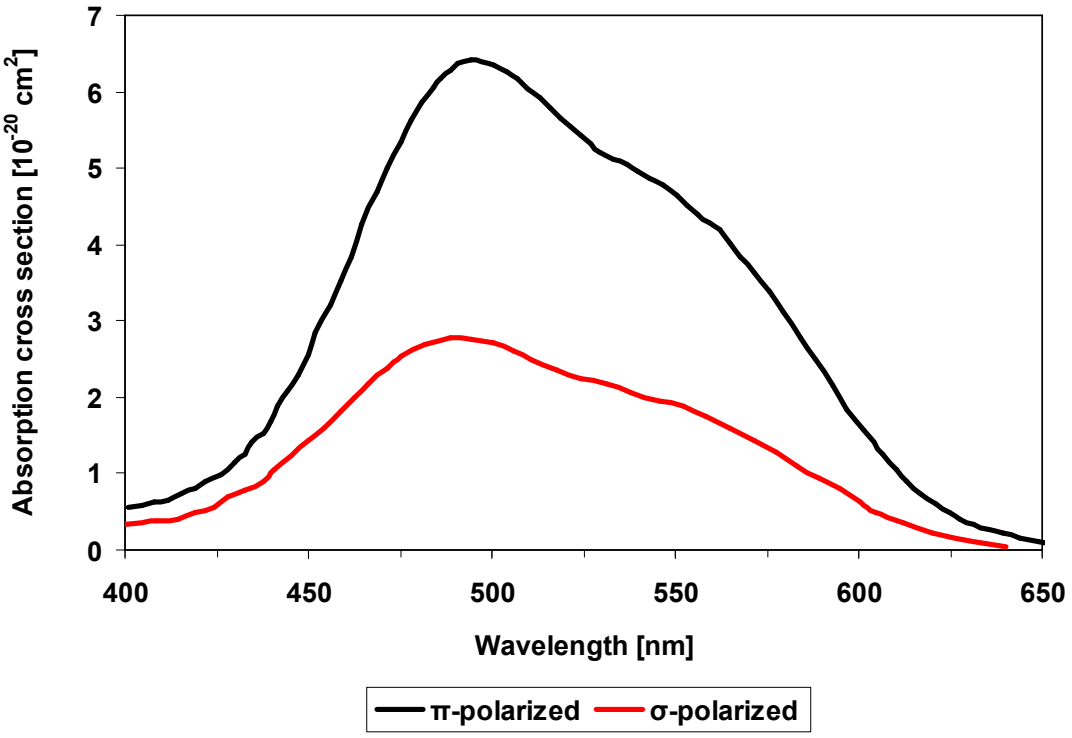

Fig. 1.3. Polarized absorption cross-sections of Ti:sapphire [1].

In addition, Ti:sapphire has a weak infrared absorption band overlapping its broad fluorescence line [1, 2, 24] which is attributed to two different processes: one is the presence Ti^{3+} - Ti^{4+} pairs in the crystal, the second is related to the Ti^{3+} concentration in the crystal but its mechanism is not yet understood [25-27]. Due to this parasitic absorption at the laser wavelength, Ti:sapphire lasers exhibit relatively high losses despite the reduction in parasitic absorption that has been achieved with annealing processes [28-30]. The amount of parasitic absorption in Ti:sapphire is usually stated

in the form of a Figure of Merit (FOM), which is the ratio between pump absorption coefficient and parasitic absorption coefficient at specific wavelengths (typically 514 nm and 820 nm respectively) [23, 25, 26], see equation (1.1). Depending on the doping concentration, commercially available crystals have FOMs between 100 and 500 [17-22] with higher doping levels resulting in lower FOMs [25, 27, 30]. A 11-mm-long Ti:sapphire crystal with doping concentration of 0.15 wt. % and a FOM of 150, which represents the sort of crystals that are typically used in commercial lasers, has a 1.7% single-pass loss (3.4% round-trip loss in a standing-wave resonator) due to parasitic absorption.

$$\text{FOM} = \frac{\alpha_{514}}{\alpha_{820}} \qquad \text{Figure of Merit for parasitic absorption in Ti:sapphire} \qquad (1.1)$$

α_{514} Pump absorption coefficient at λ_p = 514 nm [cm^{-1}]

α_{820} Parasitic absorption coefficient at λ_c = 820 nm [cm^{-1}]

The high intrinsic threshold due to a small στ-product, low pump absorption and high parasitic losses results in a requirement for a high power, high brightness pump source. With an absorption peak in the blue-green spectral region at 490 nm (see Fig. 1.3), Ti:sapphire lasers have historically been pumped with copper-vapour lasers (511 nm) [31] and argon-ion lasers (515 nm) [1, 9]. Most of today's Ti:sapphire lasers use frequency-doubled solid-state (Nd:YLF [32], Nd:YVO_4, Nd:YAG; 523 - 532 nm) or optically pumped semiconductor lasers [33] as pump source. Typical pump thresholds are of the order of a Watt. More recently Ti:sapphire lasers pumped with a frequency-doubled DBR-tapered diode laser [34] and a frequency-doubled Ytterbium-fibre laser [35] have been demonstrated.

1.2.2 Alternatives to Ti:sapphire

Of the multitude of broadly tunable laser gain materials, only a few are widely used. In the near-infrared region of the optical spectrum (0.7 - 1.1 μm), Cr:LiSAF and

Alexandrite are the most prominent vibronic laser gain materials besides Ti:sapphire. Other alternatives are dye lasers and ytterbium-doped laser gain materials.

Cr:LiSAF

Cr^{3+}-doped $LiSrAlF_6$ (Cr:LiSAF) is a vibronic 4-level laser gain material which belongs to the Colquiriite group of crystals [36]. It has an upper laser level lifetime of 67 μs and a stimulated emission cross-section of $4.8 \cdot 10^{-20}$ cm^2 [3, 16, 36]. Since the στ-product of Cr:LiSAF is 2.5 times larger than that of Ti:sapphire, it has a lower intrinsic laser threshold which makes it suitable for flash-lamp [37] and diode-laser pumping [38, 39]. Additionally it offers a fluorescent linewidth of 180 nm and low crystal scattering losses of 0.2% cm^{-1} [3]. Cr:LiSAF has two pump absorption bands at 380 - 490 nm and 550 - 750 nm [3, 36]. Diode-laser pumping has been demonstrated with AlGaInP diode lasers around 670 nm [38] and AlGaAs diode lasers at 752 nm [39]. A tuning range of 782 - 1042 nm [40] and the generation of ultrashort pulses [41, 42] have been realized under diode-laser pumping.

The thermal conductivity (3.1 W m^{-1} K^{-1}) and fracture toughness (0.40 MPa $m^{1/2}$) of Cr:LiSAF [43] are an order of magnitude lower than those of Ti:sapphire which makes Cr:LiSAF more prone to failure at high pump powers. In addition, excited-state absorption and fluorescent lifetime quenching above 50° C limit the laser performance at high pump intensities. The most significant disadvantage of Cr:LiSAF is the lack of high-brightness pump diode lasers in the red spectral region. Existing single-mode AlGaInP diode lasers have maximum output powers of around 160 mW and Cr:LiSAF laser output powers of up 260 mW have been achieved in continuous-wave operation (cw) by multiplexing four diode lasers [40]. Multi-spatial mode diode lasers offer more optical output power but at the expense of a much larger beam propagation parameter, M^2, which makes it impossible to maintain an acceptable overlap of pump and resonator modes over the length of a typical Cr:LiSAF crystal [44]. Tapered diode lasers offer higher brightness [45] but are susceptible to optical feedback. In general AlGaInP diode lasers suffer from low thermal conductivity and high electrical resistivity [46]. Absorption effects at the emitter facets lead to so-called catastrophic optical mirror damage and result in poor

reliability. Hence, even for multi-spatial mode diode lasers the maximum output power has stagnated at the Watt level.

Alexandrite

Alexandrite ($Cr:BeAl_2O_4$) is the common name for Chromium-doped chrysoberyl ($BeAl_2O_4$) in which trivalent Chromium ions (Cr^{3+}) substitute for some of the Al^{3+} ions [47]. It has a very long upper laser level lifetime ($\tau = 260$ μs at T = 300 K) [3, 16] but a small stimulated emission cross-section ($\sigma = 1.0 \cdot 10^{-20}$ cm^2) [3]. The $\sigma\tau$-product of Alexandrite is twice that of Ti:sapphire resulting in a significantly lower intrinsic laser threshold which makes it suitable for flash-lamp and diode-laser [48] pumping. Besides operating as 4-level vibronic laser gain material, it can also act as a 3-level laser with a fixed output at 680 nm. Alexandrite has two pump absorption bands at 380 – 470 nm and 500 - 650 nm [47]. Diode-laser pumping has been demonstrated with AlGaInP laser diodes emitting at 680 nm [48]. Other favourable qualities are a high fracture toughness (2.6 MPa $m^{1/2}$) [47, 49, 50] and good thermal conductivity (23 W m^{-1} K^{-1}) [3, 47], about two thirds and half that of Ti:sapphire respectively. In addition, it has good chemical stability. Unfortunately, like Cr:LiSAF, it suffers from the lack of high-power diode lasers in the yellow-red range of the optical spectrum. However, the most significant disadvantage of Alexandrite is its comparatively small laser gain bandwidth, ranging from 700 nm to 820 nm [3, 16, 47].

Ytterbium-doped laser gain materials

The rare-earth metal Ytterbium is used as a dopant in a variety of host materials (YAG, Silica, YAP, KYW, KGW, NGW, NYW, …) with trivalent ytterbium (Yb^{3+}) acting as the laser active ion [51, 52]. Ytterbium-doped laser gain materials have a simple energy level structure in which pump absorption and emission are transitions between different sublevels of the ground-state and excited-state manifolds. As a result the quantum defect is very small, keeping the amount of heat deposited in the gain medium low for a given pump power. However, because the ground state and the lower laser level are sublevels of the same manifold, the latter is thermally

populated making Ytterbium-doped laser gain media quasi-three level systems which have to be pumped to transparency before inversion can be achieved. Advantages of Ytterbium-doped materials include the absence of excited-state absorption, the ability to use very high doping concentrations up to the stoichiometric limit in some host materials, the long upper state lifetime (951 μs for Yb:YAG at room temperature [3]) and an acceptable emission cross section ($\sigma = 2.1 \cdot 10^{-20}$ cm^2 for Yb:YAG [3]). Ytterbium-doped gain materials have two pump absorption peaks at wavelengths (941 nm and 968 nm for Yb:YAG [16]) where high-power InGaAs diode lasers are commercially available (diode laser arrays achieve kW-level output powers) [53]. However, the small gain bandwidth ($\Delta\lambda_{FWHM} \sim 15$ nm around the peak at 1030 nm for Yb:YAG [51, 54]) severely limits the tuning range and pulse duration that can be achieved with Ytterbium-doped laser gain materials [55].

1.3 Gallium nitride diode lasers

While reliable high-power diode lasers emitting in the green spectral region do not yet exist, high-power GaN diode lasers with emission wavelengths in the blue spectral region have recently become commercially available. They are now produced on a large scale for applications in mass markets, most prominently optical data storage (Blu-ray™). Thus, the opportunity arises to replace the frequency-doubled solid-state lasers currently used as pump sources with GaN diode lasers. Currently, GaN diode lasers are commercially available with emission wavelengths in the ultraviolet-blue region of the optical spectrum (see Table 1.2 and Fig. 1.4).

Table 1.2. Output powers and emission wavelengths of commercially available GaN diode lasers [11-15].

Wavelength [nm]	GaN diode laser ouput power [mW]	Manufacturer / Model
405	175	Renesas NV4V31MF
448	1000	Nichia NDB7352E
473	20	Nicha NDHA210APAE1
488	60	Nichia NDS4113

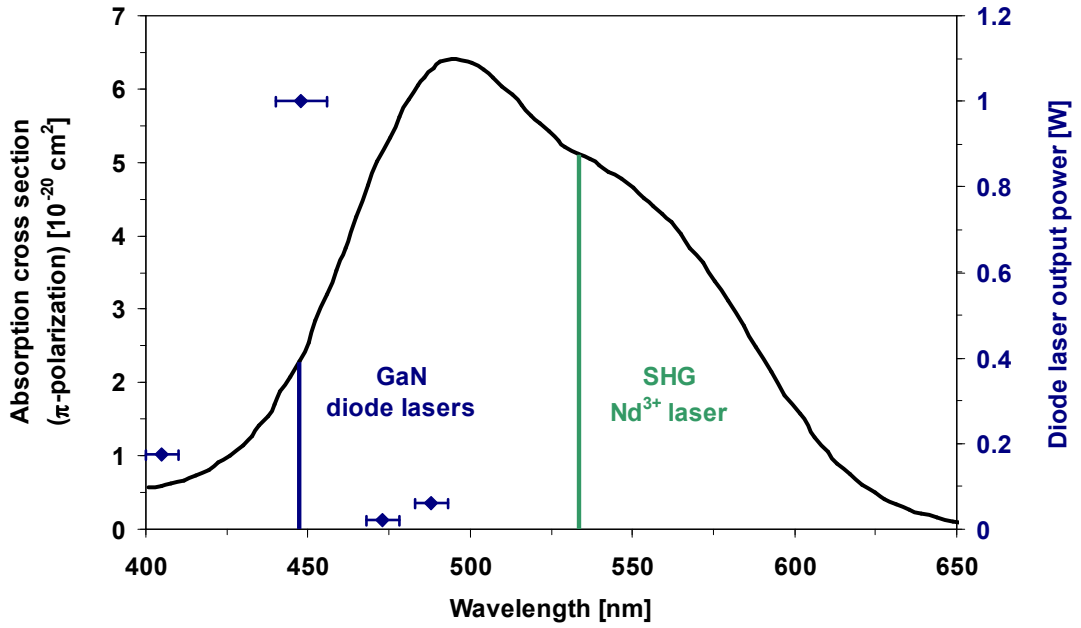

Fig. 1.4. Absorption spectrum of Ti:sapphire (π-polarization) and output powers of commercially available GaN diode lasers as a function of wavelength [1, 11-15].

However, while GaN diode lasers are commercially available with peak emission wavelengths between 370 nm and 490 nm, the diodes with the highest output power (1 W) are those emitting at 440 - 455 nm. Diodes with emission wavelengths closer to the peak absorption wavelength of Ti:Al_2O_3 at 490 nm deliver just 60 mW of output power, which makes the 440 - 455 nm diodes the best compromise [11-15].

1.4 Laser modelling

Since the GaN diode lasers have a far lower brightness than conventional pump lasers for Ti:sapphire and their emission wavelengths are not at the peak pump absorption wavelength, current approaches to Ti:sapphire laser design have to be reassessed. In order to find a low-threshold laser architecture suitable for diode laser pumping, extensive use has been made of optical and laser modelling. A theoretical model developed by A. J. Alfrey [23] has been employed to calculate and optimise the output power, pump threshold and slope efficiency. Having initially considered

several theoretical models [23, 56, 57], this rate-equation based model was chosen because it takes into account the diffraction of pump and resonator modes inside the laser gain medium – crucial for a low-threshold laser where these modes have to be tightly focussed.

Equations (1.2-9) from [23] enables us to calculate the pump power needed for a given output power and laser architecture:

$$P_{P0} = \frac{(T + 2\alpha_r L + \eta) hc\pi^2}{8\sigma\tau\lambda_p \alpha_p \int_0^L \frac{\exp[-\alpha_p z]}{w_{rx} w_{ry} w_{px} w_{py}} Q'(z)\, dz} \tag{1.2}$$

$$Q'(z) = \int_{-\infty}^{\infty}\int_{-\infty}^{\infty} \frac{\exp[-A_x x^2 - A_y y^2]}{1 + B\exp[-D_x x^2 - D_y y^2]} dx\, dy \tag{1.3}$$

$$A_{x/y} = 2\frac{w_{rx/y}^2 + w_{px/y}^2}{w_{rx/y}^2 w_{px/y}^2} \tag{1.4}$$

$$D_{x/y} = \frac{2}{w_{rx/y}^2} \tag{1.5}$$

$$B = \frac{4sP_r}{\pi w_{rx} w_{ry}} \tag{1.6}$$

$$s = \frac{\sigma\tau\lambda_r}{hc} \tag{1.7}$$

$$w_{px/y}(z) = w_{p0x/y}\sqrt{1 + \left(\frac{M^2_{px/y}\lambda_p}{\pi w_{p0x/y}^2 n_p}\right)^2 (z - z_{p0x/y})^2} \tag{1.8}$$

$$w_{rx/y}(z) = w_{r0x/y}\sqrt{1 + \left(\frac{M^2_{rx/y}\lambda_r}{\pi w_{r0x/y}^2 n_r}\right)^2 (z - z_{r0x/y})^2} \tag{1.9}$$

x	Index to denote the horizontal plane
y	Index to denote the vertical plane
p	Index to denote the pump mode

r Index to denote the resonator mode

P_{P0} Pump power incident on the crystal [W]

P_{th} Threshold pump power [W]

P_r Oscillating power inside the resonator [W]

s Saturation parameter [m^2 W^{-1}]

T Output coupler transmission

L Crystal length [m]

η Resonator roundtrip losses other than crystal and output coupler losses

α_p Pump absorption coefficient [m^{-1}]

α_r Parasitic crystal loss coefficient [m^{-1}]

σ Stimulated emission cross section [m^2]

τ Fluorescence lifetime [s]

h Plank constant [Js]

c Speed of light in vacuum [m s^{-1}]

λ Wavelength in vacuum [m]

n Index of refraction

M^2 Beam propagation parameter

w Mode radius [m]

w_0 Mode waist radius [m]

z Position along the optical axis [m]

z_0 Mode waist location [m]

At laser threshold, P_r = 0 and equations (1.2-9) can be reduced to the following expression for the threshold pump power:

$$P_{th} = \frac{\left(T + 2\alpha_r L + \eta\right) hc\pi}{4\sigma\tau\lambda_p \alpha_p \int_0^L \frac{\exp[-\alpha_p z]}{\sqrt{\left(w_{rx}^{\ 2} + w_{px}^{\ 2}\right)\left(w_{ry}^{\ 2} + w_{py}^{\ 2}\right)}} dz} \tag{1.10}$$

In case of axisymmetric (non-astigmatic) resonator and pump modes ($w_{rx} = w_{ry} = w_r$, $w_{px} = w_{py} = w_p$) equations (1.2-10) simplify to [23]:

$$P_{P0} = \frac{(T + 2\alpha_r L + \eta) hc\pi^2}{8\sigma\tau\lambda_p \alpha_p \int_0^L \frac{\exp(-\alpha_p z)}{w_r^{\,2} w_p^{\,2}} Q(z)\, dz} \tag{1.11}$$

$$Q(z) = 2\pi \int_0^\infty \frac{\exp[-A r^2]}{1 + B \exp[-D r^2]} r\, dr \tag{1.12}$$

$$A = 2\frac{w_r^{\,2} + w_p^{\,2}}{w_r^{\,2} w_p^{\,2}} \tag{1.13}$$

$$D = \frac{2}{w_r^{\,2}} \tag{1.14}$$

$$B = \frac{4sP_r}{\pi w_r^{\,2}} \tag{1.15}$$

$$s = \frac{\sigma \tau \lambda_r}{h c} \tag{1.16}$$

$$w_p(z) = w_{p0} \sqrt{1 + \left(\frac{M^2{}_p \lambda_p}{\pi w_{p0}^{\,2} n_p} \right)^2 (z - z_{p0})^2} \tag{1.17}$$

$$w_r(z) = w_{r0} \sqrt{1 + \left(\frac{M^2{}_r \lambda_r}{\pi w_{r0}^{\,2} n_r} \right)^2 (z - z_{r0})^2} \tag{1.18}$$

$$P_{th} = \frac{(T + 2\alpha_r L + \eta) hc\pi}{4\sigma\tau\lambda_p \alpha_p \int_0^L \frac{\exp[-\alpha_p z]}{w_r^{\,2} + w_p^{\,2}} dz} \tag{1.19}$$

This model, in its fully astigmatic and non-astigmatic forms, is used extensively in the following chapters to calculate and optimise the laser performance. The optimum crystal doping level, crystal length, output coupler transmission, pump and cavity mode sizes are ascertained for a low-threshold longitudinally pumped cw laser

oscillator. Since equations (1.2-9) and (1.11-18) have no analytical solution for the output power, multivariate optimisation is employed to optimise these parameters by using a conjugate gradient solver algorithm within the commercial software package MathCAD.

1.5 Mode locking

There are a multitude of techniques used to generate short laser pulses, e. g. mode locking [58], Q switching [59], gain switching [60] and cavity dumping. The shortest pulses generated directly from a laser have been achieved under mode-locked operation [8]. The basic mechanism of mode locking is the periodic modulation of the light intensity inside the laser resonator. If a resonator mode of optical frequency ν_0 is periodically modulated in time with modulation frequency f then a Fourier analysis shows that sidebands are generated in the frequency domain at $\nu_0 \pm f$ [61]. If the modulation frequency f is equal to the resonator roundtrip frequency f_r then these sidebands coincide with the neighbouring longitudinal modes of the resonator which are separated by the free spectral range $\delta\nu_r$ of the resonator, see equation (1.20).

$$\delta\nu_r = \frac{c}{2\,d_r} = f_r \qquad \text{Free spectral range of a standing-wave resonator [Hz]} \qquad (1.20)$$

f_r Resonator roundtrip frequency [Hz]

d_r Resonator optical path length [m]

All modes within the laser gain bandwidth are amplified and because they are periodically modulated as well they can generate sidebands themselves. The number of modes that can be amplified in the resonator is limited by the bandwidth of the laser gain medium. Since the amplitudes of all resonator modes synchronously reach a maximum at the position of the modulator, they are locked in phase with each other, hence the name mode locking. By contrast, in a normal laser a multitude of longitudinal (and transverse) modes can oscillate with a random phase relationship

resulting in laser output with random intensity fluctuations (noise). In mode-locked lasers with their fixed phase relationship, the mode amplitudes add constructively to produce a short pulse circulating in the resonator. Each time this pulse hits the output coupler a fraction of its power is emitted from the laser. Thus, the laser output is a periodical train of pulses separated by the resonator roundtrip time $T_r = f_r^{-1}$. The duration of these pulses $\Delta\tau$ depends on the number of amplified resonator modes N and the intensity distribution between the modes, see equation (1.21). Intensity distributions following a Gaussian function or the square of the hyperbolic secant function are common. Table 1.3 lists the intensity and spectral profiles and their associated parameters [3].

$$\Delta\tau = \frac{C_B}{\Delta\nu} \approx \frac{1}{N\,\delta\nu_R} \qquad \text{Duration-bandwidth product} \qquad (1.21)$$

$\Delta\tau$ Pulse duration (FWHM) [s]

$\Delta\nu$ Pulse spectral bandwidth (FWHM) [Hz]

C_B Pulse shape parameter (transform-limited)

N Number of amplified resonator modes

Table 1.3. Intensity and spectral profiles of the gauss function and the square of the hyperbolic secant function and their parameters.

Distribution	Intensity profile	$\Delta\tau / \tau$	Spectral profile	$\Delta\nu \cdot \tau$	C_B
hyperbolic secant^2	$sech^2 (t/\tau)$	1.763	$sech^2 (\pi\omega\tau/2)$	0.179	0.315
Gaussian	$exp[-2(t/\tau)^2]$	1.177	$exp[-(\omega\tau)^2/2]$	0.375	0.441

The duration-bandwidth product (Equation 1.21) represents Fourier's theorem which dictates that the pulse duration in the time domain and pulse bandwidth in the frequency domain are inversely proportional. Due to chromatic dispersion and nonlinearities occurring in the optical elements within the laser resonator, a pulse can acquire a chirp: that is to say the frequency components making up the pulse vary in time over its duration. A chirped pulse will exhibit a spectral bandwidth $\Delta\nu$ larger

than necessary for its duration $\Delta\tau$ and will therefore exhibit a duration-bandwidth product greater than C_B. Pulses free from chirp have a constant spectral phase and since they represent the shortest possible duration $\Delta\tau$ for a particular spectral bandwidth $\Delta\nu$ they are said to be transform limited. The optical components in the resonator of a mode-locked laser usually exhibit normal chromatic dispersion which can be compensated by introducing optical elements with anomalous dispersion to avoid chirped pulses. Such elements include prism pairs [62], diffraction grating pairs [63] or dispersive dielectric mirrors (Gires-Tournois-Interferometers [64] or chirped mirrors [65]).

The periodic modulation of the light intensity inside the resonator which is necessary to achieve mode-locked operation in a laser can be externally applied (active mode locking) [66] or induced by the resonating light itself (passive mode locking) [67]. Passive mode locking techniques are far more commonly used and allow the generation of much shorter pulses since the intensity modulation is driven by the laser light itself. The modulation mechanism for passive mode locking is based on a nonlinear element inside the resonator which exhibits an intensity-dependent loss or gain. A saturable absorber absorbs low intensity laser radiation but is saturated (or bleaches) under more intense irradiation and can therefore provide an intensity-dependent loss which leads to self amplitude modulation. Saturable absorbers based on semiconductor materials [68] can be integrated into a mirror structure resulting in a compact modulator that can be easily incorporated into a laser resonator. Such devices are generally referred to as semiconductor saturable absorber mirrors (SESAMs) [69] and, in the case where a Bragg mirror structure is used and the absorber is inserted within the topmost layer, they are also known as saturable Bragg reflectors (SBRs) [70]. The saturable absorber in a SESAM is typically a single quantum well layer although multiple quantum wells and quantum dots [71] have also been used. The properties of a SESAM, in particular the wavelength of operation, dispersion, modulation depth, saturation fluence and recovery time can be engineered by varying the design parameters, material composition and growth conditions. In chapter 3 of this thesis, an SBR will be used to mode lock a directly diode-laser-pumped Ti:sapphire laser.

In general saturable absorbers used for mode locking are classified either as fast or slow depending on their recovery time: that is to say the time taken for the induced loss to recover to its original level after saturation by the pulse. The recovery time of a fast saturable absorber is shorter than the pulse duration and the loss modulation therefore follows the light intensity. By contrast, in a slow saturable absorber which has a recovery time that is long compared to the pulse duration, only the leading edge of the pulse is loss-modulated while the trailing edge is not attenuated. Besides the self amplitude modulation provided by the intensity-dependent loss of a saturable absorber other mechanisms can be present in a mode-locked laser and influence the pulse formation and shaping (and therefore allow a slow saturable absorber to achieve stable mode locking [72, 73]). A pulse can also experiences gain narrowing and gain saturation depending on the properties of the gain medium. In the femtosecond regime chromatic dispersion and nonlinearities can be a strong influence. Most notable is the Kerr effect which leads to self-phase modulation and self-focussing (Kerr lensing). The latter is the dominant pulse shaping mechanism in Kerr lens mode-locked lasers where it provides an intensity-dependent gain (soft aperture) and potential loss (hard aperture) [7, 74]. By contrast, where a SESAM is used in the slow saturable absorber regime, and so-called soliton mode locking results, the balance between negative dispersion and self-phase modulation is the dominant pulse shaping effect [72]. In both cases, SESAMs can be used to initiate and sustain the mode locking while chromatic dispersion and the Kerr effect dominate the pulse shaping.

1.6 Synopsis

In chapter 2, the development of a continuous-wave, low-threshold Ti:sapphire laser – suitable for pumping with gallium nitride diode lasers – is described. The chapter starts with a characterisation of the pump lasers used, followed by a description of a basic Ti:sapphire laser with conventional pumping. Modelling of the resonator and Ti:sapphire crystal specifications is then used to optimise the setup for low-threshold operation. A directly diode-laser pumped Ti:sapphire laser based on the results of the modelling is subsequently demonstrated. The optimisation of this Ti:sapphire laser, under conventional pumping and under direct diode-laser pumping, is then described.

In chapter 3, direct diode-laser pumping of a mode-locked Ti:sapphire laser is reported. Based on a four-mirror resonator, this Ti:sapphire laser is passively mode-locked by a saturable Bragg reflector (SBR). The chapter begins with modelling to ascertain the pump and resonator parameters for optimum performance. A Ti:sapphire laser built using these specifications is then characterised in continuous-wave operation under conventional and diode-laser pumping. Mode-locked operation under both pump regimes is subsequently demonstrated. The optimisation of the laser performance for shorter pulse durations and the demonstration of double-sided diode-laser pumping to increase the output power are then described.

Chapter 4 deals with the pump-induced loss observed in Ti:sapphire lasers. Beginning with the observation of Ti:sapphire laser performance degradation under diode-laser pumping, this effect is subsequently characterised by collinear pumping with a frequency-doubled Nd:YVO_4 and a multi-line Argon-ion laser. The pump-induced loss is then quantified by comparison of resonator loss analyses. Fluorescence measurements lead to the observation of a reduced quantum efficiency for optically excited fluorescence at short pump wavelengths.

Chapter 5 concludes the thesis with a summary of the main achievements. An outlook is given on the future directions of directly diode-laser-pumped Ti:sapphire lasers and their possible applications. The potential impact of gallium nitride diode laser with higher output powers and longer emission wavelengths is discussed.

1.7 References

1. P. F. Moulton, "Spectroscopic and Laser Characteristics of Ti:Al_2O_3," J. Opt. Soc. Am. B **3**, 125-133 (1986).
2. P. Albers, E. Stark, and G. Huber, "Continuous-wave laser operation and quantum efficiency of titanium-doped sapphire," J. Opt. Soc. Am. B **3**, 134-139 (1986).
3. W. Koechner, *Solid-State Laser Engineering,* 6 ed. (Springer, 2006).
4. P. F. Moulton, "Ti-doped sapphire: tunable solid-state laser," OPN **8**, 9 (1982).
5. F. Schäfer, "ORGANIC DYE SOLUTION LASER," Appl. Phys. Lett. **9**, 306 (1966).
6. P. P. Sorokin and J. R. Lankard, "Stimulated Emission Observed from an Organic Dye, Chloro-aluminum Phthalocyanine," IBM J. Res. Dev. **10**, 162-163 (1966).
7. D. E. Spence, P. N. Kean, and W. Sibbett, "60-fsec pulse generation from a self-mode-locked Ti:sapphire laser," Opt. Lett. **16**, 42-44 (1991).
8. R. Ell, U. Morgner, F. X. Kärtner, J. G. Fujimoto, E. P. Ippen, V. Scheuer, G. Angelow, T. Tschudi, M. J. Lederer, A. Boiko, and B. Luther-Davies, "Generation of 5-fs pulses and octave-spanning spectra directly from a Ti:sapphire laser," Opt. Lett. **26**, 373-375 (2001).
9. A. Sanchez, R. E. Fahey, A. J. Strauss, and R. L. Aggarwal, "Room-temperature continuous-wave operation of a Ti:Al_2O_3 laser," Opt. Lett. **11**, 363-364 (1986).
10. S. Nakamura, M. Senoh, S.-I. Nagahama, N. Iwasa, T. Yamada, T. Matsushita, H. Kiyoku, and Y. Sugimoto, "InGaN-Based Multi-Quantum-Well-Structure Laser Diodes," Jpn. J. Appl. Phys. **35**, L74 (1996).
11. "Laser Diode" (Nichia Corp.), retrieved 03 October, 2011, http://www.nichia.co.jp/en/product/laser_main.html.
12. "Product information - Laser Diode [industrial use]" (Sanyo), retrieved 03 October, 2011, http://www.edc.sanyo.com/english/products/photonics/product22_2.html.

13. "Laser Diodes for BD Recording" (Sony Corp.), retrieved 03 October, 2011, http://www.sony.net/Products/SC-HP/pro/laser_diode/blu_ray_rec.html.
14. "Blue Laser" (OSRAM Opto Semiconductors GmbH), retrieved 03 October, 2011, http://catalog.osram-os.com/catalogue/catalogue.do?act=showBookmark&favOid=0000000600003f0f00ad0023.
15. "Visible Laser" (Renesas Electronics Corp.), retrieved 03 October, 2011, http://www2.renesas.com/opto/en/visiblelaser.html.
16. O. Svelto and D. C. Hanna, *Principles of lasers,* 4 ed. (Plenum Press, 1998).
17. "Titanium -Doped Sapphire Laser Crystals" (Saint-Gobain Crystals), retrieved 20 December, 2007, http://www.photonic.saint-gobain.com.
18. "Ti:Sapphire" (EKSMA Optics), retrieved 30 September, 2011, http://www.eksmaoptics.com/repository/catalogue/pdfai/NLOC/laser crystals/ti_sapphire.pdf.
19. "Ti:Sapphire Laser Crystals" (Roditi International Corporation Ltd), retrieved 30 September, 2011, http://www.roditi.com/Laser/Ti_Sapphire.html.
20. "Titanium Doped Sapphire Crystal" (GWU-Lasertechnik Vertriebsges. mbH), retrieved 30 September, 2011, http://www.gwu-group.com/cmslaser/dmdocuments/castech_tisa.pdf.
21. "Titanium doped Sapphire" (Moltech GmbH), retrieved 30 September, 2011, http://www.mt-berlin.com/frames_cryst/crystals_frameset1.htm.
22. "Ti:Sapphire Crystal" (Red Optronics), retrieved 30 September, 2011, http://www.redoptronics.com/Ti-Sapphire-crystal.html.
23. A. J. Alfrey, "Modeling of Longitudinally Pumped CW Ti:Sapphire Laser Oscillators," IEEE J. Quantum Electron. **25**, 760-766 (1989).
24. G. F. Albrecht, J. M. Eggleston, and J. J. Ewing, "Measurements of Ti^{3+}:Al_2O_3 as a lasing material," Opt. Commun. **52**, 401-404 (1985).
25. A. Sanchez, A. J. Strauss, R. L. Aggarwal, and R. E. Fahey, "Crystal-Growth, Spectroscopy, and Laser Characteristics of Ti:Al_2O_3," IEEE J. Quantum Electron. **24**, 995-1002 (1988).
26. W. R. Rapoport and C. P. Khattak, "Titanium sapphire laser characteristics," Appl. Opt. **27**, 2677-2684 (1988).

27. R. L. Aggarwal, A. Sanchez, M. M. Stuppi, R. E. Fahey, A. J. Strauss, W. R. Rapoport, and C. P. Khattak, "Residual infrared absorption in as-grown and annealed crystals of Ti:Al_2O_3," IEEE J. Quantum Electron. **24**, 1003-1008 (1988).
28. P. Lacovara, L. Esterowitz, and M. Kokta, "Growth, spectroscopy, and lasing of titanium-doped sapphire," IEEE J. Quantum Electron. **21**, 1614-1618 (1985).
29. J. F. Pinto, L. Esterowitz, G. H. Rosenblatt, M. Kokta, and D. Peressini, "Improved Ti:Sapphire Laser Performance with New High Figure of Merit Crystals," IEEE J. Quantum Electron. **30**, 2612-2616 (1994).
30. I. T. McKinnie, A. L. Oien, D. M. Warrington, P. N. Tonga, L. A. W. Gloster, and T. A. King, "Ti^{3+} Ion Concentration and Ti:sapphire Laser Performance," IEEE J. Quantum Electron. **33**, 1221-1230 (1997).
31. K. Takehisa and A. Miki, "Method for pumping a Ti:sapphire laser with a stable resonator copper vapor laser," Appl. Opt. **31**, 2734-2737 (1992).
32. G. T. Maker and A. I. Ferguson, "Ti:sapphire laser pumped by a frequency-doubled diode-pumped Nd:YLF laser," Opt. Lett. **15**, 375-377 (1990).
33. B. Resan, "Ultrashort pulse Ti:sapphire oscillators pumped by optically pumped semiconductor (OPS) pump lasers," Proc. SPIE **6871**, 687116 (2008).
34. A. Müller, O. B. Jensen, A. Unterhuber, T. Le, A. Stingl, K.-H. Hasler, B. Sumpf, G. Erbert, P. E. Andersen, and P. M. Petersen, "Frequency-doubled DBR-tapered diode laser for direct pumping of Ti:sapphire lasers generating sub-20 fs pulses," Opt. Express **19**, 12156-12163 (2011).
35. G. K. Samanta, S. C. Kumar, K. Devi, and M. Ebrahim-Zadeh, "Fiber-laser-pumped Ti:sapphire Laser," in *Lasers and Electro-Optics (CLEO) and Quantum Electronics and Laser Science Conference (QELS), 2010 Conference on*, 2010), 1-2.
36. S. A. Payne, L. L. Chase, L. K. Smith, W. L. Kway, and H. W. Newkirk, "Laser performance of $LiSrAlF_6:Cr^{3+}$," J. Appl. Phys. **66**, 1051-1056 (1989).
37. M. Stalder, "Flashlamp pumped $Cr:LiSrAlF_6$ laser," Appl. Phys. Lett. **58**, 216 (1991).

38. R. Scheps, J. F. Myers, H. B. Serreze, A. Rosenberg, R. C. Morris, and M. Long, "Diode-pumped Cr:LiSrAlF$_6$ laser," Opt. Lett. **16**, 820-822 (1991).
39. S. A. Payne, W. F. Krupke, L. K. Smith, W. L. Kway, L. D. DeLoach, and J. B. Tassano, "752 nm wing-pumped Cr:LiSrAlF$_6$ laser," IEEE J. Quantum Electron. **28**, 1188-1196 (1992).
40. U. Demirbas, D. Li, J. R. Birge, A. Sennaroglu, G. S. Petrich, L. A. Kolodziejski, F. X. Kaertner, and J. G. Fujimoto, "Low-cost, single-mode diode-pumped Cr:Colquiriite lasers," Opt. Express **17**, 14374-14388 (2009).
41. P. M. Mellish, P. M. W. French, J. R. Taylor, P. J. Delfyett, and L. T. Florez, "All-solid-state femtosecond diode-pumped Cr:LiSAF laser," Electron. Lett. **30**, 223-224 (1994).
42. M. J. P. Dymott and A. I. Ferguson, "Self-mode-locked diode-pumped Cr:LiSAF laser," Opt. Lett. **19**, 1988-1990 (1994).
43. S. A. Payne, L. K. Smith, R. J. Beach, B. H. T. Chai, J. H. Tassano, L. D. DeLoach, W. L. Kway, R. W. Solarz, and W. F. Krupke, "Properties of Cr:LiSrAlF$_6$ crystals for laser operation," Appl. Opt. **33**, 5526-5536 (1994).
44. J.-M. Hopkins, "Compact, Low-threshold Femtosecond Lasers," (University of St. Andrews, St. Andrews, Scotland, 1999).
45. U. Demirbas, M. Schmalz, B. Sumpf, G. Erbert, G. S. Petrich, L. A. Kolodziejski, J. G. Fujimoto, F. X. Kärtner, and A. Leitenstorfer, "Femtosecond Cr:LiSAF and Cr:LiCAF lasers pumped by tapered diode lasers," Opt. Express **19**, 20444-20461 (2011).
46. P. Epperlein, "Local mirror temperatures of red-emitting (Al)GaInP quantum-well laser diodes by Raman scattering and reflectance modulation measurements," Appl. Phys. Lett. **60**, 680 (1992).
47. J. Walling, O. Peterson, H. Jenssen, R. Morris, and E. O'Dell, "Tunable alexandrite lasers," IEEE J. Quantum Electron. **16**, 1302-1315 (1980).
48. R. Scheps, "Alexandrite laser pumped by semiconductor lasers," Appl. Phys. Lett. **56**, 2288 (1990).
49. B. W. Woods, S. A. Payne, J. E. Marion, R. S. Hughes, and L. E. Davis, "Thermomechanical and thermo-optical properties of the LiCaAlF$_6$:Cr^{3+} laser material," J. Opt. Soc. Am. B **8**, 970-977 (1991).

50. J. Walling, D. Heller, H. Samelson, D. Harter, J. Pete, and R. Morris, "Tunable alexandrite lasers: Development and performance," IEEE J. Quantum Electron. **21**, 1568-1581 (1985).
51. L. D. DeLoach, S. A. Payne, L. L. Chase, L. K. Smith, W. L. Kway, and W. F. Krupke, "Evaluation of absorption and emission properties of Yb^{3+} doped crystals for laser applications," IEEE J. Quantum Electron. **29**, 1179-1191 (1993).
52. R. Paschotta, "Encyclopedia of Laser Physics and Technology" (RP Photonics Consulting GmbH), retrieved http://www.rp-photonics.com/encyclopedia.html.
53. P. Lacovara, H. K. Choi, C. A. Wang, R. L. Aggarwal, and T. Y. Fan, "Room-temperature diode-pumped Yb:YAG laser," Opt. Lett. **16**, 1089-1091 (1991).
54. X. Wang, X. Xu, Z. Zhao, B. Jiang, J. Xu, G. Zhao, P. Deng, G. Bourdet, and J. C. Chanteloup, "Comparison of fluorescence spectra of Yb:$Y_3Al_5O_{12}$ and Yb:$YAlO_3$ single crystals," Opt. Mater. **29**, 1662-1666 (2007).
55. C. Hönninger, F. Morier-Genoud, M. Moser, U. Keller, L. R. Brovelli, and C. Harder, "Efficient and tunable diode-pumped femtosecond Yb:glass lasers," Opt. Lett. **23**, 126-128 (1998).
56. W. P. Risk, "Modeling of Longitudinally Pumped Solid-State Lasers Exhibiting Reabsorption Losses," J. Opt. Soc. Am. B **5**, 1412-1423 (1988).
57. E. P. Maldonado and N. D. Vieira, "Optimization of the active medium length in longitudinally pumped continuous-wave lasers," J. Opt. Soc. Am. B **12**, 2482-2485 (1995).
58. W. E. Lamb, Jr., "Theory of an Optical Maser," Physical Review **134**, A1429-A1450 (1964).
59. F. J. McClung and R. W. Hellwarth, "Giant Optical Pulsations from Ruby," Appl. Opt. **1**, 103-105 (1962).
60. P. Ho, "Picosecond pulse generation with a cw GaAlAs laser diode," Appl. Phys. Lett. **33**, 241 (1978).
61. W. Demtröder, *Experimentalphysik 3: Atome, Moleküle und Festkörper,* 2 ed. (Springer, 2000).

62. R. L. Fork, O. E. Martinez, and J. P. Gordon, "Negative dispersion using pairs of prisms," Opt. Lett. **9**, 150-152 (1984).
63. E. Treacy, "Optical pulse compression with diffraction gratings," IEEE J. Quantum Electron. **QE-5**, 454-458 (1969).
64. F. Gires and P. Tournois, "Interferometre utilisable pour la compression d'impulsions lumineuses modulees en frequence," C. R. Acad. Sci. Paris **258**, 6112-6115 (1964).
65. R. Szipöcs, K. Ferencz, C. Spielmann, and F. Krausz, "Chirped multilayer coatings for broadband dispersion control in femtosecond lasers," Opt. Lett. **19**, 201-203 (1994).
66. L. Hargrove, "LOCKING OF He-Ne LASER MODES INDUCED BY SYNCHRONOUS INTRACAVITY MODULATION," Appl. Phys. Lett. **5**, 4 (1964).
67. H. Mocker, "MODE COMPETITION AND SELF-LOCKING EFFECTS IN A Q-SWITCHED RUBY LASER," Appl. Phys. Lett. **7**, 270 (1965).
68. A. F. Gibson, M. F. Kimmitt, and B. Norris, "Generation of bandwidth-limited pulses from a TEA CO_2 laser using p-type germanium," Appl. Phys. Lett. **24**, 306-307 (1974).
69. U. Keller, K. J. Weingarten, F. X. Kärtner, D. Kopf, B. Braun, I. D. Jung, R. Fluck, C. Honninger, N. Matuschek, and J. Aus der Au, "Semiconductor saturable absorber mirrors (SESAM's) for femtosecond to nanosecond pulse generation in solid-state lasers," IEEE J. Sel. Top. Quantum Electron. **2**, 435-453 (1996).
70. S. Tsuda, W. H. Knox, E. A. de Souza, W. Y. Jan, and J. E. Cunningham, "Low-loss intracavity AlAs/AlGaAs saturable Bragg reflector for femtosecond mode locking in solid-state lasers," Opt. Lett. **20**, 1406-1408 (1995).
71. P. Guerreiro, "PbS quantum-dot doped glasses as saturable absorbers for mode locking of a Cr:forsterite laser," Appl. Phys. Lett. **71**, 1595 (1997).
72. F. X. Kärtner and U. Keller, "Stabilization of solitonlike pulses with a slow saturable absorber," Opt. Lett. **20**, 16-18 (1995).

73. R. Paschotta and U. Keller, "Passive mode locking with slow saturable absorbers," Appl. Phys. B **73**, 653-662 (2001).

74. T. Brabec, C. Spielmann, P. F. Curley, and F. Krausz, "Kerr lens mode locking," Opt. Lett. **17**, 1292-1294 (1992).

2 Continuous-wave operation of directly diode-laser-pumped Ti:sapphire lasers

2 Continuous-wave operation of directly diode-laser-pumped Ti:sapphire lasers

In this chapter, the development of a continuous-wave (cw), low-threshold Ti:sapphire laser – suitable for pumping with GaN diode lasers – is described. The chapter starts with a characterisation of the pump lasers used, followed by a description of a basic Ti:sapphire laser with conventional pumping. This then leads on to the modelling of resonator and Ti:sapphire crystal specifications to optimise for low-threshold operation. Direct diode-laser pumping of a Ti:sapphire laser based on the modelling results is subsequently demonstrated. The optimisation of this Ti:sapphire laser, under conventional 532 nm pumping and under direct diode-laser pumping at 452 nm, is then described. Where laser performance is described in this chapter, pump thresholds and slope efficiencies are always given with respect to pump power incident on the crystal.

2.1 Pump lasers

2.1.1 Frequency-doubled, diode-pumped Nd:YVO_4 laser

In order to test, evaluate and optimise Ti:sapphire lasers, a frequency-doubled, diode-pumped Nd:YVO_4 laser (Elforlight HPG5000) was initially used as the pump, see Fig. 2.1. This laser delivered up to 5 W of output power at a wavelength of 532 nm. In order to ensure a stable beam profile over the entire power range, the laser was externally attenuated by a half-wave plate and a polarizing beamsplitter cube while running at maximum output power. The laser beam was polarized in the horizontal plane. Using a scanning slit beam-profiler (DataRay Inc. Beamscope-P7) the beam propagation factor was measured to be $M_x^2 = 1.8$ in the horizontal and $M_y^2 = 1.2$ in the vertical plane.

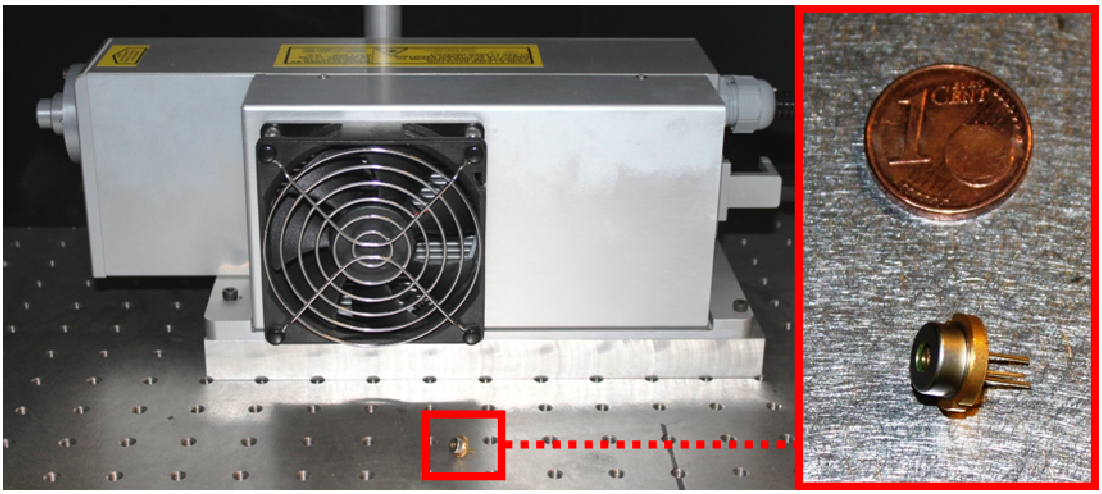

Fig. 2.1. Size comparison of a frequency-doubled neodymium laser head (5 W at 532 nm), top left, with a gallium nitride diode laser (1 W at 452 nm), bottom right.

2.1.2 GaN diode laser

Over the course of this research project GaN diode laser technology matured, resulting in higher output powers per single emitter and a shift towards longer wavelengths that are more favourable for the pumping of Ti:sapphire. The very first diode lasers used in this research were engineering samples (Nichia NDB7352E) delivering 500 mW of optical output power at wavelengths between 440 nm and 445 nm. At the time of writing, laser diodes with output powers of up to 1.0 W at wavelengths between 445 nm and 455 nm have reached production status [1]. The experiments presented in this chapter used such a diode (Nichia NDB7352, ~ 15 × 2 µm stripe) delivering 1.0 W at 452 nm. The diode sits in a water-cooled mount (T = 15° C) which also holds an aspheric collimating lens of f = 4.5 mm focal length, see Fig. 2.2. The beam propagation factor was measured to be $M_x^2 = 6.2$ in the horizontal plane and $M_y^2 = 1.8$ in the vertical plane, see Fig. 2.3 and Fig. 2.4.

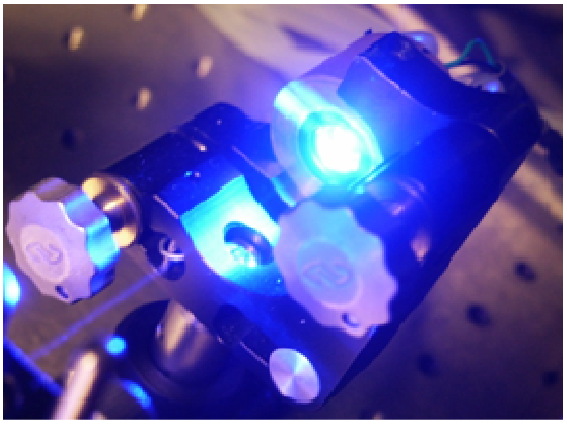

Fig. 2.2. GaN diode laser in a water-cooled mount (T = 15° C).

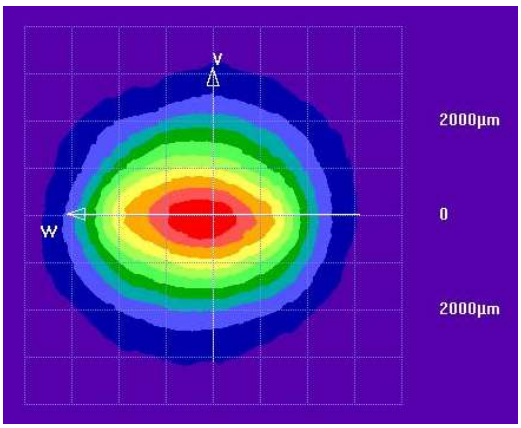

Fig. 2.3. Beam cross section of GaN diode laser (1 W) collimated with aspheric collimating lens (f = 4.5 mm).

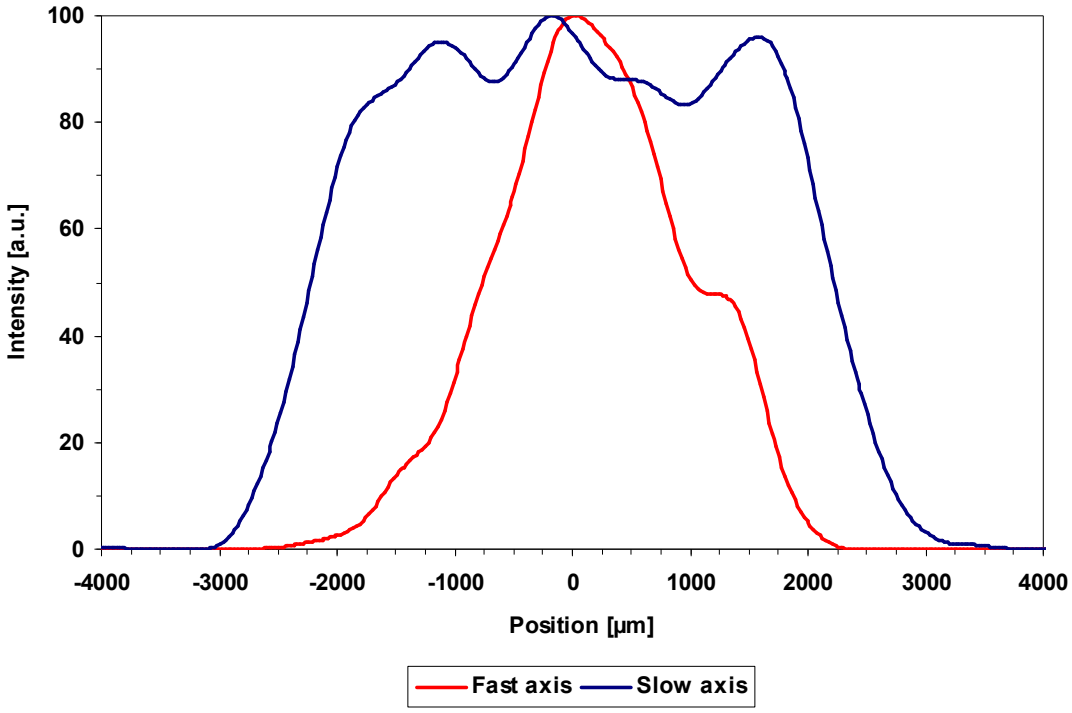

Fig. 2.4. Beam profile of a GaN diode laser (1 W, 452 nm) collimated with an aspheric collimating lens (f = 4.5 mm).

2.2 A basic Ti:sapphire laser

A Ti:Al_2O_3 crystal (4.6 mm long, 3 mm rod diameter, Brewster-cut) of the sort that is typically used in commercial lasers was provided on loan by Coherent Scotland Ltd. A basic cw 3-mirror Ti:sapphire laser was built, in order to measure the performance that could be achieved with this crystal: in particular to assess by how much the threshold would need to be reduced to make diode-laser pumping feasible. Before the laser was built, the absorption coefficient of the crystal was measured at 532 nm to assist with laser design.

2.2.1 Absorption coefficient of the Coherent Crystal at 532 nm

Since the crystal doping level was not known, the Nd:YVO_4 pump laser was used to measure the absorption coefficient at 532 nm before the laser resonator was built. With a single plano-convex lens of 125 mm focal length focussing the pump beam into the Ti:sapphire crystal, incident pump power and transmitted pump power were measured. The crystal absorbed 79% of the incident pump power. Using Beer's law, the absorption coefficient was calculated from this data to be 3.4 cm^{-1} at 532 nm. A comparison with absorption data provided by commercial crystal manufacturers [2, 3] lead to the conclusion that the crystal doping concentration is around 0.20 wt. %.

2.2.2 Laser resonator and pump optics

With existing rather than optimised components – resonator mirrors borrowed from a Cr:LiSAF laser setup – a basic 3-mirror dogleg resonator was built around the crystal, see Fig. 2.5.

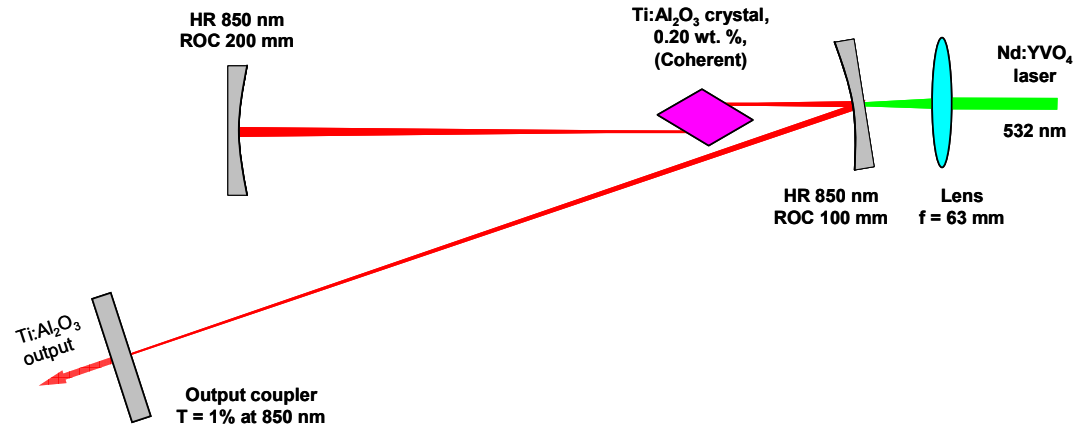

Fig. 2.5. 3-mirror resonator with Coherent crystal (4.6 mm long, 0.20 wt. % doping concentration) and Cr:LiSAF mirrors (HR: highly reflective mirror, ROC: radius of curvature, f: focal length).

The pump beam inside the resonator was characterised by recording a beam caustic with a knife-edge in place of the crystal. The measured beam profiles were non-gaussian and attempts to determine the beam widths by performing a Gaussian-fit yielded significant errors. For this reason, the clip level method was used to measure the beam widths. A clip level of 11.6 % was chosen according to [4]. A caustic was recorded in the horizontal and vertical planes, see

Fig. 2.6. The measured pump beam waist radii were w_{px} = 56 µm in the horizontal and w_{py} = 50 µm in the vertical plane in air. Given Ti:sapphire's refractive index of $n_{Ti:sapphire}$ = 1.77 at 532 nm, these correspond to w_{px} = 100 µm and w_{py} = 50 µm inside the crystal. The resonator folding mirror (radius of curvature ROC = 100 mm) acts as a plano-concave lens with a focal lengths of approximately f = -200 mm on the pump beam. The astigmatism apparent in

Fig. 2.6 is due to the pump beam's transmission through the resonator folding mirror at an angle of 9° (resonator folding angle = 18°). The beam propagation factor was calculated to be M_x^2 = 2.0 in the horizontal and M_y^2 = 1.5 in the vertical plane. Both values are slightly higher than the values for the pump laser focused by a single lens and with no other intervening optics (see section 2.1). This, as well as the non-gaussian beam profiles mentioned before, can be explained by the aberrations and multiple reflections introduced by the resonator folding mirror, which had an AR

coating for the red spectral region and transmitted only 66% of the pump power at 532 nm.

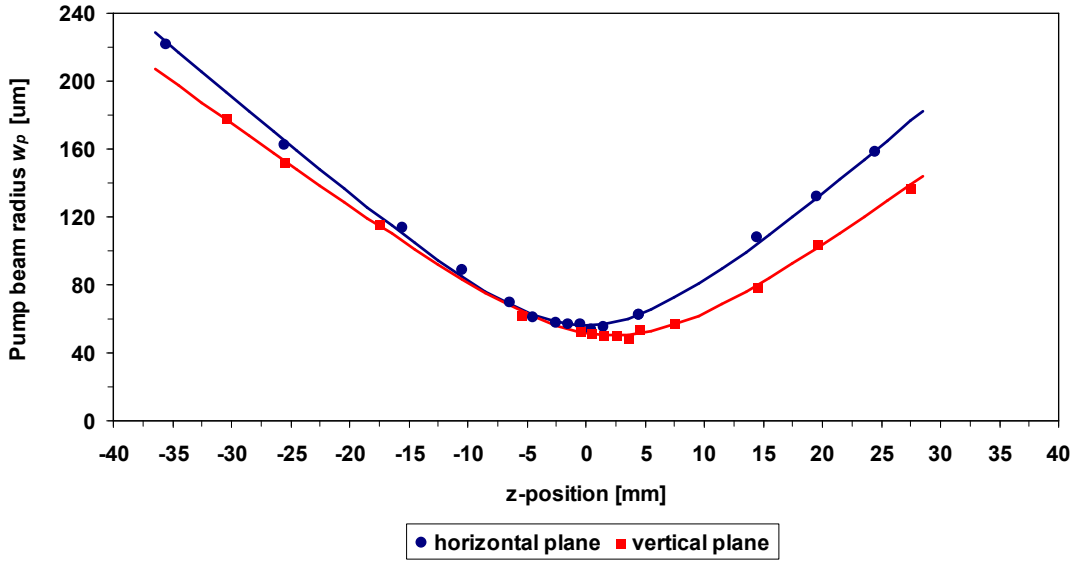

Fig. 2.6. Beam caustic of the pump beam inside the resonator.

2.2.3 Laser performance

The laser performance was optimised experimentally by varying the long arm length and alignment of the laser. By doing so, the mode overlap between resonator and pump modes was optimised. After careful alignment, a pump threshold of 1.42 W and a slope efficiency of 22% were measured with an output coupling of 1%, see Fig. 2.7. Laser emission occurred at 839 nm rather than at the peak of the stimulated emission cross-section spectrum in Ti:Sapphire (795 nm) because the Cr:LiSAF resonator mirrors had their high reflective band centred around 850 nm.

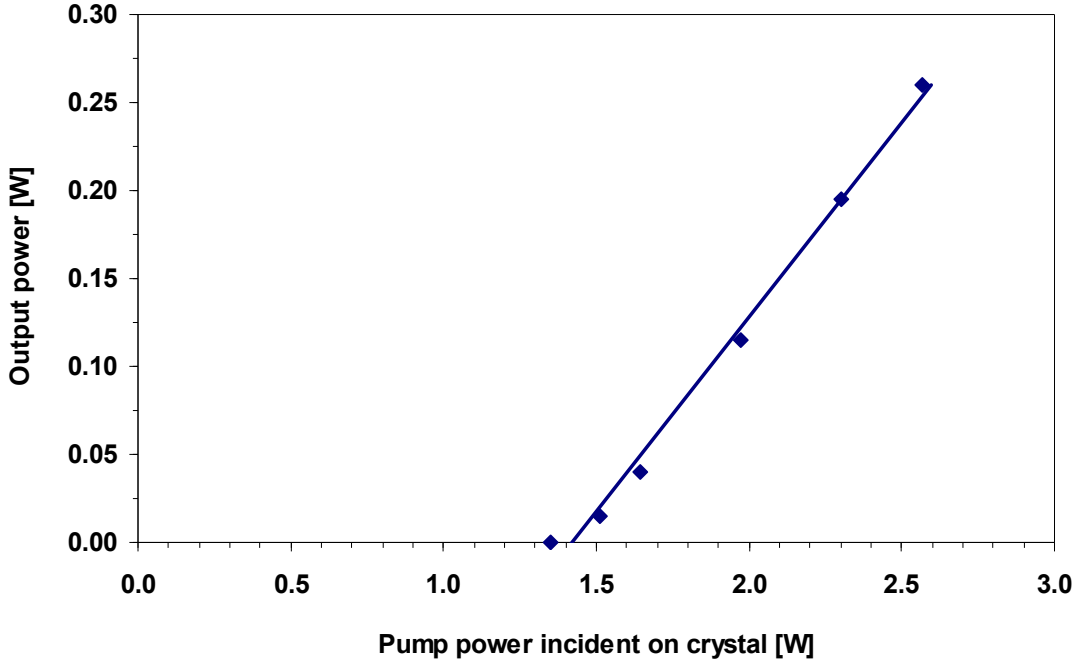

Fig. 2.7. Power transfer of the basic 3-mirror Ti:sapphire laser.

2.2.4 Discussion of results

The Watt-level pump threshold achieved at 532 nm with the crystal from Coherent Scotland Ltd. is similar to the thresholds of commercial systems. Taking into account the unfavourable emission wavelength of GaN diode lasers and their relatively low output powers, it is very unlikely that Ti:sapphire lasers with crystal and resonator specifications of the sort described in this section could be directly diode-laser pumped. Given the unsuitability of Ti:sapphire crystals used in current commercial systems, the required specification was explored using rate-equation-based modelling which is discussed in the next section.

2.3 Modelling a directly diode-laser-pumped Ti:sapphire laser

GaN diode lasers are commercially available with peak emission wavelengths between 370 nm and 490 nm, although by far the highest output powers are available from devices emitting around 450 nm – currently up to 1 W from a single emitter. Since the absorption cross-section of Ti:sapphire drops off sharply to the short wavelength side of the peak at 490 nm, the pump absorption is significantly lower at 450 nm than at the traditional green pump wavelengths of argon-ion (488, 497 or 515 nm) or frequency-doubled neodymium lasers (532 nm), as discussed in sections 1.2.1 and 1.3. Furthermore, GaN diodes have a low spatial brightness compared to the green pump lasers making it harder to maintain the pump intensities necessary to overcome Ti:sapphire's intrinsically high threshold over the length of a crystal. For these reasons, conventional Ti:sapphire laser designs, which have watt-level laser thresholds in the green (see section 2.2) are not suitable for blue diode pumping. The challenge is to develop a laser that achieves a very low laser threshold to allow pumping with the spectrally less well matched and spatially less bright GaN diode lasers.

To ascertain the optimum parameters for a laser meeting this challenge, extensive use of modelling has been made. The theoretical model introduced in chapter 1.4 [5] has been employed to calculate and optimize the pump threshold and slope efficiency. Based on rate-equation analysis, this model has been used to ascertain the optimum crystal doping level, crystal length, output coupler transmission, and mode waist sizes (pump and resonator) for a low-threshold longitudinally pumped cw laser.

2.3.1 Modelling the crystal choice

The choice of the best diode laser wavelength is a compromise between available output power and pump absorption at the diode’s emission wavelength. Similarly, the selection of the optimum crystal doping level and length is a compromise between pump absorption and parasitic losses. A higher doping concentration means higher pump absorption which allows the use of a shorter crystal. Since maintaining the

necessary pump intensity over a smaller distance is less demanding, it enables the use of spatially less bright pump sources. However, this is balanced by a higher parasitic absorption coefficient (lower figure of merit (FOM)) which increases the overall parasitic losses in the crystal despite its shorter length. Typically, Ti:sapphire crystals are commercially available with doping concentrations from 0.03 to 0.33 wt. % and figures of merit of 100 for 0.33 wt. %, 400 for 0.25 to 0.2 wt. %, and 500 for 0.15 to 0.03 wt. % [2, 3, 6-9].

To investigate the impact of parasitic crystal losses on the laser performance the output power of a number of resonator configurations and commercially available, low-loss Ti:sapphire crystals with different doping levels (0.33, 0.25, 0.20 and 0.15 wt. %) was calculated as a function of crystal lengths [10] (see Fig. 2.8). The pump power incident on the crystal was assumed to be 1 W at a wavelength of 450 nm. For these initial calculations aimed at determining the basic dependencies, nonastigmatic equations (chapter 1.4, equations 1.11-19) were used: the pump and resonator modes were assumed to be symmetric along the propagation axis with both mode waists located at the centre of the crystal. The beam propagation factor used was $M^2_p = 3.5$ for the pump mode (arithmetic mean of an assumed $M^2_{px} = 6$ and $M^2_{py} = 1$) and $M^2_r = 1.5$ for the resonator mode. Furthermore, the Ti:sapphire laser was assumed to oscillate at 795 nm, where the stimulated emission cross section of Ti:sapphire has its maximum. Intracavity losses through imperfect mirror coatings and Fresnel reflections at the crystal facets were estimated to be 0.1% per mirror bounce or crystal facet transit. With four passes through a crystal facet and three mirror bounces (output coupler not included) this loss amounts to a total of 0.7% per resonator round-trip. The remaining parameters – pump and resonator mode waist sizes, crystal length and output coupler transmission – were optimised for each configuration to give maximum laser output power. Since there is no analytical solution for the output power (see chapter 1.4, equations 1.11-18), multivariate optimisation was employed to optimise these parameters by using a conjugate gradient solver algorithm within the commercial software package MathCAD.

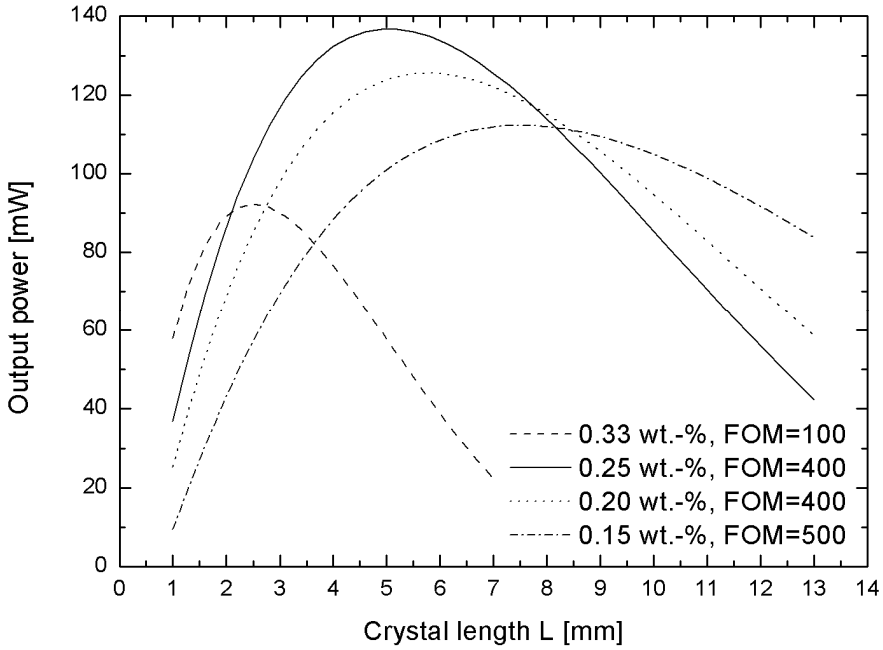

Fig. 2.8. Calculated output power for 1 W of incident pump power (λ_p = 450 nm) as a function of crystal length for various commercially available Ti:sapphire crystals. The resonator parameters (w_r: resonator waist radius, w_p: pump waist radius, T: output coupling) were optimized for each crystal: 0.33 wt. %, FOM = 100: w_r = 13 µm, w_p = 13 µm, T = 6.3%; 0.25 wt. %, FOM = 400: w_r = 20 µm, w_p = 18 µm, T = 3.6%; 0.20 wt. %, FOM = 400: w_r = 21 µm, w_p = 19 µm, T = 3.2%; 0.15 wt. %, FOM = 500: w_r = 23 µm, w_p = 22 µm, T = 2.6% [10].

This analysis shows that the best laser performance can be expected from a Ti:sapphire crystal with 0.25 wt. % doping concentration. In this case the maximum output power of 137 mW was predicted for a pump mode radius of w_p = 18 µm and a resonator mode waist radius of w_r = 20 µm, a crystal length of L = 5.0 mm and an output coupler transmission of T = 3.6%. For these parameters a pump threshold of 276 mW and a slope efficiency of 19% were calculated.

2.3.2 Low-parasitic-loss Ti:sapphire crystal

On the basis of the modeling results, a 5.2-mm-long, Brewster-cut Ti:sapphire crystal with 0.25 wt. % doping concentration and FOM ≥ 400 was procured (Saint-Gobain Crystals). This crystal provides a good compromise between the shorter crystal

lengths that can be used at higher doping levels and the increased loss per unit length (lower figure of merit) typically associated with such crystals.

The crystal's absorption was measured at the diode laser wavelengths of 445 nm and 452 nm, the Ar-Ion laser wavelengths of 458 nm, 477 nm, 488 nm, 497 nm, 502 nm and 515 nm as well as at the frequency-doubled Nd:YVO_4 laser wavelength of 532 nm. The power incident on the anti-reflection-coated lens (f = 60 mm, Reflectivity < 0.5% at 350 – 650 nm) used to focus the pump laser light into the crystal and the pump power transmitted by the crystal without the laser oscillating were both measured. Neglecting the reflection and scattering losses of the focusing lens, the absorption coefficients were calculated according to Beer's Law, see Fig. 2.9. Table 2.1 also shows the fraction of incident pump power absorbed in a single pass through the crystal.

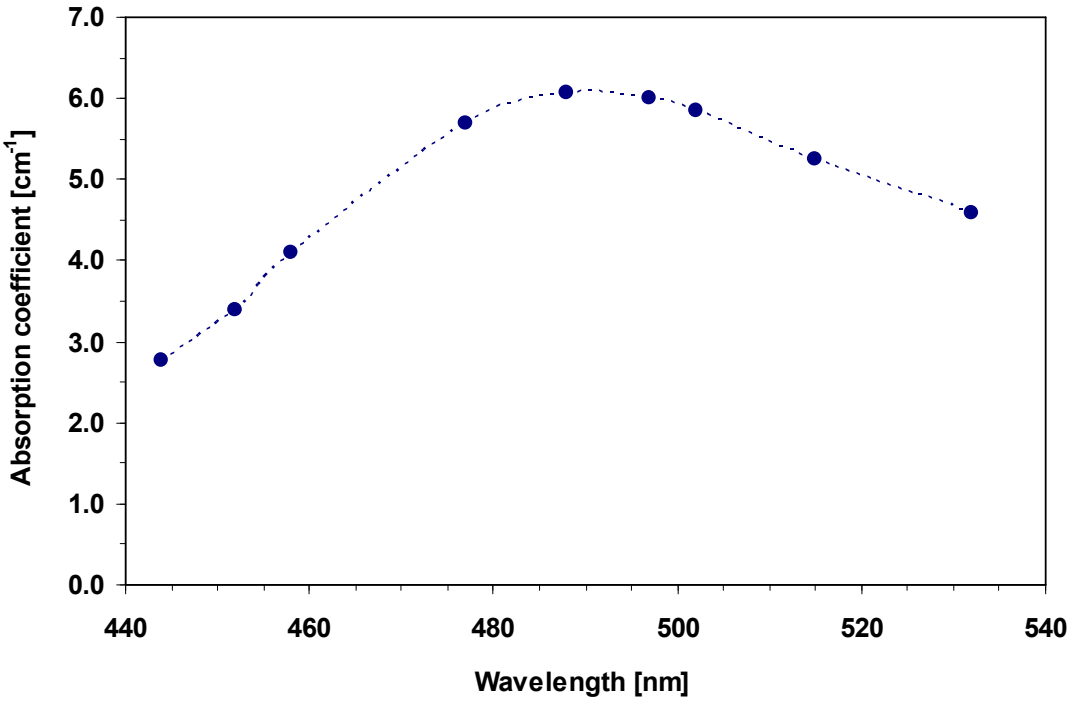

Fig. 2.9. Measured absorption coefficients at various wavelengths of the low parasitic loss crystal from Saint-Gobain Crystals.

Table 2.1. Absorption coefficients and fractions of incident pump power absorbed in a single pass through the low parasitic loss crystal from Saint-Gobain Crystals.

Wavelength [nm]	Absorption coefficient [cm^{-1}]	Single pass absorption [%]
445	2.8	76
452	3.4	83
458	4.1	88
477	5.7	95
488	6.1	96
497	6.0	96
502	5.8	95
515	5.3	93
532	4.6	91

2.4 A low-threshold Ti:sapphire laser

2.4.1 Modelling

In order to build a low-threshold resonator, the new low-parasitic-loss crystal and mirrors specifically designed for a diode-laser-pumped Ti:sapphire laser (HR 695 - 870 nm, HT 420 – 490 nm and AR 750 – 820 nm on the reverse side) were used. To help optimise the performance, the non-astigmatic rate-equation-based model introduced in section 2.3.1 was used to ascertain the best pump and resonator waist sizes and output coupling. Where necessary, the model parameters were changed: the pump laser wavelength was assumed to be 452 nm consistent with the emission wavelength of the diode laser introduced in section 2.1.2. The parameters of the Saint-Gobain crystal – crystal length = 5.2 mm, doping concentration = 0.25 wt. %, FOM = 400, measured absorption coefficient = 3.4 cm^{-1} at 452 nm – were used in the model. Overall resonator losses were assumed to be 2.1% per roundtrip with 0.7% due to imperfect mirror coatings and Fresnel reflections on the crystal facets and 1.4% due to parasitic absorption in the crystal, according to equation 1.1 in chapter 1.2.1. Based on previous measurements (see section 2.1.2), the beam propagation factor used was $M^2_p = 4.0$ for the pump mode (arithmetic mean of $M^2_{px} = 6.2$ and $M^2_{py} = 1.8$) and $M^2_r = 1.3$ for the resonator mode. With a pump power of 1.0 W incident on the crystal, the multivariate optimisation for maximum output power suggested a pump waist radius of $w_{p0} = 21$ μm, a resonator waist radius of

$w_{r0} = 24$ µm and an output coupling of 4%. In this case, a pump threshold of 295 mW, a slope efficiency of 24% and a maximum output power of 171 mW were predicted.

2.4.2 Resonator setup

ABCD matrix calculations of the mode radii resulting from the resonator and pump optics used were made with the commercial software Winlase. This resulted in the resonator design shown in Fig. 2.10. The folding angle of the resonator was chosen to eliminate astigmatism in the Ti:sapphire laser output beam which, as in any folded resonator, results in astigmatism within the crystal [11]. Furthermore the Brewster-cut of the crystal introduces astigmatism. The calculated resonator waist sizes and locations within the crystal therefore differ substantially from the simplified assumptions used in the non-astigmatic model ($w_{rx0} = w_{ry0}$, $z_{ry0} = 2.6$ mm). Instead the resonator waist radii and locations are $w_{rx0} = 32$ µm at $z_{rx0} = 3.5$ mm in the horizontal plane and $w_{ry0} = 19$ µm at $z_{ry0} = 1.1$ mm in the vertical plane.

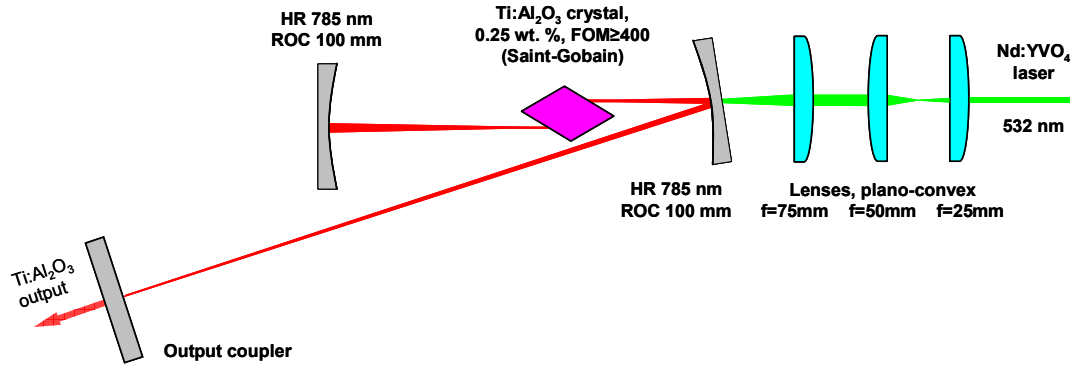

Fig. 2.10. 3-mirror resonator with low parasitic loss Ti:sapphire crystal.

2.4.3 Laser performance with 532 nm pump

In order to align and evaluate the resonator the frequency-doubled Nd:YVO_4 laser was used as pump source before moving on to diode pumping, as shown in Fig. 2.10. With a two-element Keplerian telescope (f = 25 mm and f = 50 mm) in front of the

focussing lens (f = 75 mm), pump waist radii of w_{px0} = 32 µm and w_{py0} = 15 µm were calculated. After careful alignment, a pump threshold of 106 mW and a slope efficiency of 16% were obtained with a T_{oc} = 0.5% output coupling. The power transfers with output couplings of Toc = 1, 2, 3, and 5% were also recorded (see Fig. 2.11 and Table 2.2). Although the design parameters of this laser were chosen to allow efficient operation with a 452 nm GaN diode laser pump, the performance when pumped at 532 nm was comparable with low-threshold cw Ti:sapphire lasers optimized for argon-ion or frequency-doubled neodymium laser pumping [12-15].

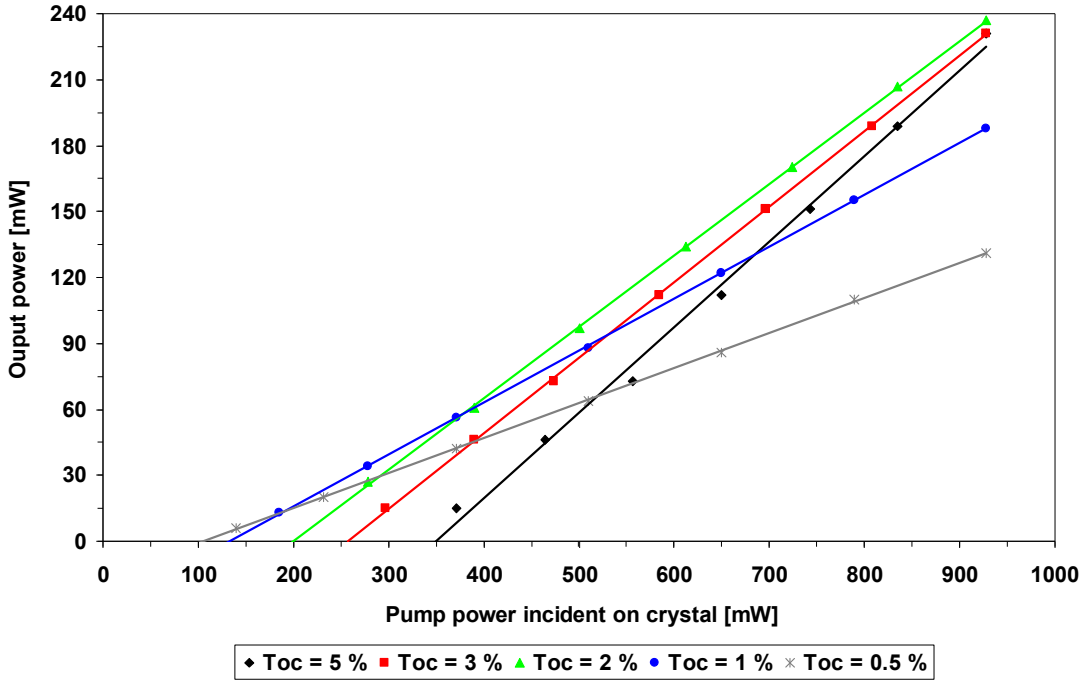

Fig. 2.11. Power transfer measurements of the low-threshold Ti:sapphire laser with various output couplings pumped at 532 nm.

Table 2.2. Performance of the low-threshold Ti:sapphire laser with various output couplings pumped at 532 nm.

Output coupling [%]	Pump threshold [mW]	Slope efficiency [%]
0.5	106	15.9
1	134	23.6
2	200	32.5
3	256	34.3
5	337	36.8

Based on these measurements, Findlay-Clay [16] and Caird [17] analyses of the resonator losses were performed. Resulting in round-trip losses of 1.4% for the Findlay-Clay method and 0.9% for the Caird method, see Fig. 2.12 and Fig. 2.13.

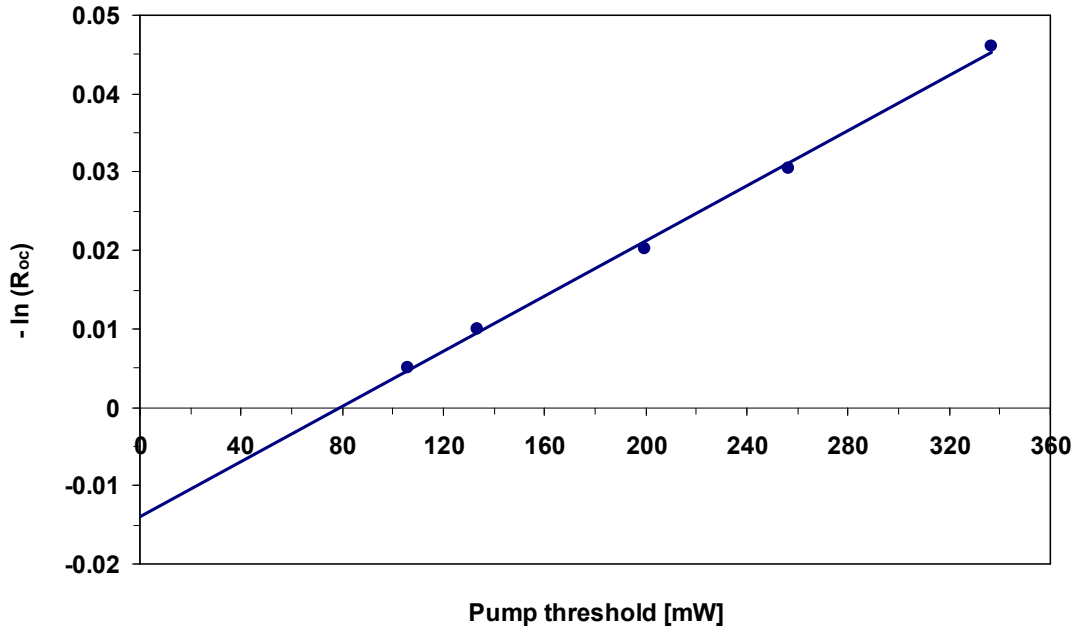

Fig. 2.12. Findlay-Clay plot of the low-threshold Ti:sapphire laser pumped at 532 nm.

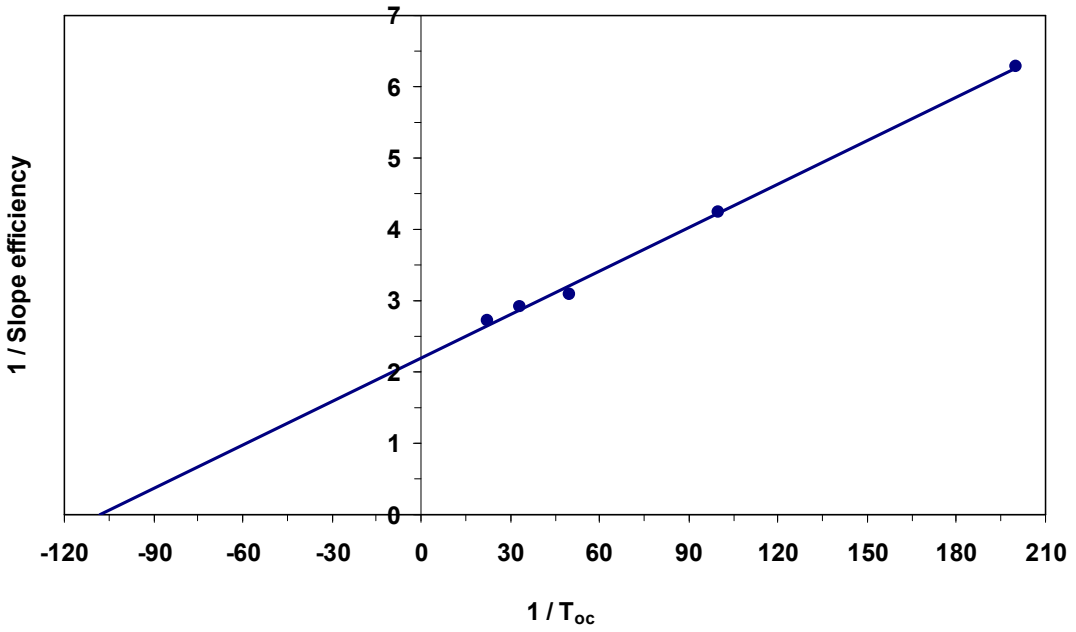

Fig. 2.13. Caird plot of the low-threshold Ti:sapphire laser pumped at 532 nm.

2.4.4 Laser performance with 452 nm pump

After evaluating the performance of the low-threshold Ti:sapphire laser with the frequency-doubled Nd:YVO_4 laser, the switch to diode-laser pumping was made. To allow an easy transition between the two pump regimes, a dichroic mirror (Chroma Technology Corp. z488bcm-xr) was used to combine both pump beams. The dichroic mirror was highly reflective for wavelengths below 500 nm and transmissive for wavelengths above 520 nm. Pump optics calculations led to a setup consisting of a cylindrical, Galilean telescope (f_x = -25.4 mm and f_x = 250 mm) to shape the diode laser beam in the horizontal plane and a spherical focusing lens of f = 75 mm focal length. As a result diode laser pump waist radii of $w_{px0} = 26$ µm and $w_{py0} = 12$ µm were predicted. (N.B. Some lensing in the thin dichroic beamsplitter resulting from mechanical stress induced by the lens mount was subsequently identified which caused the actual pump waist sizes to be much larger than the calculated values.)

The Ti:sapphire laser performance was measured for output couplings of T_{oc} = 0.5, 1, and 2% (see Table 2.3 and Fig. 2.14). This represents the first demonstration of a directly diode-laser-pumped Ti:sapphire laser [10]. Laser oscillation could not be achieved with higher output couplings.

Table 2.3. Performance of the low-threshold Ti:sapphire laser with various output couplings pumped at 452 nm.

Output coupling [%]	Pump threshold [mW]	Slope efficiency [%]	Output wavelength [nm]
0.5	483	3.4	770
1	572	5.4	783
2	796	6.5	770

The diode laser pump was attenuated by adjusting the electric current of the diode, which also changes the beam parameters of the diode laser. This, and the fact that data is only available for three different output couplings means that these measurements cannot be used for a reliable resonator loss analysis.

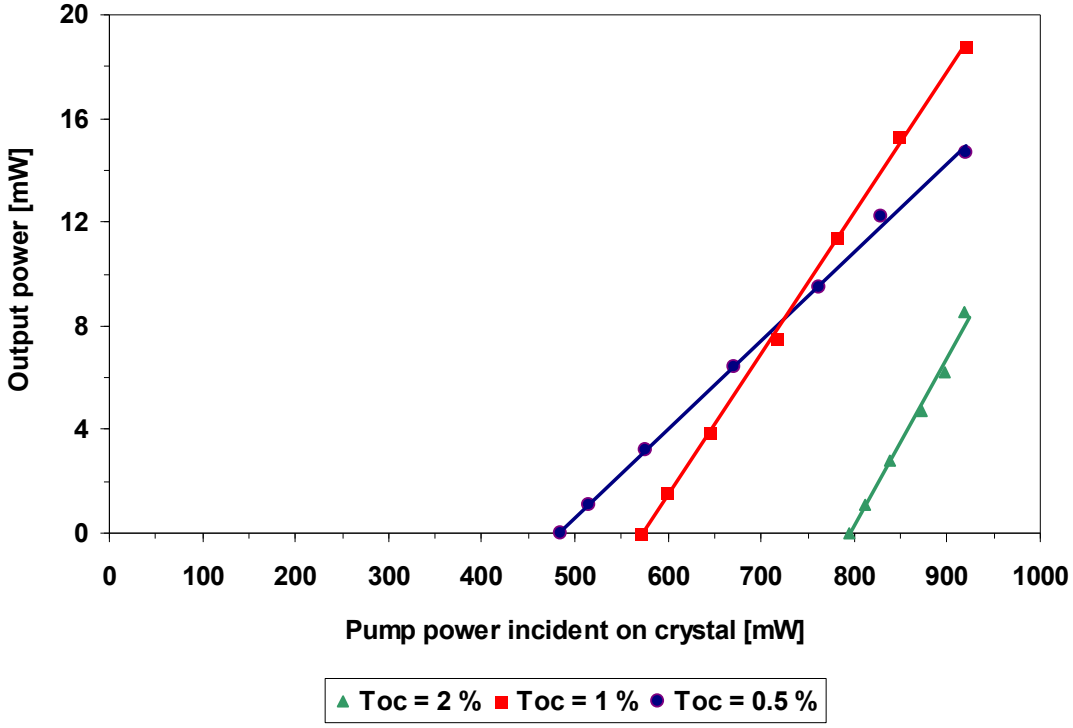

Fig. 2.14. Power transfer measurements of the low-threshold Ti:sapphire laser with various output couplings pumped at 452 nm.

2.4.5 Discussion of results

Despite the very low thresholds achieved under 532 nm pumping, the maximum output power under GaN diode-laser pumping was only 19 mW (at 783 nm with T_{oc} = 1%), a mere fraction of the 171 mW predicted by the modelling (see 2.4.1). There are a number of reasons for this: first, the additional lensing introduced by the dichroic mirror resulted in pump waist sizes much larger than those suggested by the modelling; second, the non-astigmatic model was to simplistic, failing to account for astigmatism it lead to a non-ideal overlap between pump and resonator modes; and third, there is a pump-induced loss and a reduction in pump quantum efficiency present at pump wavelengths below 458 nm. The latter is the dominating effect and will be discussed in more detail in chapter 4.

2.5 Improved low-threshold Ti:sapphire laser pumped at 532 nm

2.5.1 Modelling and optimisation of resonator and pump optics

To accurately model and optimise the laser performance the astigmatism of the pump and resonator modes needs to be taken into account. Accordingly the astigmatic equations provided by Alfrey [18] (chapter 1.4, equations 1.2-10) were used for all further modelling. The Ti:sapphire laser was assumed to oscillate at 795 nm, where the stimulated emission cross section of Ti:sapphire has its maximum. Based on previous measurements (Chapter 2.1.1) the assumption for the beam propagation factors were $M^2_{px} = 1.8$ and $M^2_{py} = 1.2$ for the pump mode and $M^2_{rx/y} = 1.3$ for the resonator mode. The pump power incident on the crystal was assumed to be 1.0 W at a wavelength of 532 nm. Intracavity losses through imperfect mirror coatings and Fresnel reflections on the crystal facets were estimated to be 0.35% per round-trip. As a result the overall roundtrip resonator loss is assumed to be 1.7% with 1.4% due to parasitic absorption in the crystal. The pump absorption coefficient was measured to be $\alpha_p = 4.6\ cm^{-1}$ at 532 nm. To assess the pump and resonator waist locations inside the crystal, the rate-equation model was coupled with ABCD matrix calculations of the resonator and pump modes (using commercial software: Winlase). The remaining parameters – pump and resonator mode waist sizes and output coupler transmission – were optimised to give maximum laser output power.

The optimisation procedure predicted that maximum output power would be achieved with pump waist radii of $w_{px0} = 16$ µm, $w_{py0} = 12$ µm, resonator waist radii of $w_{rx0} = 25$ µm, $w_{ry0} = 14$ µm and an output coupling of $T_{oc} = 6\%$. ABCD matrix calculations aimed at delivering these mode radii resulted in the resonator design shown in Fig. 2.15.

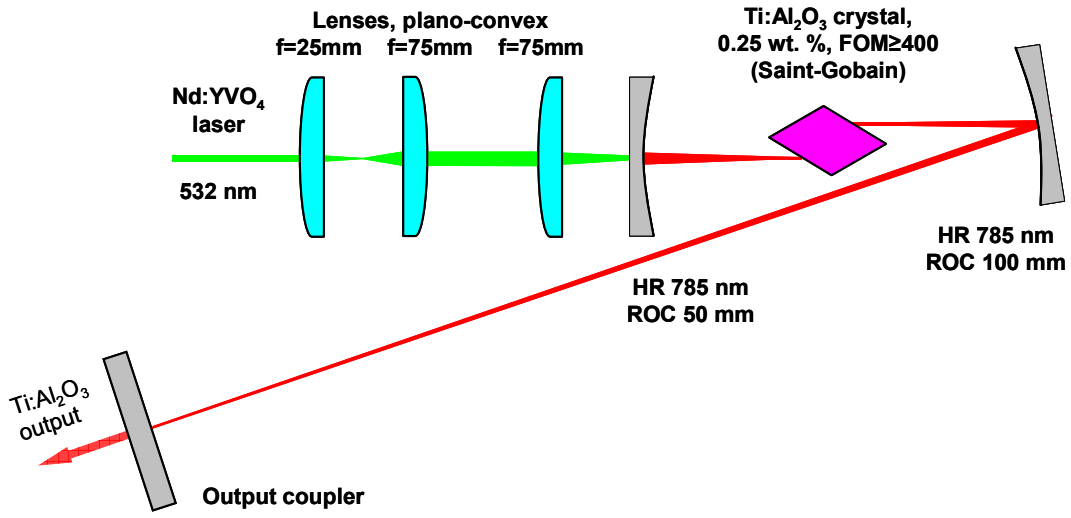

Fig. 2.15. Improved 3-mirror resonator with low-parasitic-loss Ti:sapphire crystal for pumping at 532 nm.

This resonator design results in waist radii of w_{rx0} = 26 µm and w_{ry0} = 14 µm at z_{rx0} = 3.9 mm and z_{ry0} = 1.3 mm which are very close to those suggested by the model. Calculations of the pump optics led to the selection of a setup consisting of a Keplerian telescope (f = 25mm and f = 75 mm) and a focusing lens of f = 75 mm focal length. As a result, pump waist radii of w_{px0} = 23 µm and w_{py0} = 10 µm at z_{px0} = 4.0 mm and z_{py0} = 1.1 mm were predicted. While resonator and pump waist locations are well matched, the pump waist radii are not an ideal fit to the values suggested by the model. However, a better fit would have required the use of an additional cylindrical telescope to reshape the pump beam of the frequency-doubled Nd:YVO_4 laser, adding unwanted complexity to the experimental set-up.

2.5.2 Laser performance

After careful optimization, a pump threshold of 67 mW and a slope efficiency of 16% were achieved with a T_{oc} = 0.5% output coupler at a laser wavelength of 791 nm. While the Ti:sapphire crystal and resonator parameters were optimised for GaN diode laser pumping at 450 nm, the laser's pump threshold at 532 nm is a significantly better than a range of cw Ti:sapphire lasers which have been

specifically optimised for low-threshold pumping at 532 nm or 514 nm [12-15]. So far, the lowest threshold for such a system, to my knowledge, was reported by Harrison et al. [13] at 90 mW with a slope efficiency of 6% and output coupling of 0.4%. The laser performance with output couplings of T_{oc} = 1, 2, 3 and 5% was also recorded (see Fig. 2.16 and Table 2.4).

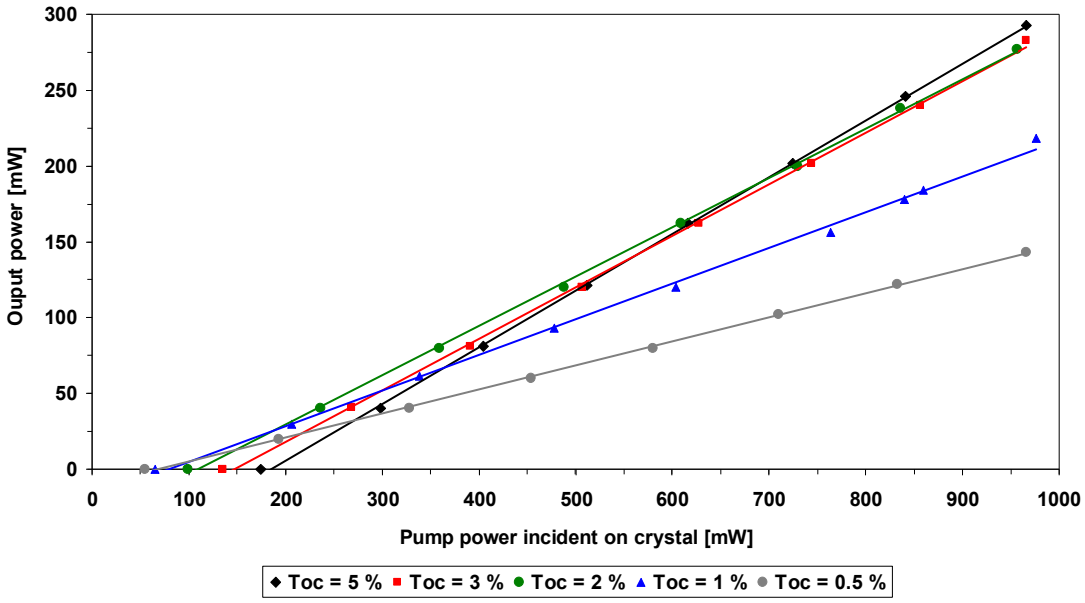

Fig. 2.16. Power transfer measurements of the improved low-threshold Ti:sapphire laser with various output couplings pumped at 532 nm.

Table 2.4. Performance of the improved low-threshold Ti:sapphire laser with various output couplings pumped at 532 nm.

Output coupling [%]	Pump threshold [mW]	Slope efficiency [%]	Output wavelength [nm]
5	185	37.4	807
3	147	34.0	812
2	110	32.6	781
1	79	23.5	777
0.5	67	15.8	791

Based on these measurements, Findlay-Clay [16] and Caird [17] analyses of the resonator losses were performed. These give round-trip loss of 1.2% for the Findlay-Clay method (see Fig. 2.17) and 1.1% for the Caird method (see Fig. 2.18). The

roundtrip loss values calculated are 30 – 35% lower than the value of 1.7% assumed in the model suggesting a higher crystal FOM and/or lower mirror and Fresnel losses.

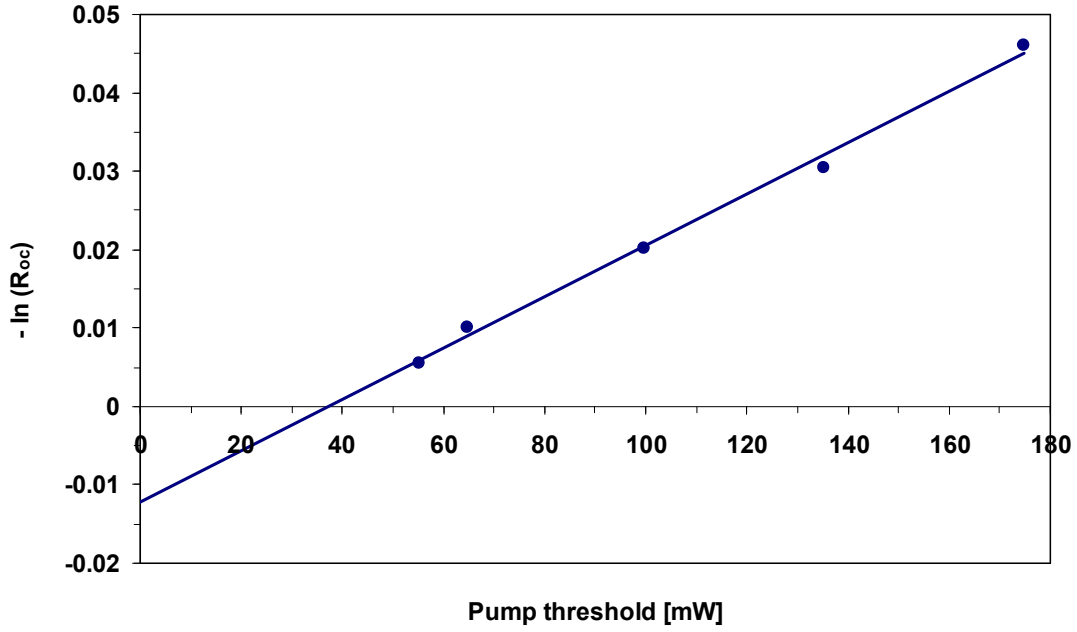

Fig. 2.17. Findlay-Clay plot of the improved low-threshold Ti:sapphire laser pumped at 532 nm.

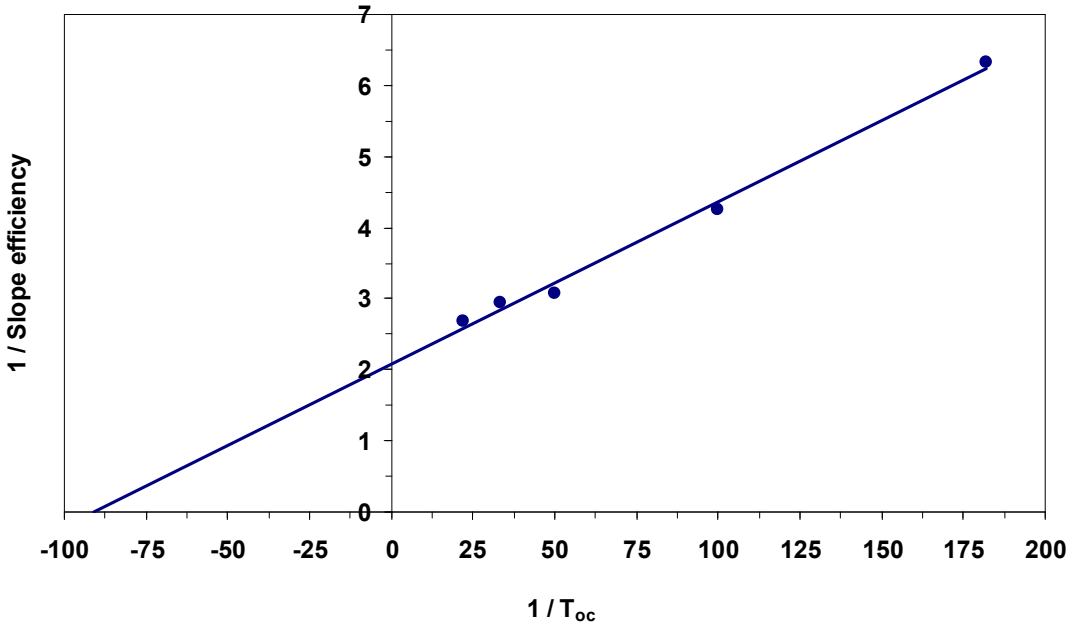

Fig. 2.18. Caird plot of the improved low-threshold Ti:sapphire laser pumped at 532 nm.

The calculations of the pump optics setup were based on previous measurements of the laser beam characteristics. To check whether the chosen setup achieves the calculated mode radii, the crystal was removed from the resonator and replaced by a knife-edge rotating-drum beam profiler (Coherent Inc. BeamMaster) to measure the pump waist radii. The results (w_{px0} = 11 µm and w_{py0} = 8 µm in air which, given $n_{Ti:sapphire}$ = 1.76, corresponds to w_{px0} = 19 µm and w_{py0} = 8 µm inside the crystal) agree reasonably well with the calculations.

2.5.3 Discussion of results

The modelling in 2.5.1 suggested a pump threshold of 183 mW, a slope efficiency of 40% and a maximum output power of 350 mW for 1.0 W of pump power incident on the crystal with 6% output coupling. A pump threshold of 53 mW is calculated for 0.5% output coupler. The measured laser thresholds are about 25% higher than the model suggestions, which might be due to the non-ideal fit of the pump waist radii (see 2.5.1).

2.6 Improved low-threshold Ti:sapphire laser pumped at 452 nm

2.6.1 Modelling and optimisation of resonator and pump optics

The performance of the diode-pumped Ti:sapphire laser was modelled in a fashion similar to the system pumped by the frequency-doubled Nd:YVO_4 laser discussed in section 2.5.1. Where necessary, the model parameters were changed as discussed below. The beam propagation factors used were M^2_{px} = 6.2 and M^2_{py} = 1.8 for the pump mode, based on previous measurements (Chapter 2.1.2), and $M^2_{rx/y}$ = 1.3 for the resonator mode. Resonator losses were increased by an additional 1.4% per roundtrip to take into account the pump-induced loss present under diode-pumping (see chapter 4.3), giving a combined resonator roundtrip loss of 3.1%.

The pump absorption coefficient was measured to be $\alpha_p = 3.4\ cm^{-1}$ at a wavelength of 452 nm. The pump power incident on the crystal was assumed to be 1.0 W. Multivariate optimisation of the remaining parameters for maximum output power suggested pump waist radii of $w_{px0} = 34$ µm, $w_{py0} = 12$ µm at $z_{px0} = 4.0$ mm, $z_{py0} = 1.2$ mm, resonator waist radii of $w_{rx0} = 30$ µm, $w_{ry0} = 17$ µm at $z_{rx0} = 4.0$ mm, $z_{ry0} = 1.2$ mm and an output coupling of 4.2%. ABCD matrix calculations of resonator and pump optics coupled to this model resulted in the design shown in Fig. 2.19.

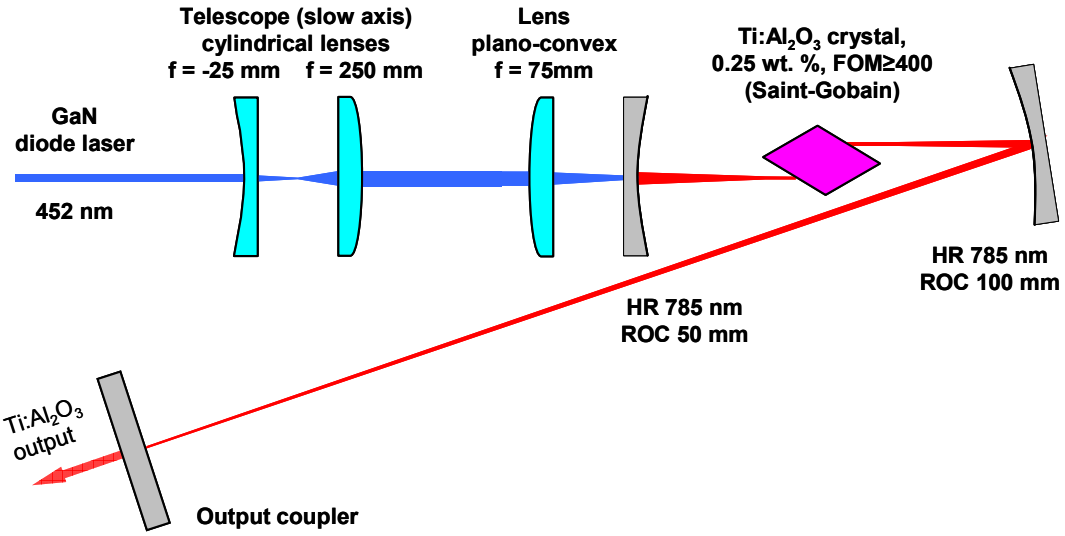

Fig. 2.19. Improved 3-mirror resonator with low parasitic loss Ti:sapphire crystal for pumping at 452 nm.

It gives resonator waist sizes identical to the model suggestions ($w_{rx0} = 30$ µm, $w_{ry0} = 17$ µm) at well matched waist locations of $z_{rx0} = 4.0$ mm in the horizontal and $z_{ry0} = 1.3$ mm in the vertical plane. Pump optics calculations led to a setup consisting of a cylindrical, Galilean telescope (f_x = -25.4 mm and f_x = 250 mm) to shape the diode laser beam in the horizontal plane and a spherical focusing lens of f = 75 mm focal length. As a result pump waist radii of $w_{px0} = 31$ µm and $w_{py0} = 18$ µm at $z_{px0} = 4.0$ mm and $z_{py0} = 1.0$ mm were predicted.

2.6.2 Laser performance

After careful optimization, a pump threshold of 540 mW and a slope efficiency of 7% were achieved with 1% output coupling at a laser wavelength of 777 nm (see Fig. 2.20). The maximum output power was 24 mW. This represents a significant performance improvement over the previous design (pump threshold 572 mW, slope efficiency 5%, maximum output power 19 mW at 783 nm with 1% output coupling, see section 2.4.4).

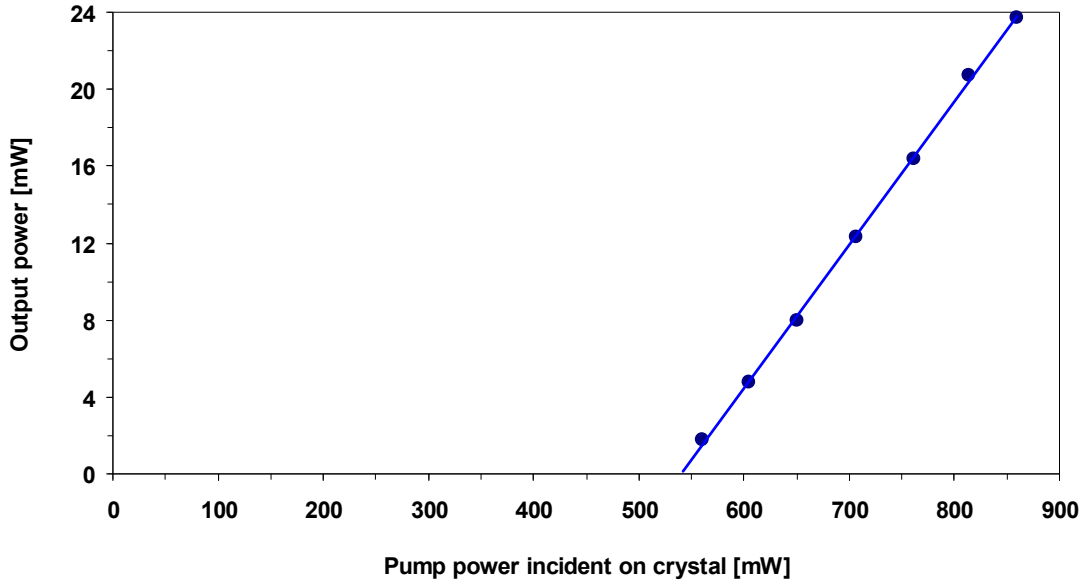

Fig. 2.20. Power transfer of the diode-laser pumped Ti:sapphire laser with T_{oc} = 1%.

2.6.3 Pump beam characterisation

The calculations of the setup of the pump optics were based on previous measurements of the laser beam characteristics. To check whether the chosen setup achieves the calculated performance, the crystal was removed from the resonator and replaced by a knife-edge rotating-drum beam profiler (Coherent Inc. BeamMaster) to record the pump beam caustic, see Fig. 2.21. The measured pump beam waist radii were w_{px0} = 20 µm in the horizontal and w_{py0} = 17 µm in the vertical plane in air which corresponds to w_{px0} = 35 µm and w_{py0} = 17 µm inside the crystal. These values are in line with the calculated waist radii presented in section 2.6.1. The beam

propagation parameters were calculated to be $M_x^2 = 6.5$ in the horizontal and $M_y^2 = 1.6$ in the vertical plane which agrees with previous measurements, see section 2.1.2. The pump transmission of the AR-coated resonator end mirror was measured to be 99% at 452 nm.

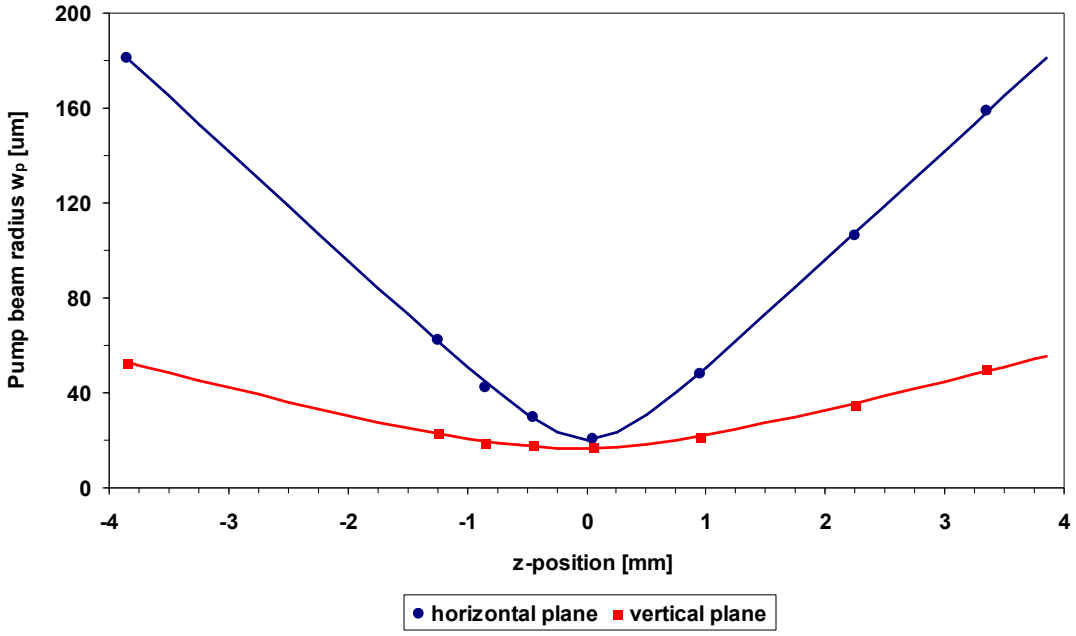

Fig. 2.21. Pump beam caustic for the 450nm diode laser at the focus within the laser resonator shown in Error! Reference source not found.**.**

2.6.4 Discussion of results

The modelling in section 2.6.1 suggested a pump threshold of 377 mW, a slope efficiency of 20% and a maximum output power of 127 mW for 1.0 W of pump power incident on the crystal with 4.2% output coupling. A pump threshold of 186 mW is calculated for 0.5% output coupling. While the modelling gave a fair indication of the laser performance under 532 nm pumping the measured output powers under GaN diode laser pumping are only a fraction of the values suggested by the model. This is despite accounting for the pump-induced loss in the model. It indicates that the reduction in pump quantum efficiency is the dominating factor for the performance deterioration under diode-laser pumping. Chapters 4.4 and 4.5 will investigate this effect.

2.7 Conclusions

Laser architectures suitable for pumping of Ti:sapphire with GaN laser diodes have been identified through rate-equation based modelling. A 3-mirror resonator with a highly doped, low-parasitic-loss crystal (doping concentration = 0.25 wt. %, FOM = 400) achieved thresholds as low as 67 mW have for pumping at 532 nm.

Direct diode laser pumping of Ti:sapphire has been demonstrated, using a single 1.0 W GaN laser diode emittting at 452 nm. The output power was 24 mW, with a slope efficiency of 7% and a threshold of 540 mW. The results shown in this chapter represent the first demonstration of a directly diode-laser-pumped Ti:sapphire laser.

The previous hurdles to such a demonstration have been overcome in part by the improvement in GaN diode lasers but importantly also via a resonator design and choice of crystal specifications informed by detailed modelling. Ti:sapphire lasers with resonator and crystal specifications of the sort that are typically used in commercial lasers were demonstrated to be unsuitable for diode-laser pumping.

The output power of the directly diode-pumped laser is lower than might have at first been expected from this modelling – this is due to pump-induced losses in the crystal and a reduction in pump quantum efficiency at short pump wavelengths, a phenomenon that is explored in more detail in chapter 4. Nevertheless it was possible to increase the cw laser output power further which will be reported in chapter 3 alongside the mode locking of a directly diode-laser pumped Ti:sapphire laser.

2.8 References

1. "Laser Diode" (Nichia Corp.), retrieved 03 October, 2011, http://www.nichia.co.jp/en/product/laser_main.html.
2. "Ti:Sapphire" (EKSMA Optics), retrieved 30 September, 2011, http://www.eksmaoptics.com/repository/catalogue/pdfai/NLOC/laser crystals/ti_sapphire.pdf.
3. "Titanium -Doped Sapphire Laser Crystals" (Saint-Gobain Crystals), retrieved 20 December, 2007, http://www.photonic.saint-gobain.com.
4. A. E. Siegman, M. W. Sasnett, and T. F. Johnston, "Choice of Clip Levels for Beam Width Measurements Using Knife-Edge Techniques," IEEE J. Quantum Electron. **27**, 1098-1104 (1991).
5. A. J. Alfrey, "Modeling of Longitudinally Pumped CW Ti:Sapphire Laser Oscillators," IEEE J. Quantum Electron. **25**, 760-766 (1989).
6. "Ti:Sapphire Laser Crystals" (Roditi International Corporation Ltd), retrieved 30 September, 2011, http://www.roditi.com/Laser/Ti_Sapphire.html.
7. "Titanium doped Sapphire" (Moltech GmbH), retrieved 30 September, 2011, http://www.mt-berlin.com/frames_cryst/crystals_frameset1.htm.
8. "Titanium Doped Sapphire Crystal" (GWU-Lasertechnik Vertriebsges. mbH), retrieved 30 September, 2011, http://www.gwu-group.com/cmslaser/dmdocuments/castech_tisa.pdf.
9. "Ti:Sapphire Crystal" (Red Optronics), retrieved 30 September, 2011, http://www.redoptronics.com/Ti-Sapphire-crystal.html.
10. P. W. Roth, A. J. Maclean, D. Burns, and A. J. Kemp, "Directly diode-laser-pumped Ti:sapphire laser," Opt. Lett. **34**, 3334-3336 (2009).
11. H. W. Kogelnik, C. V. Shank, A. Dienes, and E. P. Ippen, "Astigmatically Compensated Cavities for Cw Dye Lasers," IEEE J. Quantum Electron. **QE 8**, 373-& (1972).
12. P. Albers, E. Stark, and G. Huber, "Continuous-wave laser operation and quantum efficiency of titanium-doped sapphire," J. Opt. Soc. Am. B **3**, 134-139 (1986).

13. J. Harrison, A. Finch, D. M. Rines, G. A. Rines, and P. F. Moulton, "Low-Threshold, Cw, All-Solid-State Ti-Al2o3 Laser," Opt. Lett. **16**, 581-583 (1991).
14. J. F. Pinto, L. Esterowitz, G. H. Rosenblatt, M. Kokta, and D. Peressini, "Improved Ti:Sapphire Laser Performance with New High Figure of Merit Crystals," IEEE J. Quantum Electron. **30**, 2612-2616 (1994).
15. A. J. Tiffany, I. T. McKinnie, and D. M. Warrington, "Low-threshold, single-frequency, coupled cavity Ti:Sapphire laser," Appl. Optics **36**, 4989-4992 (1997).
16. D. Findlay and R. A. Clay, "The measurement of internal losses in 4-level lasers," Physics Letters **20**, 277-278 (1966).
17. J. A. Caird, S. A. Payne, P. R. Staver, A. J. Ramponi, L. L. Chase, and W. F. Krupke, "Quantum Electronic-Properties of the $Na_3Ga_2Li_3F_{12}:Cr^{3+}$ Laser," IEEE J. Quantum Electron. **24**, 1077-1099 (1988).
18. A. J. Alfrey, "Modeling of Longitudinally Pumped CW Ti- Sapphire Laser-Oscillators," IEEE J. Quantum Electron. **25**, 760-766 (1989).

3 Direct diode-laser pumping of mode-locked Ti:sapphire lasers

3 Direct diode-laser pumping of mode-locked Ti:sapphire lasers

In this chapter, direct diode-laser pumping of a mode-locked Ti:sapphire laser is reported. Based on a four-mirror resonator, this Ti:sapphire laser is passively mode-locked by a saturable Bragg reflector (SBR). The chapter starts with modelling to ascertain the pump optics and resonator parameters for optimum performance. A Ti:sapphire laser following these specifications is then characterised in cw operation under conventional and GaN diode-laser pumping. Mode-locked operation under both pump regimes is subsequently demonstrated. Double-sided diode-laser pumping to increase the output power is then described. All pump thresholds and slope efficiencies are given with respect to pump power incident on the crystal.

3.1 Modelling

To design a mode-locked Ti:sapphire laser suitable for diode-laser pumping the astigmatic rate-equation-based model (see chapter 1.4) introduced in the chapter 2 (sections 2.5.1 and 2.6.1) was employed again. Where necessary, the model parameters were changed as discussed below. Because an SBR is used for mode-locking, the Ti:sapphire laser is based on an asymmetric four-mirror resonator to allow for both a tight focus on the SBR in one resonator arm, and the inclusion of a prism pair for dispersion compensation in a second arm where the mode is near-collimated. In chapter 2, the round-trip loss of a three mirror resonator pumped at 532 nm was measured to be around 1.2% (see 2.5.2) – significantly lower than the 1.7% estimated in the previous model (see 2.5.1). However, additional losses due to Fresnel reflections on the prism facets and an additional mirror had to be taken into account here. The associated losses were estimated to be 0.2% per round-trip. Therefore the 4-mirror resonator's round-trip loss was assumed to be 1.4% at 532 nm pumping. For diode-laser pumping at 452 nm an additional 1.3% of pump-induced loss (see chapter 4.2 and 4.3) was added resulting in a round-trip loss of 2.7%. As

before, the rate-equation-based model was coupled with ABCD-matrix calculations of the resonator and pump waist locations inside the crystal. Multivariate optimisation for maximum output power suggested the pump and resonator parameters shown in Table 3.1. The predicted performance – pump threshold and slope efficiency – of a Ti:sapphire laser with these parameters is included in Table 3.1.

Table 3.1. Pump and resonator parameters suggested by the modelling and predicted performance.

	λ_p = 452 nm	λ_p = 532 nm
w_{cx0} [µm]	32	25
w_{cy0} [µm]	18	14
w_{px0} [µm]	28	16
w_{py0} [µm]	13	12
T [%]	4.5	5.9
P_{th} [mW]	332	183
η [%]	24	40

The design of the resonator and pump optics used to achieve these parameters are discussed separately for both pump wavelengths in the following sections.

3.2 Cw operation: conventionally pumped Ti:sapphire laser

3.2.1 Resonator and pump optics

To find a resonator and pump optics design which meets the parameters suggested by the modelling (see section 3.1), ABCD-matrix calculations of the resonator and pump mode radii were made with the commercial software Winlase. The resulting design for pumping at 532 nm, an asymmetric, Z-folded 4-mirror Ti:sapphire laser, is shown in Fig. 3.1 and gives resonator waist radii of w_{cx0} = 24 µm at z_{cx0} = 2.6 mm in the horizontal plane and w_{cy0} = 14 µm at z_{cy0} = 2.3 mm in the vertical plane. The resonator includes two fused-silica prisms for dispersion compensation in mode-

locked operation and a slit for adjusting the oscillation wavelength and bandwidth. The angles of the two resonator folding mirrors were chosen to eliminate astigmatism in the Ti:sapphire laser output beam. The folding (full) angles were 11.5° for the short arm and 13.9° for the long arm of the resonator.

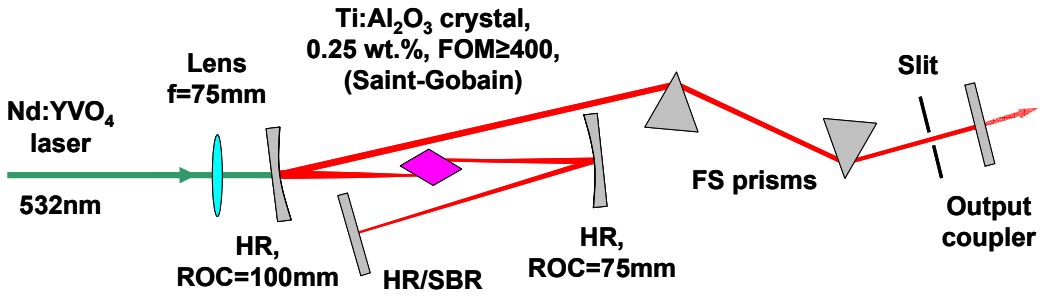

Fig. 3.1. Asymmetric, Z-folded 4-mirror resonator for conventional pumping (532 nm).

The pump optics, consisting of a two-element Keplerian telescope (f = 25 mm and f = 75 mm) and a spherical focusing lens (f = 75 mm), focus the output of the frequency-doubled Nd:YVO_4 laser into the crystal with calculated pump waist radii of $w_{px0} = 20$ µm at $z_{px0} = 4.4$ mm in the horizontal plane and $w_{py0} = 9$ µm at $z_{py0} = 1.0$ mm in the vertical plane. While the resonator waist radii are very well matched to the values suggested by the modelling (compare Table 3.1), the pump waist radii are not an ideal fit. Furthermore, the pump and resonator waist locations are about 1.5 mm apart in both planes. However, a better fit would have required the use of an additional cylindrical telescope to reshape the pump beam of the frequency-doubled Nd:YVO_4 laser, adding unwanted complexity to the experimental setup.

3.2.2 Laser performance

After the resonator and pump optics were set up according to the calculated design, the Ti:sapphire laser was characterised under conventional pumping (532 nm). The performance was recorded with output couplings of $T_{oc} = 0.5$, 1, 2, 3, and 5% and the oscillation wavelength adjusted to around 800 nm (see Fig. 3.2 and Table 3.2). A pump threshold of 60 mW and a slope efficiency of 15% was obtained with an output

coupling of T_{oc} = 0.5% [1]. Replacing the output coupler with a HR mirror resulted in a pump threshold of 44 mW. Although the Ti:sapphire crystal parameters were optimised for GaN diode-laser pumping, the cw pump threshold at 532 nm is, to my knowledge, the lowest yet reported for a Ti:sapphire laser [2-11]. Compared to the performance data of the 3-mirror Ti:sapphire laser described in section 2.5, this laser delivers lower pump thresholds but also smaller slope efficiencies. This is due to the pump waist radii of this laser being about 15% smaller.

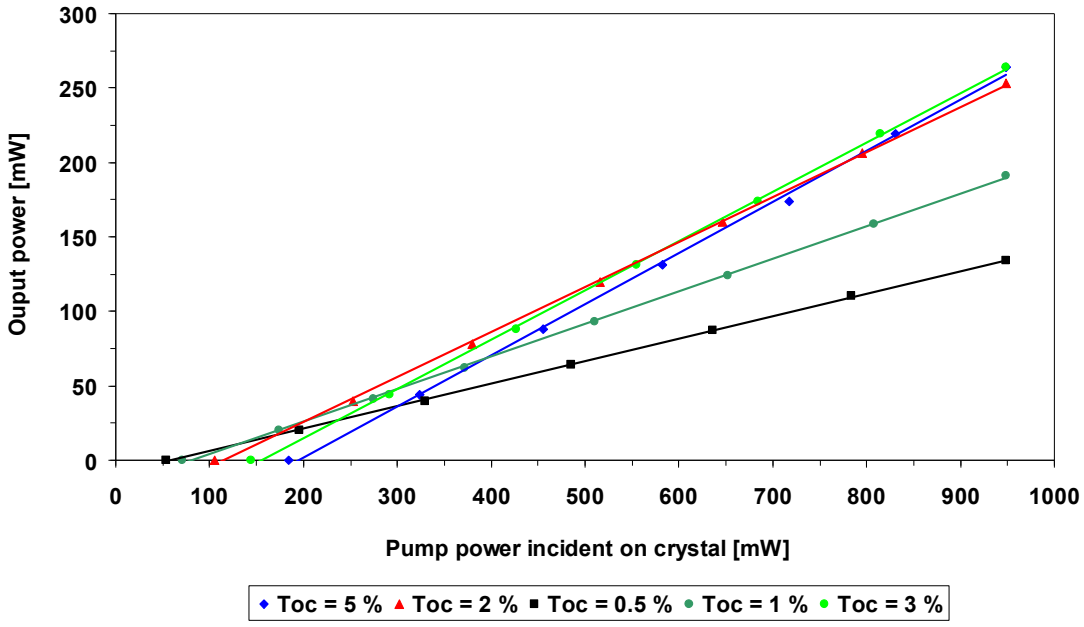

Fig. 3.2. Power transfer measurements of the 4-mirror Ti:sapphire laser with various output couplings pumped at 532 nm.

Table 3.2. Performance data of the 4-mirror Ti:sapphire laser with various output couplings pumped at 532nm.

Output coupling [%]	Pump threshold [mW]	Slope efficiency [%]	Output wavelength [nm]
HR	44	-	801
0.5	60	15.1	800
1	82	21.9	800
2	116	30.2	797
3	154	33.0	800
5	195	35.2	799

Resonator loss analyses using the Findlay-Clay [12] and Caird [13] approaches were conducted using the measured pump thresholds and the calculated slope efficiencies

(see Fig. 3.3 and Fig. 3.4). The resulting resonator round-trip loss of 1.2% for the Findlay-Clay method and 1.1% for the Caird method agree very well. The value is lower than the 1.4% assumed in the model (compare section 3.1). Despite having one additional resonator mirror and two prisms the 4-mirror Ti:sapphire laser has resonator round-trip losses identical to the 3-mirror resonator described in section 2.5.

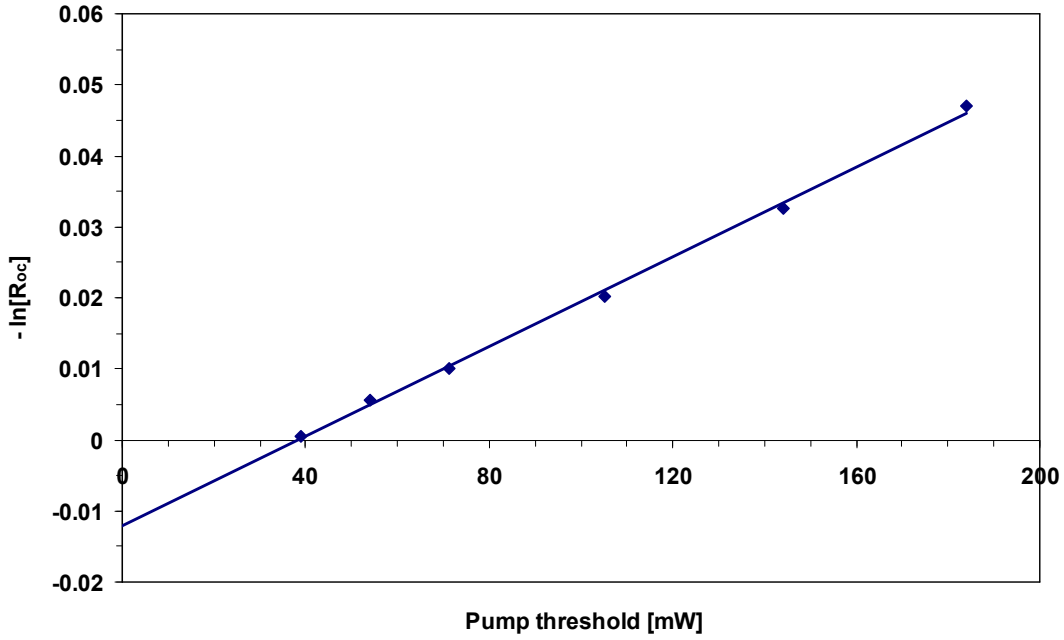

Fig. 3.3. Findlay-Clay plot for the 4-mirror Ti:sapphire laser pumped at 532 nm.

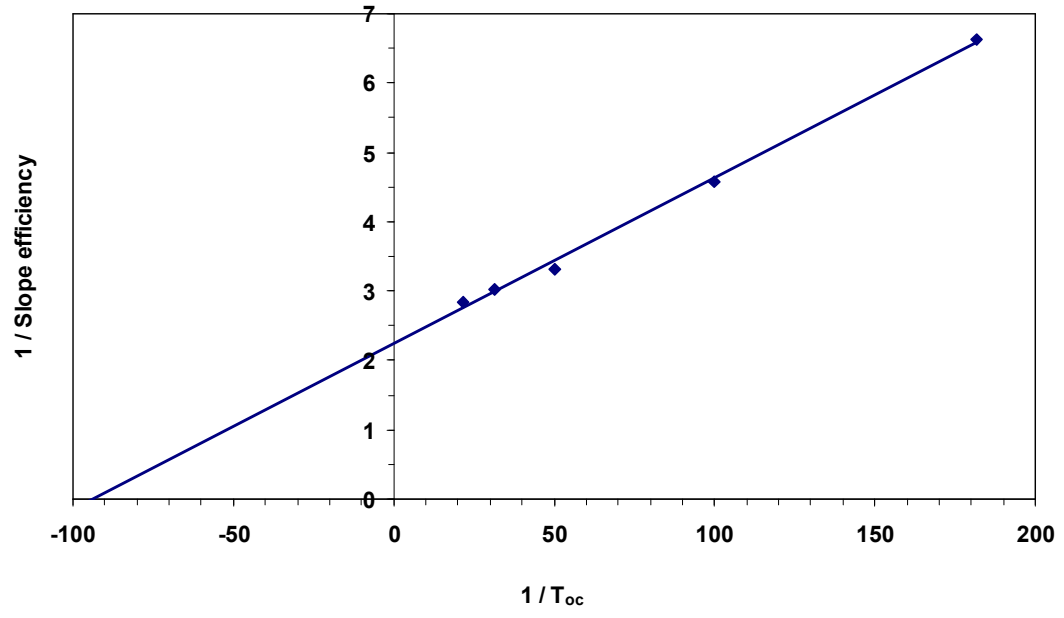

Fig. 3.4. Caird plot for the 4-mirror Ti:sapphire laser pumped at 532 nm.

Along with the power transfers, the beam propagation factor of the Ti:sapphire laser was measured with a scanning-slit beam-profiler (Dataray Inc. Beamscope-P7). The measurements were done with 1.00 W of pump power at 532 nm incident on the focussing lens (corresponding to 949 mW incident on the crystal) for all output couplers. The resulting propagation factors were $M^2 \leq 1.1$ in the horizontal and in the vertical plane indicating diffraction-limited Ti:sapphire laser output.

The oscillation wavelength of the Ti:sapphire laser was tuned by moving the slit perpendicularly to the axis of the resonator mode. With 1.00 W of pump power at 532 nm incident on the focussing lens (corresponding to 949 mW incident on the crystal) the oscillation wavelength and output power were recorded for 0.5% output coupling and with an HR mirror instead of an output coupler (see Fig. 3.5). The recorded tuning curves are determined by the reflectivity of the resonator mirrors ($R \geq 99.95\%$ at 695 - 870 nm) and the output coupler ($T_{oc} \approx 0.5\%$ at 750 – 860 nm) rather than representing the gain spectrum of Ti:sapphire (compare chapter 1.2.1).

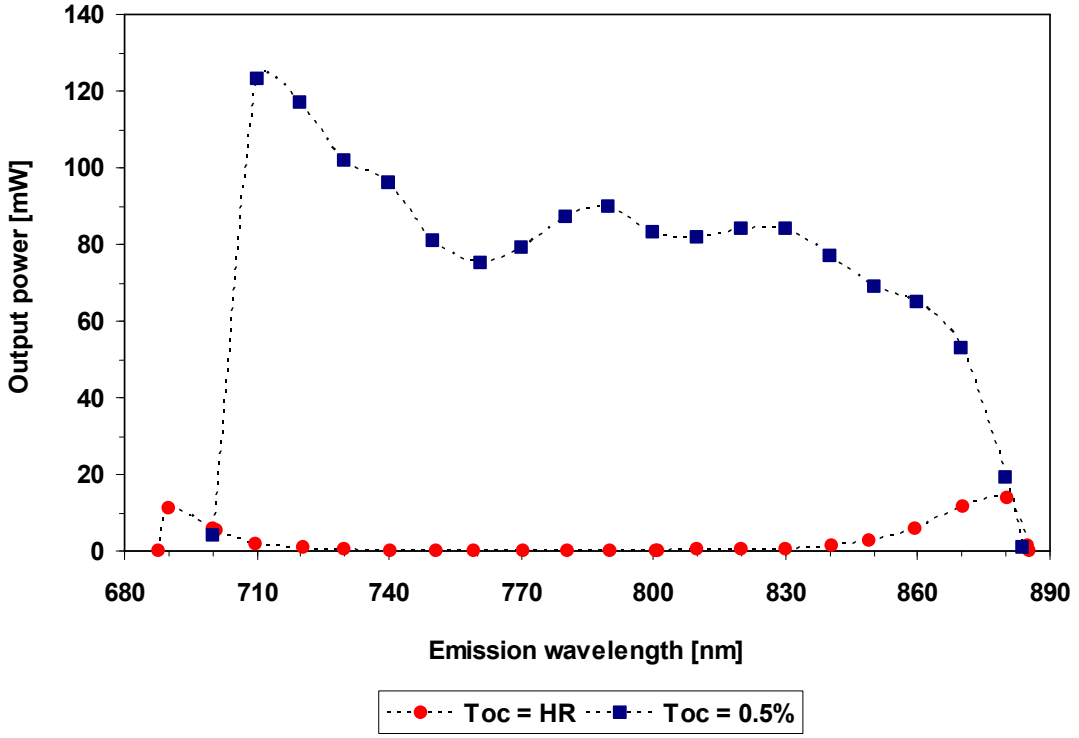

Fig. 3.5. Tuning curve of the 4-mirror Ti:sapphire laser pumped with 1.00 W at 532 nm with an output coupling of 0.5% and with an HR mirror used instead of an output coupler.

3.3 Cw operation: directly diode-laser-pumped Ti:sapphire laser

3.3.1 Resonator and pump optics

The 4-mirror Z-folded resonator was designed from the outset to suit both conventional and diode-laser pumping. The resonator design for pumping at 452 nm, shown in Fig. 3.6, is therefore almost identical to the 532 nm pumped setup presented in section 3.2.1. To achieve the larger resonator mode radii suggested by the modelling (in section 3.1), the distances between the resonator folding mirrors and the crystal were adjusted resulting in resonator waist radii of $w_{cx0} = 32$ µm at $z_{cx0} = 2.9$ mm in the horizontal plane and $w_{cy0} = 18$ µm at $z_{cy0} = 2.3$ mm in the vertical plane. The resonator waist radii perfectly match the modelling suggestions (compare section 3.1).

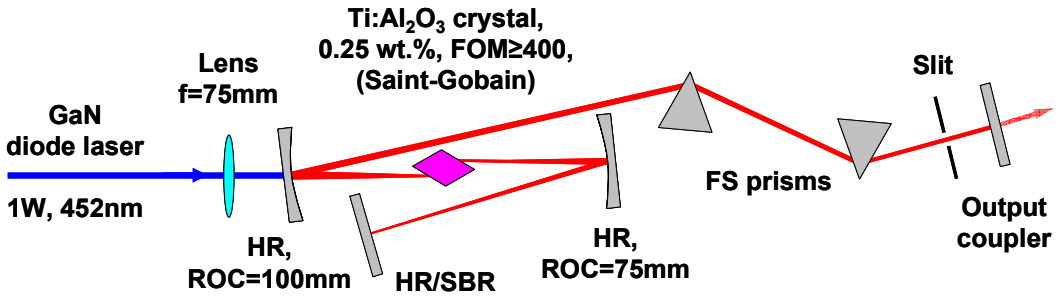

Fig. 3.6. Asymmetric, Z-folded 4-mirror resonator for diode-laser pumping (452 nm) (FS: Fused Silica).

ABCD-matrix calculations with the commercial software Winlase led to a pump optics setup consisting of a two-element, cylindrical lens Galilean telescope ($f_x = -25.4$ mm and $f_x = 250$ mm) to shape the diode laser beam in the horizontal plane and a spherical focusing lens (f = 75 mm). The output of the diode laser was focused into the crystal with calculated pump waist radii of $w_{px0} = 25$ µm at $z_{px0} = 2.9$ mm in the horizontal plane and $w_{py0} = 12$ µm at $z_{py0} = 2.2$ mm in the vertical plane. The pump waist radii are close to the optimised values from the model (compare 3.1) and, in principle, the pump and resonator waist locations overlap ideally in both planes. The diode laser was externally attenuated with a halfwave-

plate and a polarizing beamsplitter cube to ensure a stable beam profile over the entire power range.

3.3.2 Laser performance

For pumping with the 452 nm diode laser, the power transfers were recorded with output couplings of T_{oc} = 0.5, 1, 2, and 3% and the oscillation wavelength adjusted to 800 nm using the slit (see Fig. 3.7 and Table 3.3). Laser oscillation could not be achieved with 5% output coupling. A pump threshold of 334 mW and a slope efficiency of 3.5% were obtained with an output coupling of T_{oc} = 0.5%. Replacing the output coupler with a HR mirror resulted in a pump threshold of 264 mW. These pump thresholds are the lowest yet reported for a directly diode-laser-pumped Ti:sapphire laser. Compared to the performance data of the 3-mirror Ti:sapphire lasers described in sections 2.4.4 and 2.6.2, this laser delivers ~30% lower pump thresholds. This is due to a better overlap between the pump and resonator modes.

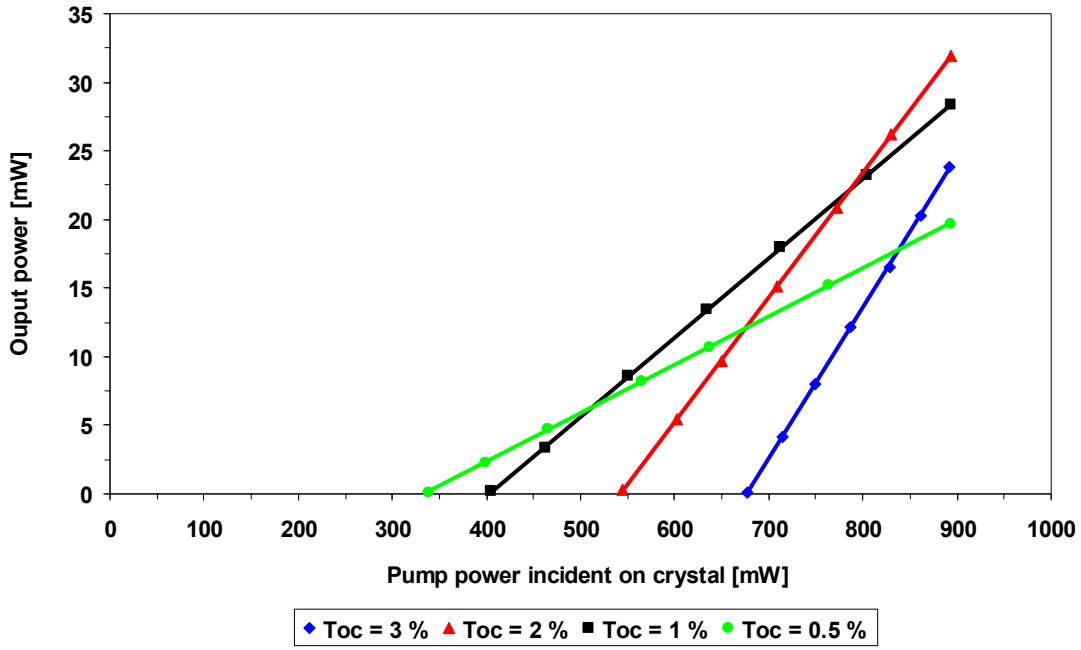

Fig. 3.7. Power transfer measurements of the 4-mirror Ti:sapphire laser with various output couplings pumped at 452 nm.

Table 3.3. Performance data of the 4-mirror Ti:sapphire laser with various output couplings pumped at 452nm.

Output coupling [%]	Pump threshold [mW]	Slope efficiency [%]	Output wavelength [nm]
HR	264	-	800
0.5	334	3.5	800
1	402	5.8	800
2	543	9.1	800
3	677	11.0	800

The measured pump thresholds and the calculated slope efficiencies were used to analyze the resonator losses, resulting in round-trip losses of 2.1% for the Findlay-Clay method [12] (Fig. 3.8) and 2.7% for the Caird method [13] (Fig. 3.9). The values agree with the 2.6% assumed in the model (compare 3.1). In comparison to the round-trip losses obtained with the very same resonator under 532 nm pumping (see 3.2.2) the values are 0.9% to 1.6% higher which represents the pump-induced loss at 452 nm.

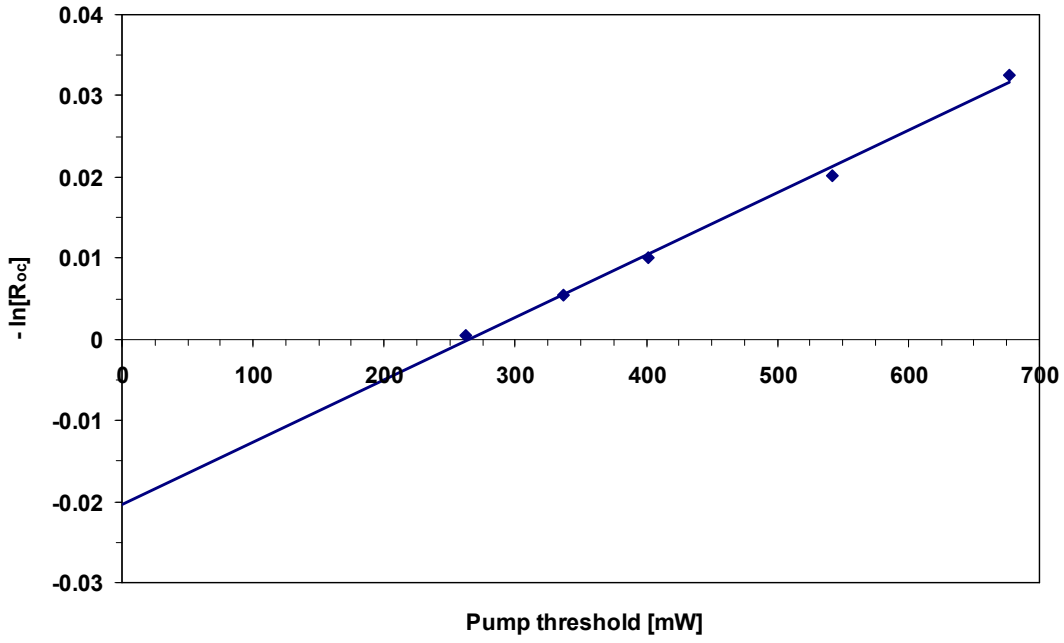

Fig. 3.8. Findlay-Clay plot for the 4-mirror Ti:sapphire laser pumped at 452 nm.

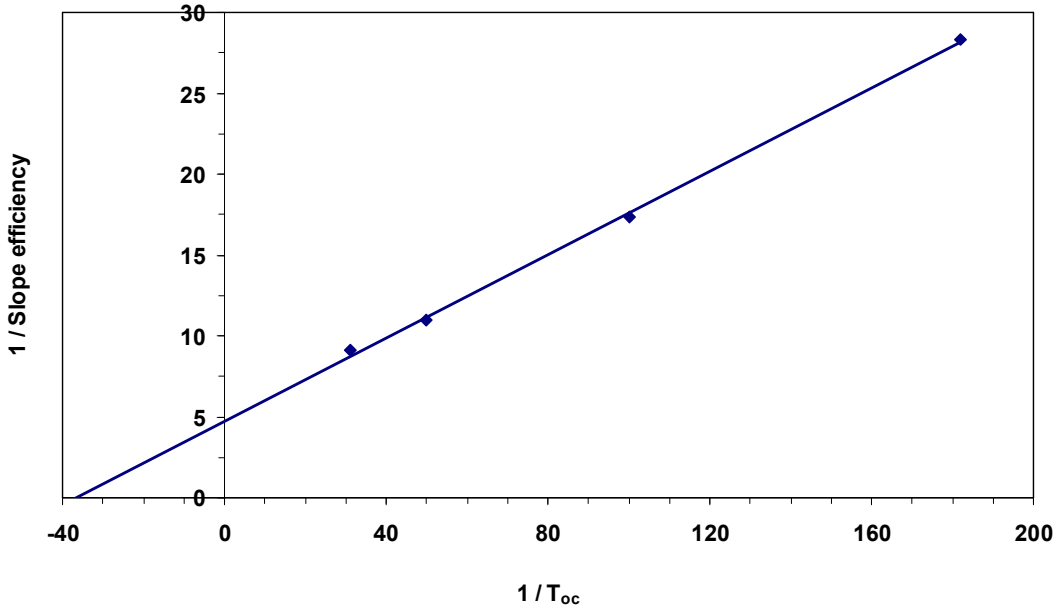

Fig. 3.9. Caird plot for the 4-mirror Ti:sapphire laser pumped at 452 nm.

The beam propagation factor of the Ti:sapphire laser was measured with a scanning-slit beam-profiler (Beamscope-P7). The measurements were done at maximum pump power (1 W) resulting in $M^2_x = 2.3$ in the horizontal and $M^2_y = 2.1$ in the vertical plane. These values suggest that the actual fundamental resonator mode size was smaller than calculated and hence led to the amplification higher-order modes.

With the maximum of pump power at 452 nm of 919 mW incident on the crystal, the tuning range of the Ti:sapphire laser was recorded, see Fig. 3.10. The oscillation wavelength was tuned by moving the slit perpendicularly to the axis of the resonator mode. The output coupling was 2%, which gave the highest output power (32 mW at 800 nm, see Fig. 3.7). The maximum output power of 40 mW occurs at 770 nm rather than at Ti:sapphire's peak gain wavelength of 795 nm (compare chapter 1.2.1). At wavelengths shorter than 735 nm or longer than 825 nm the tuning curve is determined by the reflectivity of the output coupler ($T_{oc} \approx 2\%$ at 735 - 825 nm) and resonator mirrors ($R \geq 99.95\%$ at 695 – 870 nm). Compared to the 3-mirror Ti:sapphire lasers, the maximum output power with a single diode laser pump increased to 40 mW (at 770 nm with $T_{oc} = 2\%$) from 24 mW (at 777 nm with $T_{oc} = 1\%$, see 2.6.2) and 19 mW (at 783 nm with $T_{oc} = 1\%$, see 2.4.4) respectively.

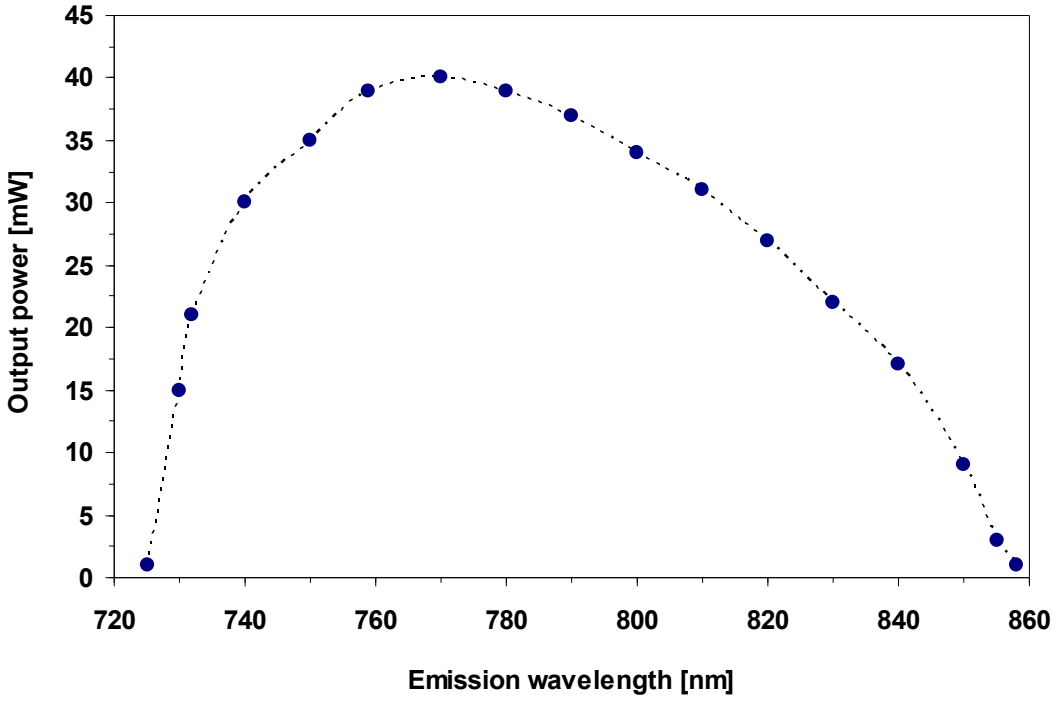

Fig. 3.10. Tuning curve of the 4-mirror Ti:sapphire laser (2% output coupling) pumped at 452 nm with 919 mW incident on the crystal.

3.4 Mode locking

3.4.1 Setup

In the four-mirror Ti:sapphire laser shown in Fig. 3.6 the flat HR resonator mirror was replaced with a saturable Bragg reflector (SBR) to obtain robust mode locking. The SBR used here was designated for use in a low-threshold Cr:LiSAF laser and was therefore designed to operate at a wavelength around 850 nm. As a result, the laser had to be tuned to this wavelength region for mode-locked operation rather than closer to the peak gain wavelength of Ti:sapphire at 795 nm or closer to 770 nm where maximum output power in cw operation was achieved (see Fig. 3.10). The Bragg mirror structure of the SBR consisted of 30 pairs of $Al_{0.15}Ga_{0.85}As$ and AlAs quarter-wave layers on a 0.5-mm-thick GaAs substrate. Saturable absorption was provided by a 5-nm-thick $In_{0.08}Ga_{0.92}As$ quantum well in the middle of the topmost

AlGaAs layer [14]. The SBR was grown at temperatures optimised for low non-saturable losses (typically less than 0.5% in such devices, dominated by the transmission of the rear mirror [15]). During the experiments, the calculated spot size of the fundamental resonator mode on the SBR was 20 × 21 μm ($1/e^2$ half-width). The tip-to-tip separation of the fused-silica prism pair for dispersion compensation was set to 52.5 cm.

3.4.2 Laser performance in mode-locked operation

With an output coupling of 0.5%, mode-locked operation was initiated and sustained for incident pump powers above 105 mW for 532 nm pumping or above 439 mW for diode-laser pumping at 452 nm, see Fig. 3.11 [1]. The repetition rate was 127 MHz in both cases. An average output power of 13 mW and a pulse duration (FWHM) of 142 fs were achieved under diode-laser pumping with 890 mW of pump power [1]. The pulse durations were measured using a standard Michelson-type autocorrelator with two-photon absorption in a AlGaInP single-mode diode laser (Sanyo Ltd., DL3147-060) used for nonlinear detection [16]. At a lower pump power of 662 mW, and consequently a lower average output power of 7 mW, pulse durations as short as 114 fs were measured under diode-laser pumping, see Fig. 3.12 [1]. The spectral bandwidth (FWHM) was 7.2 nm (3.0 THz) with a centre wavelength of 841 nm as shown in Fig. 3.13, giving a duration–bandwidth product of 0.35 [1].

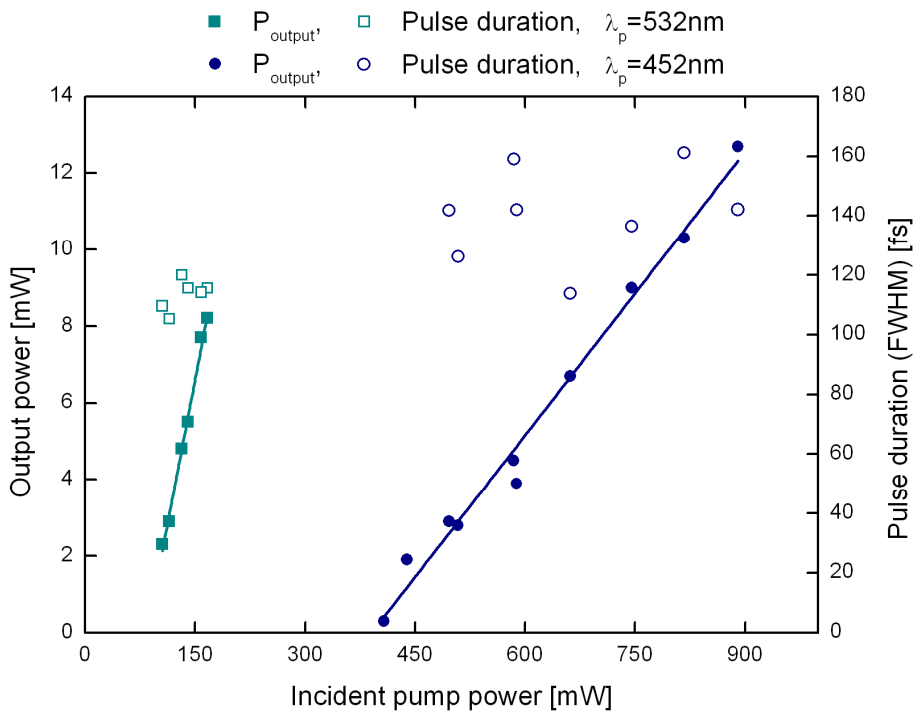

Fig. 3.11. Output power and pulse duration in mode-locked operation as a function of pump power incident on the crystal (0.5% output coupling) under conventional pumping (532 nm) and diode-laser pumping (452 nm) [1].

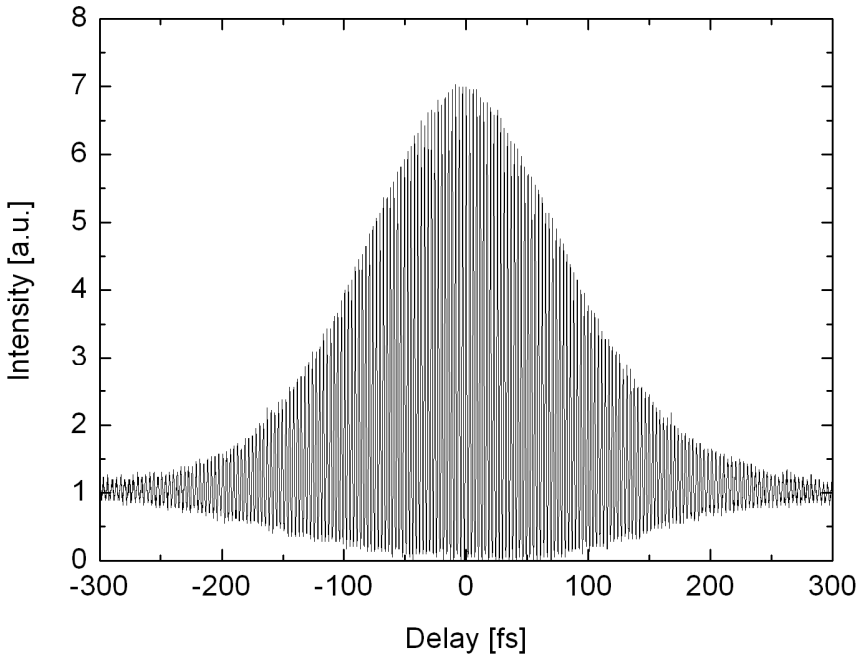

Fig. 3.12. Interferometric autocorrelation of the pulses at 662 mW of diode-laser pump power and 7 mW of average output power (0.5% output coupling) [1]. The divergence from the ideal 8:1 ratio resulted from a difference in reflectivity between the two corner cube mirrors used in the interferometer arms of the autocorrelator.

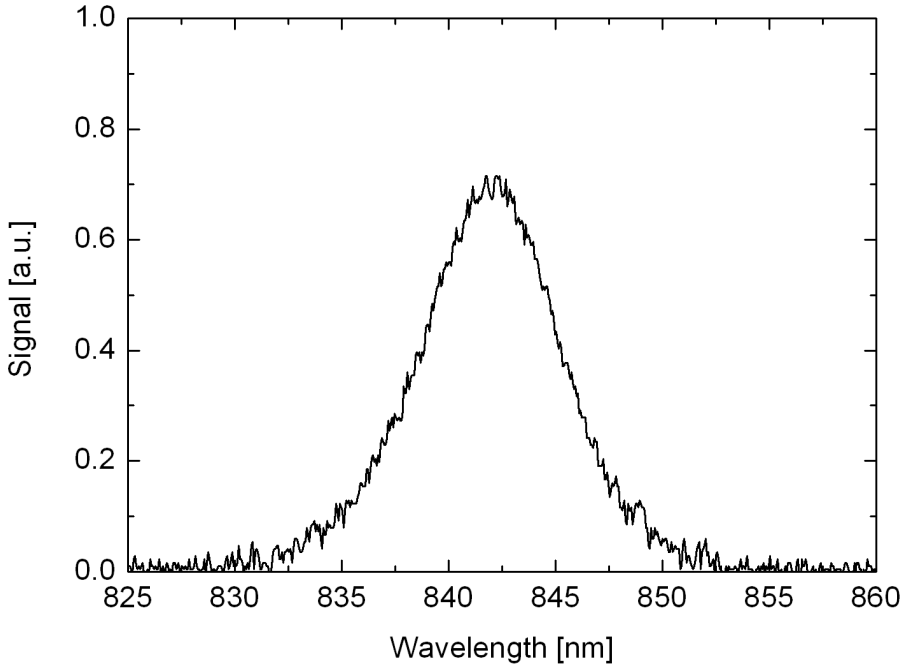

Fig. 3.13. Spectrum of the pulses at 662 mW of diode-laser pump power and 7 mW of average output power (0.5% output coupling). The centre wavelength was 841 nm [1].

3.5 Double-sided diode-laser pumping

Increasing the pump power by adding more GaN diode lasers to the setup was considered in order to achieve output powers of about 100 mW, a target which would demonstrate the suitability of directly diode-laser-pumped Ti:sapphire lasers for low-power applications like multi-photon microscopy. Pumping the four-mirror resonator through both folding mirrors (double-sided pumping) with a pair of polarization beam combined GaN diode lasers on either side would provide up to 4 W of combined pump power. However within the scope of this thesis only double-sided pumping with two diode lasers was realized. Double-sided pumping is more difficult to align than pumping from one side with a polarization combined pair of diode lasers. Nonetheless, it was used here because the pump absorption of Ti:sapphire is significantly lower for light polarized perpendicular (σ-polarized) rather than parallel (π-polarized) to the crystal c-axis (see chapter 1.2.1) [17]. The Ti:sapphire crystal

used here (0.25 wt. %, FOM ≥ 400, Saint-Gobain Crystals) absorbs 83% of the incident, π-polarized light at 452 nm in a single pass (see chapter 2.3.2) while the calculated single-pass absorption of σ-polarized light at the same wavelength was only 61%.

3.5.1 Resonator and pump optics

The resonator design is identical to that used for single diode laser pumping (see section 3.3.1) while the pump optics were reconfigured for double-sided pumping, see Fig. 3.14. Besides the GaN diode laser used before (1 W at 452 nm, Nichia NDB7352E), a second diode laser of the same type, delivering 1 W at 454 nm, was used to pump the Ti:sapphire resonator. ABCD-matrix calculations with the commercial software Winlase led to an identical pump optics setup for both diode lasers, consisting of a two-element, cylindrical lens Galilean telescope (f_x = -25.4 mm and f_x = 250 mm) to shape the diode laser beam in the horizontal plane and a spherical focusing lens (f = 75 mm). The output of the 452 nm diode laser was focused into the crystal through the long-arm folding mirror (radius of curvature (ROC) = 100 mm) resulting in calculated pump waist radii of w_{px0} = 25 µm at z_{px0} = 2.9 mm in the horizontal plane and w_{py0} = 12 µm at z_{py0} = 2.2 mm in the vertical plane.

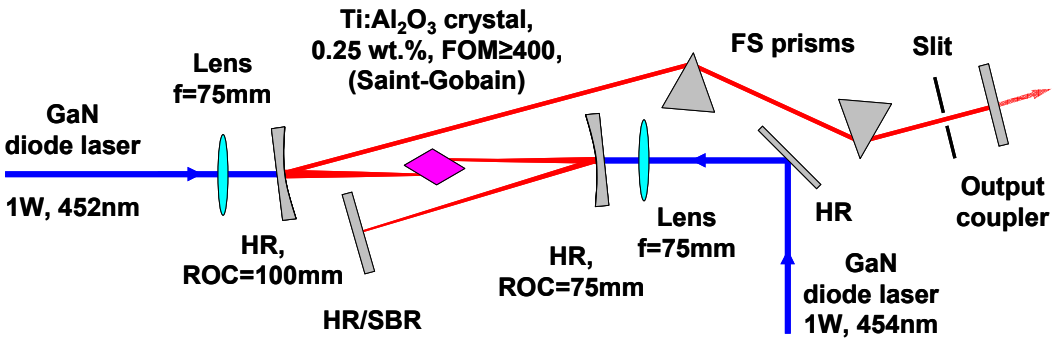

Fig. 3.14. Asymmetric, Z-folded 4-mirror resonator for double-sided, diode-laser pumping (452 nm and 454 nm GaN diode lasers).

The output beam of the 454 nm diode laser was characterized with a knife-edge rotating-drum beam profiler (Coherent Inc. BeamMaster). The recorded caustic, shown in Fig. 3.15, gives a beam propagation factor of M^2 = 5.9 x 1.1. Based on these measurements, pump waist radii of w_{px0} = 27 µm at z_{px0} = 2.6 mm in the horizontal plane and w_{py0} = 12 µm at z_{py0} = 2.6 mm in the vertical plane were calculated with the 454 nm diode laser beam focused into the crystal through the short-arm folding mirror (ROC = 75 mm). Both diode lasers were externally attenuated with half-wave plates and a polarizing beamsplitter cubes to ensure a stable beam profile over the entire power range. The resonator waist radii were calculated to be w_{cx0} = 32 µm at z_{cx0} = 2.9 mm in the horizontal plane and w_{cy0} = 18 µm at z_{cy0} = 2.3 mm in the vertical plane.

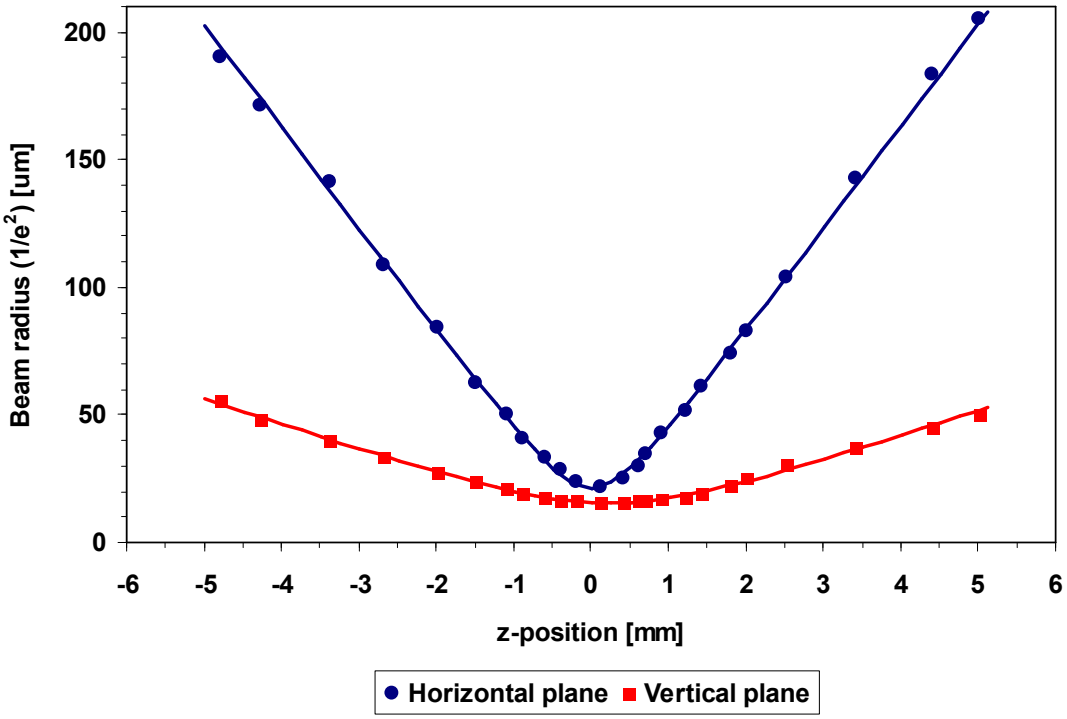

Fig. 3.15. Beam caustic of the 454 nm GaN diode laser including the cylindrical Galilean telescope (f_x = -25.4 mm and f_x = 250 mm) used to shape the beam in the horizontal plane. Caustic measured with a f = 150 mm spherical focusing lens.

3.5.2 Laser performance in cw operation

With an output coupling of 0.5% and the emission wavelength adjusted to 800 nm, the power transfer of the double-sided, diode-laser-pumped Ti:sapphire laser was recorded. Fig. 3.16 shows the Ti:sapphire laser output power as a function of the combined pump power of both diodes with the diode lasers power being added sequentially: first the 452 nm diode laser until full power is reached (919 mW incident on the crystal) followed by the 454 nm pump laser until a combined maximum pump power of 1862 mW is reached. The slope efficiencies taken for each pump regime separately were 3.4% for the 452 nm diode laser pumping (0 – 919 mW) and 3.3% for the combined 452 and 454 nm pump regime (919 – 1862 mW). The nearly identical slope efficiencies indicate good mode matching between the two pump modes and the resonator mode. The slope efficiencies and the pump threshold of 326 mW were close to the values measured with the single-diode laser pumped setup presented in 3.3.2. At maximum pump power, an output power of 51 mW was recorded.

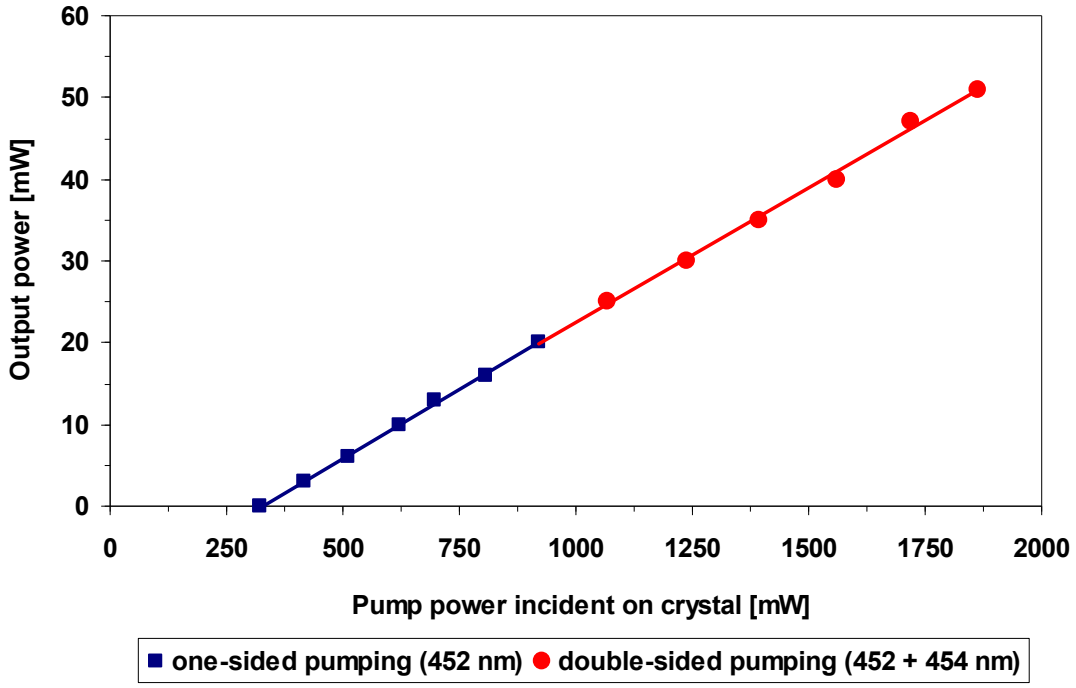

Fig. 3.16. Ti:sapphire laser output power at 800 nm as a function of the combined GaN diode laser pump power at 452 nm and 454 nm (T_{oc} = 0.5%). The diode lasers were powered up sequentially.

With the emission wavelength tuned to 800 nm, the 4-mirror Ti:sapphire laser output power was measured for the output couplings of Toc = 0.5, 1, 2, 3, and 5% (see Fig. 3.17). This was done at maximum pump power from the 452 nm diode only (919 mW) and from both diode lasers (1862 mW combined). With the 452 nm diode laser alone the maximum output power was 31 mW with 2% output coupling. Pumping with both diodes and using 3% output coupling gave 118 mW.

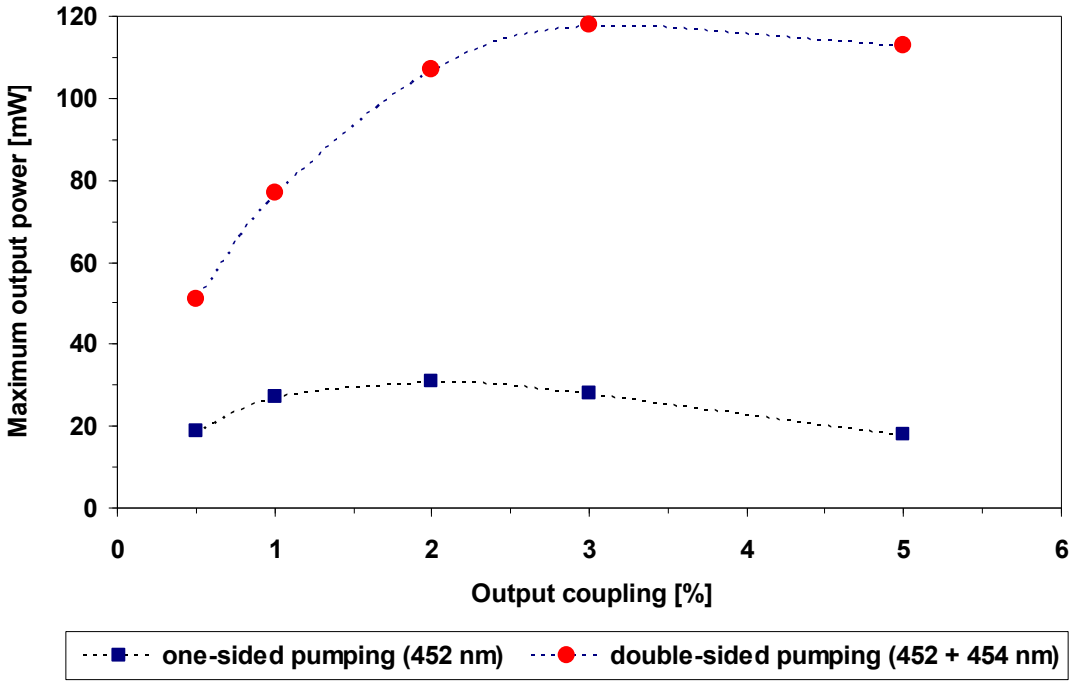

Fig. 3.17. Maximum output power of the 4-mirror Ti:spphire laser at 800 nm for various output couplings under single diode laser pumping (919 mW at 452 nm) and double-sided pumping (1862mW at 452 + 454 nm).

The tuning range of the Ti:sapphire laser was recorded at maximum pump power for output couplings of 2% and 3%, see Fig. 3.18. The oscillation wavelength was tuned by moving the slit perpendicularly to the axis of the resonator mode. The maximum output power of 129 mW occurred at 770 nm rather than at Ti:sapphire's peak gain wavelength of 795 nm (compare section 1.2.1). At wavelengths shorter than 730 nm or longer than 860 nm, the tuning curve is determined by the reflectivity of the output coupler and resonator mirrors ($R \geq 99.95\%$ at 695 - 870 nm). Nevertheless

output powers greater than 100 mW were maintained over a tuning range of 80 nm (740 - 820 nm).

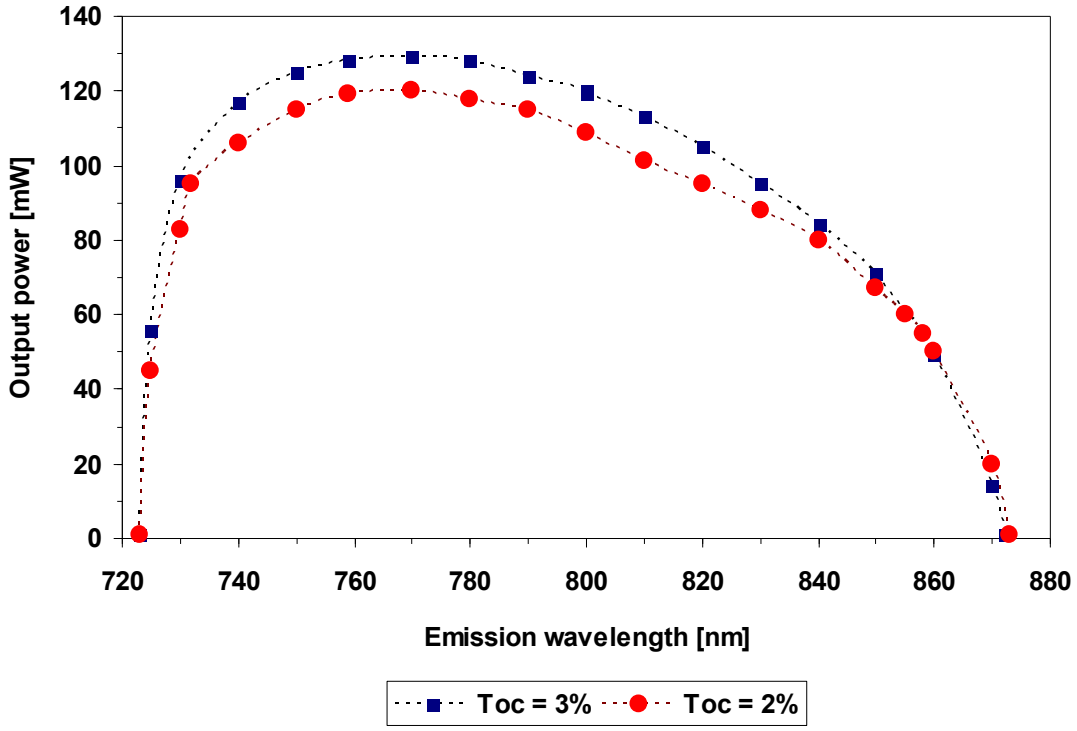

Fig. 3.18. Tuning curve of the 4-mirror Ti:sapphire laser (2 and 3% output coupling) pumped with 919 mW at 452 nm and 943 mW at 454 nm incident on the crystal.

3.5.3 Laser performance in mode-locked operation

In comparison to the previous mode locking experiments (section 3.4) only two changes were made in the resonator setup. First, the SBR used to initiate and sustain mode-locked operation was designed to operate at a wavelength around 825 nm rather than at 850 nm. Apart from a different operation wavelength this SBR was of the same design as the one introduced in section 3.4.1. As a result, the laser was allowed to oscillate at a wavelength closer to the peak gain wavelength of Ti:sapphire at 795 nm and closer to the wavelength where maximum output power was achieved in cw operation (770 nm, see Fig. 3.18). Second, the tip-to-tip separation of the fused-silica prism pair was changed to 60 cm for in order to achieve shorter pulses.

With an output coupling of 2%, an average output power of 101 mW and a pulse duration (FWHM) of 111 fs were achieved under double-sided diode-laser pumping with a combined 1862 mW of pump power, see Fig. 3.19. The spectral bandwidth (FWHM) was 8.0 nm (3.6 THz) with a centre wavelength of 818 nm as shown in Fig. 3.20, giving a duration–bandwidth product of 0.40.

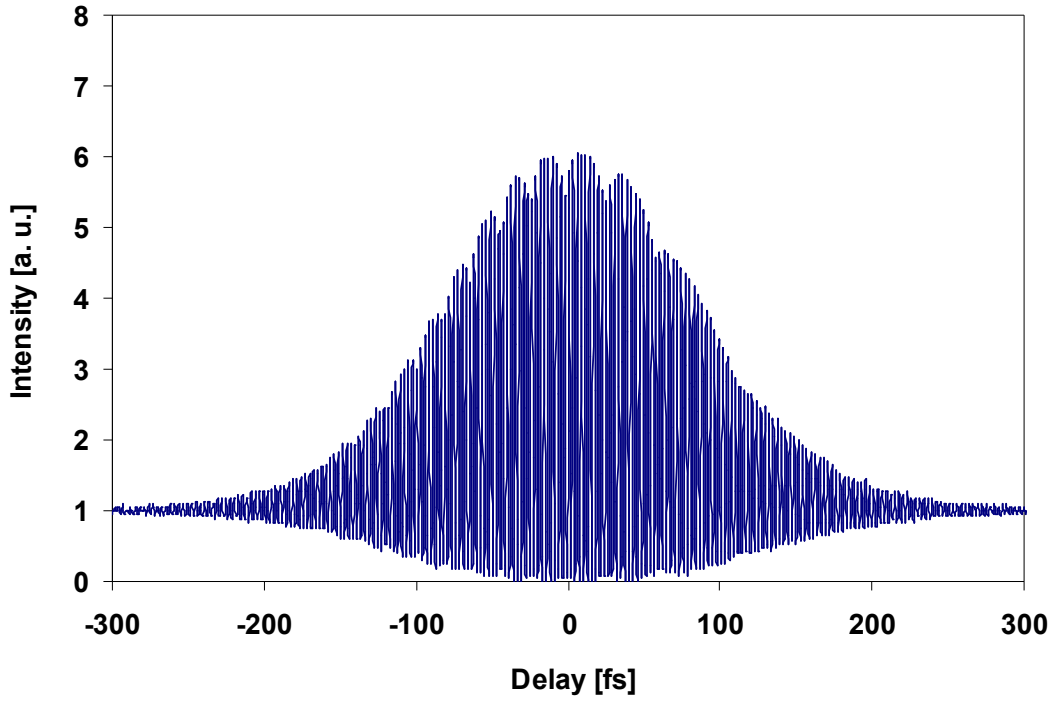

Fig. 3.19. Interferometric autocorrelation of the pulses at maximum double-sided diode-laser pump power (1862 mW) and 101 mW of average output power (2% output coupling). The divergence from the ideal 8:1 ratio resulted from a difference in reflectivity between the two corner cube mirrors used in the interferometer arms of the autocorrelator.

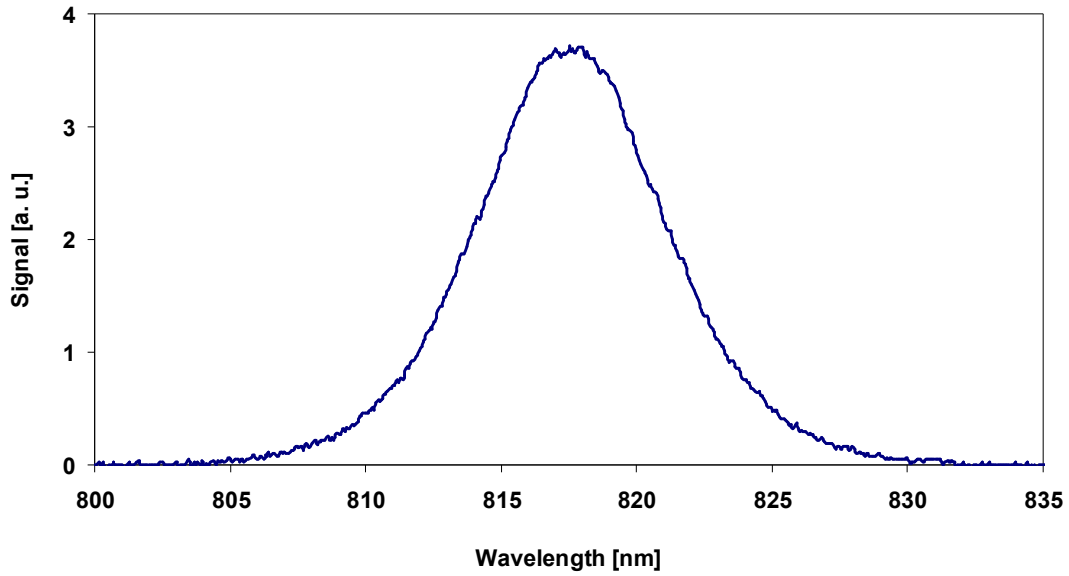

Fig. 3.20. Spectrum of the pulses at maximum double-sided diode-laser pump power (1862 mW) and 101 mW of average output power (2% output coupling). The centre wavelength was 818 nm.

3.6 Conclusions

The design and characterisation of a mode-locked Ti:sapphire laser suitable for direct diode-laser pumping was described in this chapter. The resonator parameters that the modelling indicated would result in optimised performance dictated the use of an asymmetric, Z-folded four-mirror resonator.

In cw operation, a maximum output power of 40 mW at a wavelength of 770 nm was achieved by pumping with a single GaN diode laser. For conventional pumping at 532 nm, a threshold of only 60 mW and a slope efficiency of 15% were demonstrated with 0.5% output coupling. Although the laser design was optimized for GaN diode-laser pumping, the cw threshold when pumped at 532 nm is, to my knowledge, the lowest yet reported for a Ti:sapphire laser.

By using a saturable Bragg reflector, mode-locked operation of a directly diode-laser-pumped Ti:sapphire laser was demonstrated for the first time. With a single GaN diode laser pump pulses as short as 114 fs were generated. A maximum output power of 13 mW and a mode-locking threshold of 408 mW were achieved.

In order to increase the output power of the laser, a double-sided pumping configuration with two GaN diode lasers was subsequently employed. Cw output powers of more than 100 mW were obtained over a tuning range of 740 – 820 nm. In mode-locked operation a maximum output power increased to 101 mW at a pulse duration of 111 fs.

3.7 References

1. P. W. Roth, A. J. Maclean, D. Burns, and A. J. Kemp, "Direct diode-laser pumping of a mode-locked Ti:sapphire laser," Opt. Lett. **36**, 304-306 (2011).
2. J. Harrison, A. Finch, D. M. Rines, G. A. Rines, and P. F. Moulton, "Low-Threshold, Cw, All-Solid-State Ti-Al2o3 Laser," Opt. Lett. **16**, 581-583 (1991).
3. J. F. Pinto, L. Esterowitz, G. H. Rosenblatt, M. Kokta, and D. Peressini, "Improved Ti:Sapphire Laser Performance with New High Figure of Merit Crystals," IEEE J. Quantum Electron. **30**, 2612-2616 (1994).
4. K. Torizuka, H. Takada, and K. Miyazaki, "Low-Threshold Self-Mode-Locked Ti Sapphire Laser," IEICE Trans. Electron. **E78C**, 85-87 (1995).
5. K. Read, F. Blonigen, N. Riccelli, M. E. Murnane, and H. Kapteyn, "Low-threshold operation of an ultrashort-pulse mode-locked Ti:sapphire laser," Opt. Lett. **21**, 489-491 (1996).
6. K. Torizuka, H. Takada, and K. Miyazaki, "Low-threshold self-mode-locked Ti:sapphire laser with double dispersion compensators," Jpn. J. Appl. Phys. Part 1 - Regul. Pap. Short Notes Rev. Pap. **36**, 710-713 (1997).
7. A. J. Tiffany, I. T. McKinnie, and D. M. Warrington, "Low-threshold, single-frequency, coupled cavity Ti:Sapphire laser," Appl. Optics **36**, 4989-4992 (1997).
8. A. M. Kowalevicz, T. R. Schibli, F. X. Kartner, and J. G. Fujimoto, "Ultralow-threshold Kerr-lens mode-locked Ti : Al2O3 laser," Opt. Lett. **27**, 2037-2039 (2002).
9. A. Sennaroglu, A. M. Kowalevicz, F. X. Kartner, and J. G. Fujimoto, "High,performance, compact, prismless, low-threshold 30-MHz Ti : Al2O3 laser," Opt. Lett. **28**, 1674-1676 (2003).
10. B. Stormont, I. G. Cormack, M. Mazilu, C. T. A. Brown, D. Burns, and W. Sibbett, "Low-threshold, multi-gigahertz repetition-rate femtosecond Ti : sapphire laser," Electron. Lett. **39**, 1820-1822 (2003).
11. W. J. Ling, Y. L. Jia, J. H. Sun, Z. H. Wang, and Z. Y. Wei, "Low-threshold self-starting femtosecond Ti : sapphire laser," Appl. Optics **45**, 2495-2498 (2006).

12. D. Findlay and R. A. Clay, "The measurement of internal losses in 4-level lasers," Phys. Lett. **20**, 277-278 (1966).
13. J. A. Caird, S. A. Payne, P. R. Staber, A. J. Ramponi, L. L. Chase, and W. F. Krupke, "Quantum electronic properties of the $Na_3Ga_2Li_3F_{12}:Cr^{3+}$ laser," IEEE J. Quantum Electron. **24**, 1077-1099 (1988).
14. Z. Zhang, T. Nakagawa, H. Takada, K. Torizuka, T. Sugaya, T. Miura, and K. Kobayashi, "Low-loss broadband semiconductor saturable absorber mirror for mode-locked Ti:sapphire lasers," Opt. Commun. **176**, 171-175 (2000).
15. S. Tsuda, W. H. Knox, S. T. Cundiff, W. Y. Jan, and J. E. Cunningham, "Mode-locking ultrafast solid-state lasers with saturable Bragg reflectors," IEEE J. Sel. Top. Quantum Electron. **2**, 454-464 (1996).
16. D. T. Reid, W. Sibbett, J. M. Dudley, L. P. Barry, B. Thomsen, and J. D. Harvey, "Commercial semiconductor devices for two photon absorption autocorrelation of ultrashort light pulses," Appl. Optics **37**, 8142-8144 (1998).
17. P. F. Moulton, "Spectroscopic and Laser Characteristics of $Ti:Al_2O_3$," J. Opt. Soc. Am. B **3**, 125-133 (1986).

4 Pump-induced loss and reduced quantum efficiency

4 Pump-induced loss and reduced quantum efficiency

In order to achieve laser oscillation in a Ti:sapphire laser with a GaN diode laser pump, the resonator must be optimised for low pump thresholds. The typical approach used to achieve this was to employ a frequency-doubled Nd:YVO_4 pump laser emitting at 532 nm (see section 2.1.1) to optimise the resonator and subsequently switch to GaN diode laser pumping. However, on switching from frequency-doubled Nd:YVO_4 laser pumping to GaN diode laser pumping, the Ti:sapphire laser's output power deteriorated over the first few minutes before reaching a steady state. This was an unexpected result. The laser's performance was significantly lower than might have been expected from the rate equation-based modelling presented in chapter 2. It is the lower output power, steady-state results that are of interest from a laser engineering perspective and which are reported for continuous-wave and mode-locked operation in chapters 2 and 3 respectively. In this chapter, however, the nature of the reduction in output power itself is characterised. All pump thresholds and slope efficiencies are given with respect to pump power incident on the crystal unless otherwise stated.

4.1 Ti:sapphire laser performance deterioration over time under GaN diode laser pumping

The typical laser setup used experimentally is shown in Fig. 4.1. It employed the low parasitic loss crystal from Saint-Gobain Crystals Ltd. (5.2 mm long, 0.25 wt. % doping concentration, FOM ≥ 400, Brewster-cut), see section 2.3.2. The pump source was a 445 nm GaN diode laser delivering 800 mW (Nichia NDB7352E). The beam propagation factor, M^2, was measured with a scanning slit beam profiler (DataRay Inc. Beamscope-P7) and a knife-edge rotating-drum beam profiler (Coherent Inc. BeamMaster) and was found to be 6.0 × 1.4 in the horizontal and vertical planes respectively. A cylindrical, Keplerian telescope (f_x = 10 mm and f_x = 130 mm) was used to shape the beam in the horizontal plane (slow axis of the diode laser). To

allow an easy transition between the two pump regimes, a dichroic mirror (Chroma Technology Corp. z488bcm-xr) was used to combine both pump beams. The dichroic mirror was highly reflective for wavelengths below 500 nm and transmissive for wavelengths above 520 nm. Once the Ti:sapphire laser had been optimised with the frequency-doubled Nd:YVO_4 pump laser, the GaN diode laser beam was aligned collinear to the 532 nm pump beam.

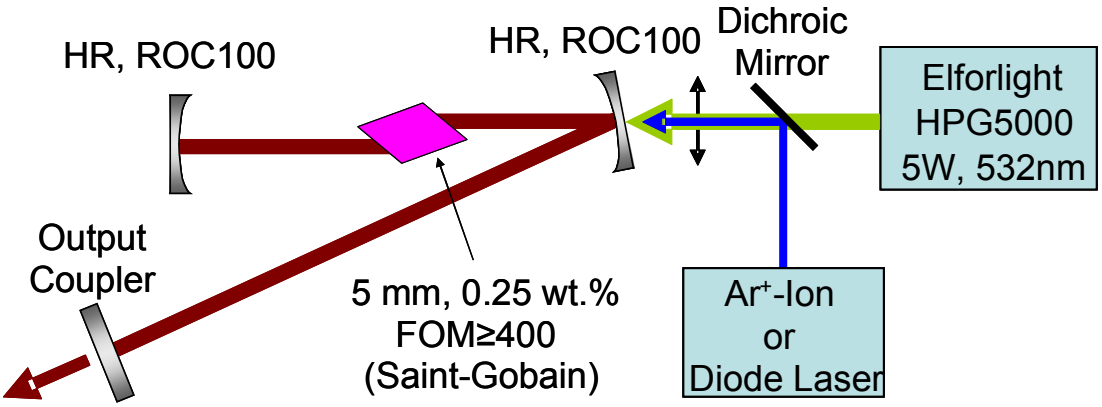

Fig. 4.1. Schematic diagram of the Ti:sapphire laser resonator (HR: high reflector, ROC: radius of curvature).

With the 532 nm pump laser, a slope efficiency of 15% and a pump threshold of 140 mW were achieved with 0.5% output coupling. Having 712 mW of pump power at 532 nm incident on the crystal resulted in 80 mW of output power from the Ti:sapphire laser. Adding another 712 mW of pump power at 445 nm from the collinearly aligned GaN diode laser led to an immediate output power increase to 94 mW. However, the output power of the Ti:sapphire laser began to deteriorate and 13 minutes after adding the 445 nm pump light, it had dropped to a stable level of 53 mW (see Fig. 4.2). Switching off the GaN diode laser resulted in 39 mW of output power from the same 712 mW of pump power at 532 nm. The laser output power then recovered while being pumped at 532 nm: it reached 66 mW forty minutes after switching off the 445 nm pump and was continuing to rise.

While a similar deterioration in output power was observed when pumping at 445 nm alone, the recovery only occurred when pumping with 532 nm alone. The Ti:sapphire laser output power did not recover if both pump lasers were switched off, even after being switched off overnight. This behaviour rules out thermal lensing or quenching of the upper state lifetime as reasons for the performance deterioration. Furthermore, the Ti:sapphire laser operated with pump powers up to 2.5 W at 532 nm with no sign of a rollover in output power (reduction in slope efficiency). Resetting the Ti:sapphire laser to its initial output power level required more than two hours of exposure to 712 mW of 532 nm pump light. This indicates that the cause for this behaviour is neither thermal nor mechanical instability.

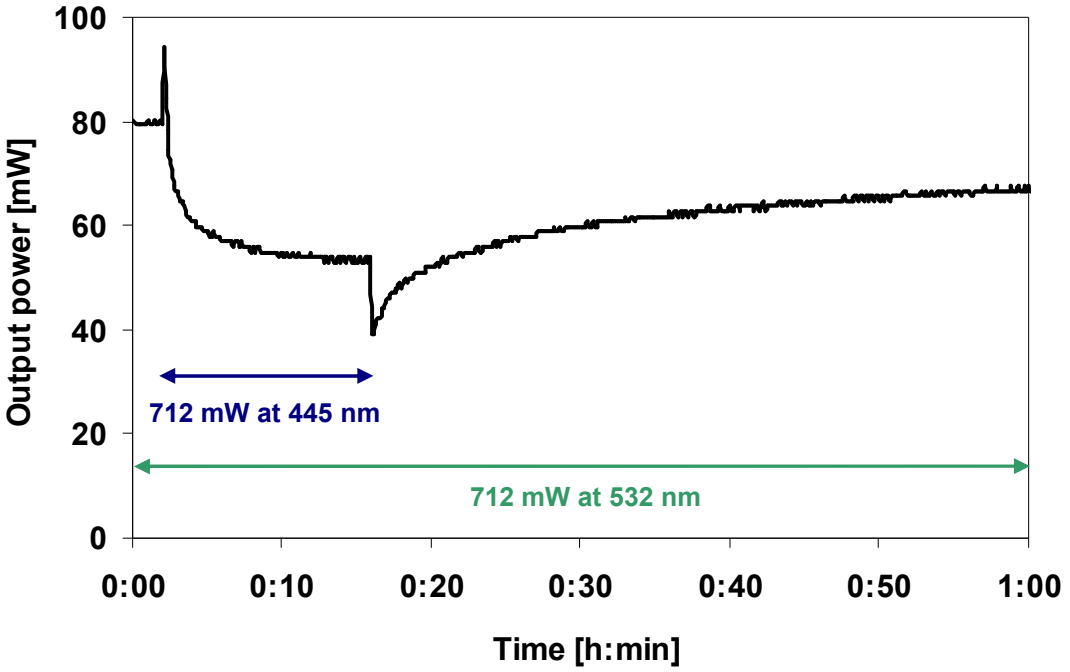

Fig. 4.2. Output power as a function of time for the Ti:sapphire laser (0.5% output coupling) co-pumped with a frequency-doubled Nd:YVO_4 laser ($\lambda = 532$ nm) and a GaN diode laser ($\lambda = 445$ nm), the latter only from minutes 2 to 16.

In otherwise the same setup, the low parasitic loss Saint-Gobain crystal was then replaced by a crystal of the sort that is typically used in commercial lasers (4.6 mm long, ~0.20 wt. % doping concentration, Brewster-cut, provided on loan by Coherent Scotland Ltd.), see chapter 2.2. After realignment of the resonator, the Ti:sapphire

laser with the Coherent crystal showed similar performance degradation and recovery behaviour over time when pumped with the GaN diode laser and the frequency-doubled Nd:YVO_4 laser.

In order to make a relative measurement of the power emitted from the Ti:sapphire crystal as fluorescence in the absence of laser oscillation, a silicon photodetector (Newport Corp. 818-SL) equipped with an interference filter ($\lambda_0 = 800$ nm, $\Delta\lambda_{FWHM} = 65$ nm, Comar Instruments 800IW25) was placed inside the resonator in front of the output coupler. An optical power meter head (Coherent Inc. FieldMate PM10) was placed between the crystal and the curved end mirror to simultaneously measure any changes in the amount of pump power absorbed in the crystal. With the resonator blocked and the Ti:sapphire laser not oscillating, the fluorescence signal and transmitted pump power were recorded under simultaneous pumping at 445 nm and 532 nm for both crystals. No deterioration of the fluorescence signal or change in absorbed pump power was observed over a period of more than 10 min for either the Saint-Gobain or the Coherent crystal. However, when the Ti:sapphire laser was subsequently oscillating again pumped at 532 nm only, the output power started from a deteriorated level which means that Ti:sapphire laser oscillation is not required for the performance deterioration under diode laser pumping to occur. The constant fluorescence signal and pump absorption suggests that the performance deterioration over time is due to an increase in crystal loss induced by the 445 nm pump light rather than a reduction in gain or pump absorption.

4.2 Collinear pumping with a multi-line Argon-Ion laser

For further examination of the pump-induced loss mechanism, the setup with the low parasitic loss Saint-Gobain crystal shown in Fig. 4.1 was modified by replacing the 445 nm GaN diode laser with an Argon-ion laser that could be tuned between multiple lines (Coherent Inc. Innova Sabre). The output of the frequency-doubled Nd:YVO_4 laser combined with that of the Argon-ion laser was then used to pump the Ti:sapphire laser (0.5% output coupling). Fig. 4.3 shows the deterioration and recovery of the Ti:sapphire laser output power under dual-wavelength pumping [1]. Pump mode waist radii were calculated to be 31 × 14 μm and 26 × 14 μm ($1/e^2$) for the frequency-doubled Nd:YVO_4 laser and the Argon-ion laser respectively; the cavity waist radii were calculated to be 31 × 18 μm ($1/e^2$). (N.B. Some lensing in the thin dichroic beamsplitter resulting from mechanical stress induced by the lens mount was subsequently identified which may cause some inaccuracy in the estimates of the pump mode sizes in this section.)

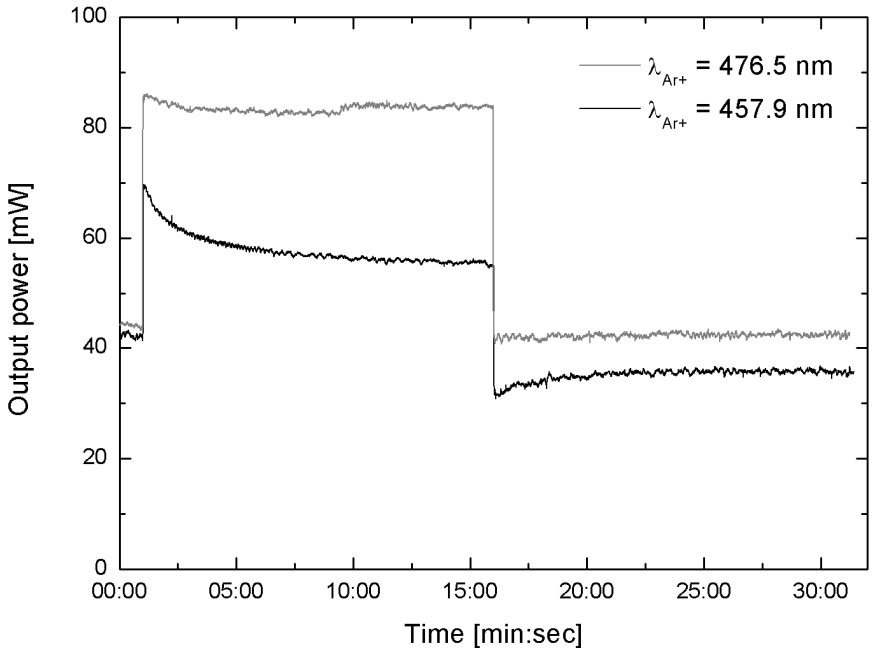

Fig. 4.3. Output power as a function of time for the Ti:sapphire laser (0.5% output coupling) co-pumped with a frequency-doubled Nd:YVO_4 laser ($\lambda = 532$ nm) and an Argon-ion laser ($\lambda_{Ar+} = 457.9$ nm or $\lambda_{Ar+} = 476.5$ nm), the latter only from minutes 1 to 16 [1].

The results of the dual wavelength pumping experiment are shown in Fig. 4.3. Initially, with the Ti:sapphire laser pumped only by the frequency-doubled Nd:YVO_4 with 500 mW incident on the crystal at 532 nm, no output power degradation was observed. As expected, the Ti:sapphire laser output power initially increased after adding another 500 mW from the Argon-ion pump laser (at Time 01:00 min:sec in Fig. 4.3), but significantly different temporal behavior was observed thereafter depending on the wavelength of the Argon-ion laser [1]. For an Argon-ion laser wavelength of 477 nm, no degradation in the output power of the Ti:sapphire laser was seen. When the 477 nm beam was blocked (at Time 16:00 min:sec in Fig. 4.3), the Ti:sapphire laser output power immediately returned to its original level for pumping with 532 nm only. By contrast, when co-pumping at 458 nm the output power degraded over a period of several minutes after the expected initial increase. Blocking the 458 nm beam resulted in the Ti:sapphire laser output power dropping below its original level for pumping with 532 nm alone. The output power would then recover under pumping at 532 nm and returned to its original level after tens of minutes of exposure. Without the 532 nm pump light incident on the crystal, the performance degradation was stable overnight.

Pumping with the Argon-ion laser only (without co-pumping at 532 nm), the power transfer characteristics were measured for each of the available Argon-ion lines, see Fig. 4.4 and Table 4.1 [1]. The measurements were taken after the performance deterioration had occurred and the output power had reached a steady state. The output coupling was 2% and the pump and resonator waist radii were calculated to be 26×14 μm and 26×16 μm ($1/e^2$) respectively. The clear change in performance between pump wavelengths of 477 nm and 458 nm is indicated by a sharp increase in threshold (240 mW to 337 mW) and reduction in the slope efficiency (29% to 18%) [1], see Table 4.1. [N.B. The slope efficiencies and thresholds are referenced to absorbed pump power in this case to account for the reduced pump absorption at shorter wavelengths.] Unfortunately, the Argon-ion laser lines between 458 nm and 477 nm could not be accessed due to aging of the laser tube and hence the wavelength of onset of the pump-induced loss could not be more closely determined.

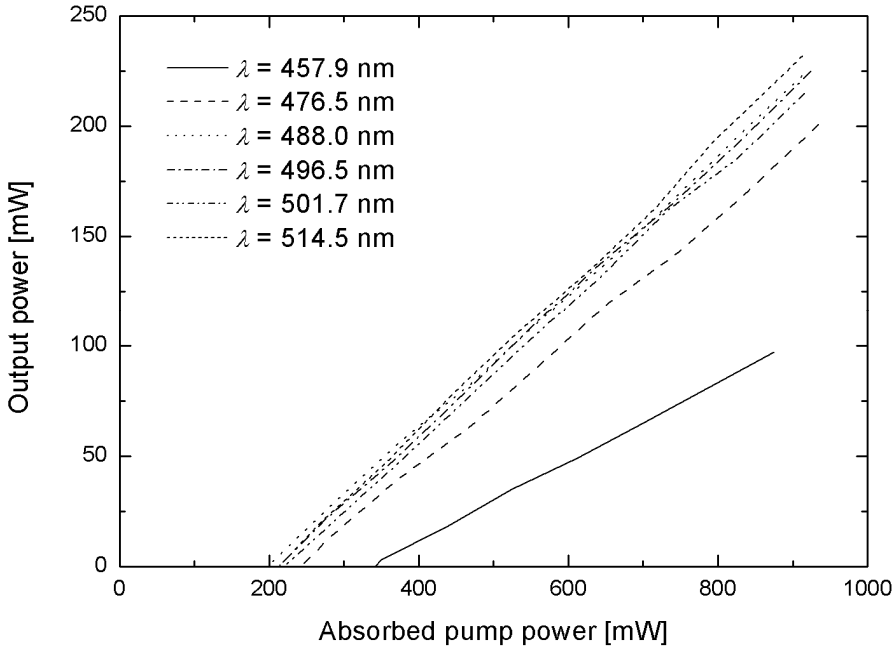

Fig. 4.4. Power transfer of the Ti:sapphire laser (2% output coupling) pumped with an Argon-ion laser operating on a range of emission wavelengths [1].

Table 4.1. Data extracted from the power transfer characteristics shown in Fig. 4.4 including the fraction of incident pump power absorbed in the Ti:sapphire crystal. Slope efficiencies and pump thresholds are referenced to absorbed pump power.

Pump wavelength [nm]	Slope efficiency [%]	Pump threshold [mW]	Pump absorption [%]
457.9	18.0	337	88
476.5	28.6	240	95
488.0	30.9	197	96
496.5	31.4	210	96
501.7	30.9	219	95
514.5	32.9	212	93

The slope efficiency and pump threshold as a function of the Argon-ion pump laser wavelength, shown in Table 4.1, are compared in Fig. 4.5 to the results obtained with the 4-mirror resonator under 452 nm diode-laser pumping and 2% output coupling (see section 3.2). The sharp increase in pump threshold and reduction in slope efficiency in moving from a pump wavelength of 477 nm to 458 nm indicates the onset of the pump-induced loss. Assuming that the beam parameters of the

Argon-ion laser are similar for the 458 nm and 477 nm line, the change in pump threshold by a factor of 1.4 suggests a similar change in the sum of the resonator losses and output coupling; Since the output coupling is 2%, and assuming that the resonator roundtrip losses at 477 nm are similar to the value measured at 532 nm (1.1 - 1.2%, see section 2.5.2), it indicates an additional loss of 1.3% at 458 nm. However, possible changes in the pump quantum efficiency with pump wavelength also need to be taken into account, as is discussed in section 4.4.4. The further increase in pump threshold and reduction in slope efficiency (all with respect to pump power absorbed in the crystal) in moving to GaN diode laser pumping (452 nm, blue points in Fig. 4.5) is besides of a possible change in pump quantum efficiency the result of poor GaN diode laser beam quality and a possible further increase in pump-induced loss at shorter pump wavelengths.

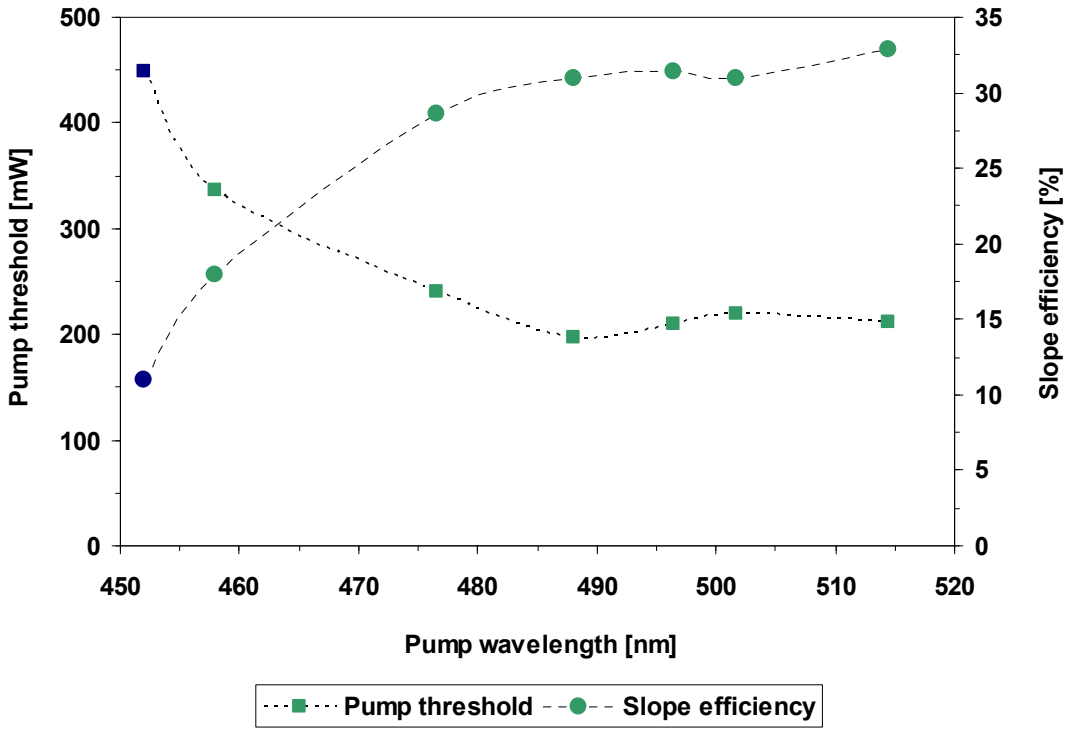

Fig. 4.5. Threshold and slope efficiency of an Argon-ion laser-pumped (green points) and an GaN diode-laser-pumped (blue points) Ti:sapphire laser (2% output coupling) as a function of the pump wavelength. Slope efficiencies and pump thresholds are referenced to absorbed pump power to account for the reduced absorption at shorter pump wavelengths. The dotted lines joining the points are intended only to guide the eye.

4.3 Loss analysis

Direct measurement of the additional loss caused by pumping Ti:sapphire at wavelengths around 450 nm – for example by measuring the fraction of a probe beam transmitted – is difficult for two reasons: first, the background and additional losses are small, around 1% per resonator roundtrip; and second, the additional loss will be restricted to the small pump mode volume within the crystal, which a probe beam would have to match. Hence the pump-induced loss was instead derived from resonator-based loss measurements of Ti:sapphire lasers pumped with the 452 nm GaN diode laser or the frequency-doubled Nd:YVO_4 laser.

In order to quantify the resonator losses, Findlay-Clay [2] and Caird [3] analyses were undertaken. For the conventionally pumped, 3-mirror Ti:sapphire laser introduced in chapter 2.5, both methods agreed, giving a resonator roundtrip loss of 1.2% according to the Findlay-Clay method and 1.1% according to the Caird method (see section 2.5.2). Unfortunately the power transfer characteristics of the 3-mirror Ti:sapphire laser under diode-laser pumping could not be used for a reliable resonator loss analysis (see section 2.4.4). However, this data is available for the two 4-mirror resonators presented in chapters 3.2 and 3.3 with the additional benefit of having, except for the mode sizes, identical resonators for conventional and diode-laser pumping. The 4-mirror Ti:sapphire laser gave a roundtrip loss of 1.2% (Findlay-Clay) and 1.1% (Caird) for 532 nm pumping (see section 3.2.2) confirming the values measured with the 3-mirror resonators. 452 nm diode-laser pumping resulted in resonator roundtrip losses of 2.1% from the Findlay-Clay analysis and 2.7% from the Caird method (see section 3.3.2). The difference in resonator loss between the two pump regimes suggests a pump-induced loss of 0.9% to 1.6% per resonator roundtrip. This represents an increase in resonator loss by a factor of 1.8 to 2.5 between those two pump wavelengths (452 nm and 532 nm). The values calculated here agree with the pump-induced loss estimate of 1.3% made in the previous section (see 4.2).

4.4 Fluorescence measurements

The measurements discussed in this chapter so far were largely based on Ti:sapphire laser resonators. The acquisition of three additional Ti:sapphire crystals opened the opportunity to make further investigations on the performance degradation in parallel to the laser experiments. Measurements of fluorescence and absorption, with all of these crystals (the details of which are given in Table 4.2) in order to consider sample to sample variation, will be discussed in this section. These as yet unpublished measurements were carried out by Dr Alexander Maclean but are included here for completeness and to allow comparison to the results presented elsewhere in this chapter.

Table 4.2. Ti:sapphire crystal specifications (HEM: Heat exchanger method).

Doping concentration [wt. %]	FOM	Length [mm]	Growth method	Manufacturer
0.10	400	8.5	HEM	Crystal Systems Inc.
0.15	400	4.5	Czochralski	Saint-Gobain Crystals
0.25	208	6	HEM	Crystal Systems Inc.

4.4.1 Experimental setup

The setup that was used for the experiments discussed in this section is shown in Fig. 4.6. A line-tuneable Argon-ion laser (Coherent Inc. Innova Sabre), the 445 nm GaN diode laser introduced in section 4.1 and a 405 nm GaN diode laser were used as pump light sources. The Argon-ion laser beam and the collimated, 405 nm diode laser beam were focussed into the crystal with a lens of f = 100 mm focal length. Additionally, the 445 nm diode laser used a cylindrical, Keplerian telescope (f_x = 10 mm and f_x = 130 mm) to shape the beam in the horizontal plane. A gold coated parabolic mirror of 71 mm focal length and 76 mm diameter (with a hole in the centre to transmit the pump light) collected the fluorescence emitted through the pump-facing facet of the crystal. The fluorescence intensity integrated over the solid angle covered by the parabolic mirror was then measured with a photodiode. A thermal power meter head (Coherent Inc. FieldMate PM10) was used to measure both the pump power incident on the focussing lens and the amount of pump power

transmitted through the crystal. Angled towards the back-facet of the crystal was the input fibre of a spectrometer (Ocean Optics Inc. S2000) allowing measurement of the fluorescence spectrum.

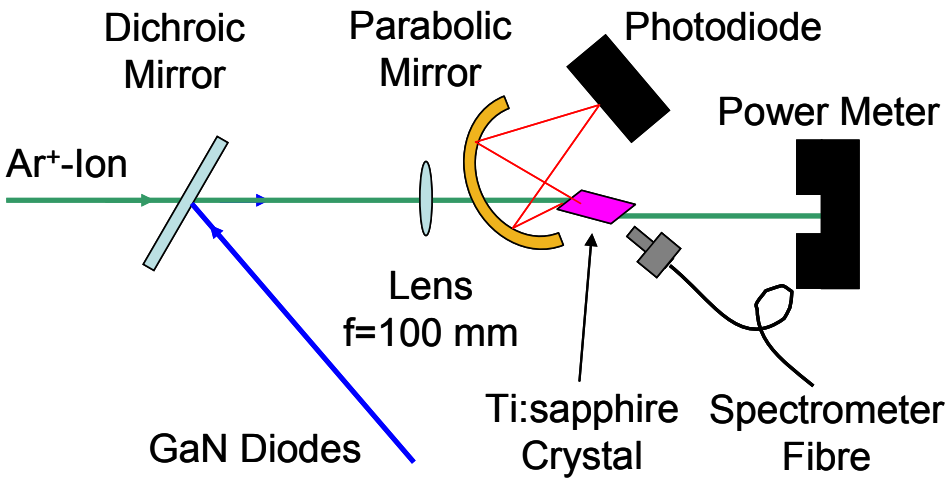

Fig. 4.6. Setup for fluorescence and absorption measurements.

4.4.2 Fluorescence intensity over time

Previous experiments with the 0.25 wt. % Saint-Gobain (Czochralski-grown) and the 0.20 wt. % Coherent (growth method unknown) crystals showed no deterioration of the fluorescence signal or the absorbed pump power over time under collinear pumping at 532 nm and 445 nm (see section 4.1). Using the experimental setup shown in Fig. 4.6 with the Argon-ion laser tuned to a wavelength of 458 nm, where Ti:sapphire laser performance deterioration over time was previously observed (see section 4.2), the 0.10 wt. % Crystal Systems and the 0.15 wt. % Saint-Gobain crystals were pumped with 2.5 W of power. For both crystals neither the integrated fluorescence intensity nor the absorbed pump power showed any deterioration over a 10 min observation period. This confirms the previous conclusion that the performance deterioration over time is due to a pump-induced crystal loss rather than a reduction in gain or pump absorption.

4.4.3 Fluorescence spectra as a function of pump wavelength

So far the underlying mechanism responsible for the reduced Ti:sapphire laser performance at blue pump wavelengths has not been identified. It is not, however, implausible that this mechanism might involve a radiative electronic transition with an energy difference corresponding to a wavelength in the fluorescence spectrum of Ti:sapphire. In this case the fluorescence spectrum would show some sort of signature in the presence of this effect. To investigate whether this is the case, fluorescence spectra of the three Ti:sapphire crystals listed in Table 4.2 were recorded for all pump wavelengths (GaN diode laser: 405, 445 nm; Argon-ion laser: 458, 477, 488, 497, 502, 515 nm). To correct for the change in quantum defect and absorption with the pump wavelength, each spectrum was normalized to its maximum. The normalized spectra did not show any change in shape, which is illustrated in Fig. 4.7 for the particular case of the 0.25 wt. % Crystal Systems crystal. This indicates that the reduced laser performance does not result from absorption by a centre that generates any significant emission or absorption within the fluorescence bandwidth of Ti:sapphire.

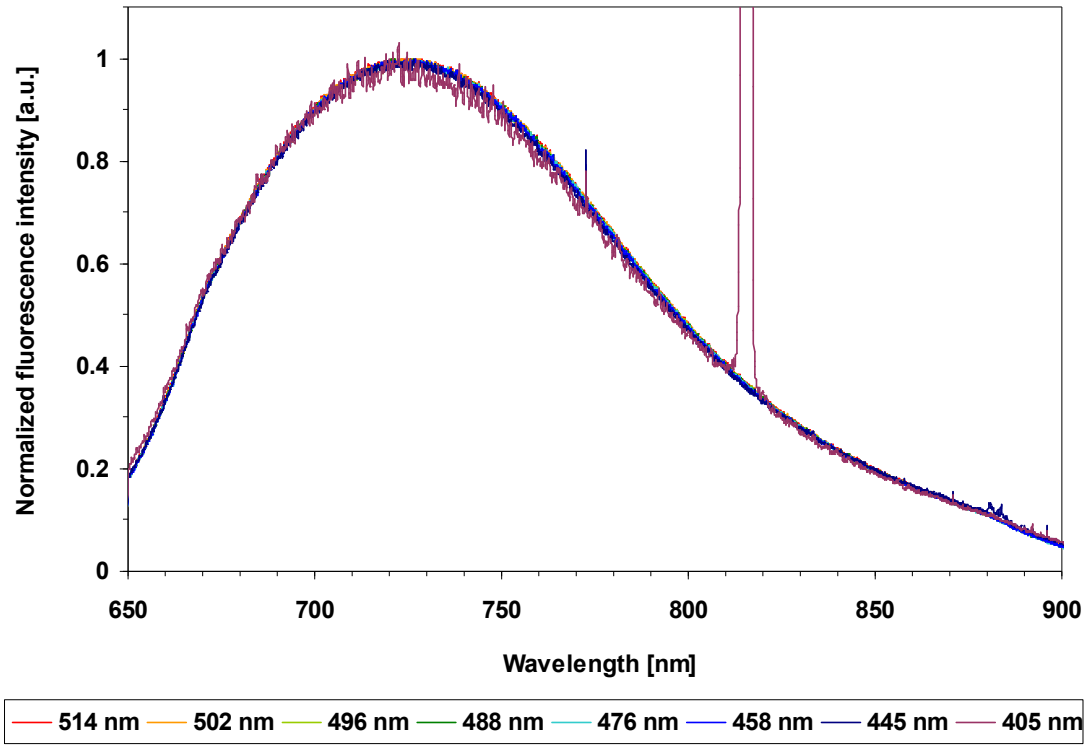

Fig. 4.7. Normalized fluorescence spectra of the 0.25 wt. % Crystal Systems crystal for various pump wavelengths. The peak at 810 nm is caused by the second-order diffraction signal of the 405 nm GaN diode laser pump. The peak at 770 nm is caused by a rogue pixel in the detector.

4.4.4 Quantum efficiency

Along with the fluorescence spectra, the integrated fluorescence intensity was measured as a function of the pump wavelength for all three crystals. Since the fluorescence mean photon energy is independent of the pump wavelength – the fluorescence spectra do not change as seen in the previous section (4.4.3) – the fluorescence intensity and fluorescence photon emission rate are proportional to each other. Dividing the integrated fluorescence intensity by the pump photon absorption rate (absorbed pump power divided by photon energy) gives a measure that is proportional to the quantum efficiency of the optically excited fluorescence. Normalized to the highest value for a range of pump wavelengths, this 'normalized quantum efficiency' represents the relative fraction of absorbed pump photons contributing to fluorescence. Fig. 4.8 shows the normalized quantum efficiency to be almost constant for all wavelengths above 458 nm; however, there is a strong

reduction for the GaN diode laser wavelengths of 445 and 405 nm. This suggests that compared to pumping at longer wavelengths, the quantum efficiency of the optically excited fluorescence may be reduced by a factor of two for pumping at 445 nm and by a factor of five for pumping at 405 nm.

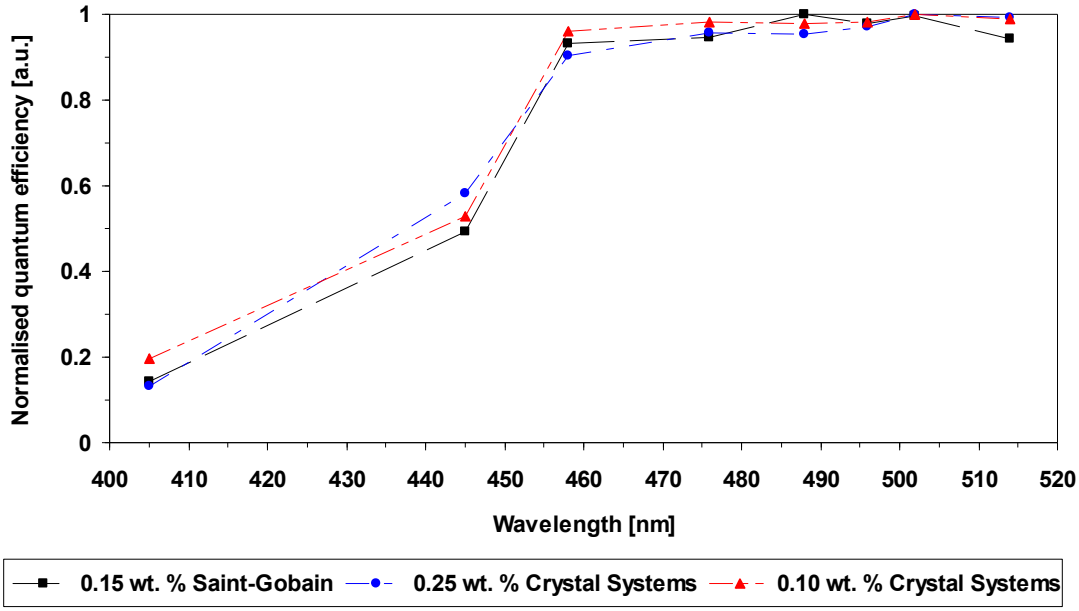

Fig. 4.8. Normalized quantum efficiency of optically excited fluorescence as a function of pump wavelength.

The quantum efficiency of optically excited fluorescence itself is a product of the pump quantum efficiency and the fluorescence quantum efficiency. The former is the percentage of absorbed pump photons which contributes to the population of the upper laser level and reduced values at the GaN diode laser wavelengths could be due to absorption of pump photons in non-laser active centres (e.g. impurities or the optical modification of existing centres). The fluorescence quantum efficiency is the percentage of laser-active ions excited to the upper laser level which contribute to fluorescence and a reduction of this value under GaN diode laser pumping could be due to excited state life time quenching through nonradiative processes. For both possible causes, either a reduction in upper laser level lifetime or a smaller effective pump absorption, the laser pump threshold would increase by a factor equal to the reduction in optically excited fluorescence under GaN diode-laser pumping (see

equation 1.19). However, once the laser starts oscillating the population inversion becomes clamped. The laser slope efficiency would therefore not be affected by a reduction in fluorescence quantum efficiency. The laser slope efficiencies measured under GaN diode-laser pumping, presented in chapters 2 and 3, were only a fraction of the values measured under conventional pumping (compare sections 2.4.3 with 2.4.4 and 3.2.2 with 3.3.2) [1, 4]. This behaviour strongly suggests that the reduction in the quantum efficiency of optically excited fluorescence at GaN diode laser wavelengths is due to absorption of pump photons in non-laser-active centres (e.g. impurities or the optical modification of existing centres).

4.5 Absorption measurements

Following discussion of these results at a conference [5], Dr Peter Moulton of Q-Peak Inc. – who was responsible for the original development of Ti:sapphire as a laser material [6] – very kindly re-analysed some existing data he had on the absorption spectrum of Ti:sapphire [7]. As shown in Fig. 4.9, Dr Moulton fitted two Gaussians to the absorption data to account for the Jahn-Teller splitting of the upper laser level in Ti:sapphire [8]. There was a residual on the short wavelength side of this fit which Dr Moulton interpreted as suggesting that the absorption below about 460 nm may not be explicable by Ti^{3+} alone. A similar poor fit to a two Gaussian model of the Ti^{3+} absorption was obtained for measurements on the samples used in this work (see Fig. 4.10). Although by no means conclusive and requiring significant further study before any firm conclusion can be drawn, this observation adds credence to the idea that below about 460 nm, there may be pump absorption by some species other than Ti^{3+} alone. It would seem plausible that this absorption process is driving the process that produces the pump induced loss and contributing to the reduction in pump quantum efficiency observed in the fluorescence measurements.

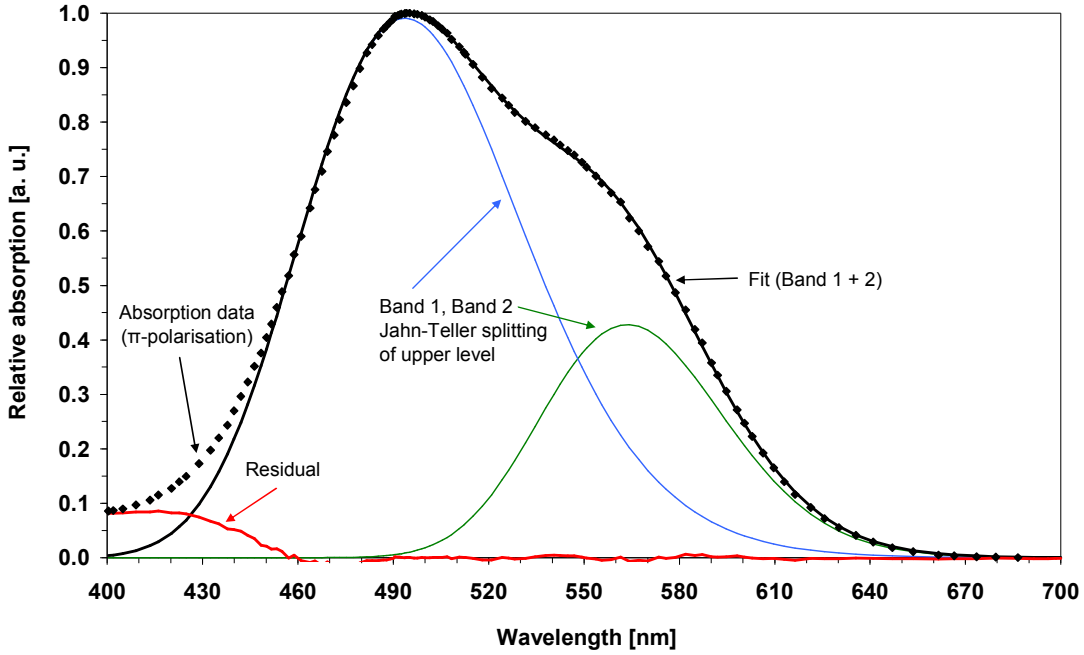

Fig. 4.9. Fit to the absorption spectrum in Ti:sapphire accounting for the Jahn-Teller splitting of the upper laser level and showing a residual at the short wavelength side. Data and analysis from Dr Peter Moulton [9].

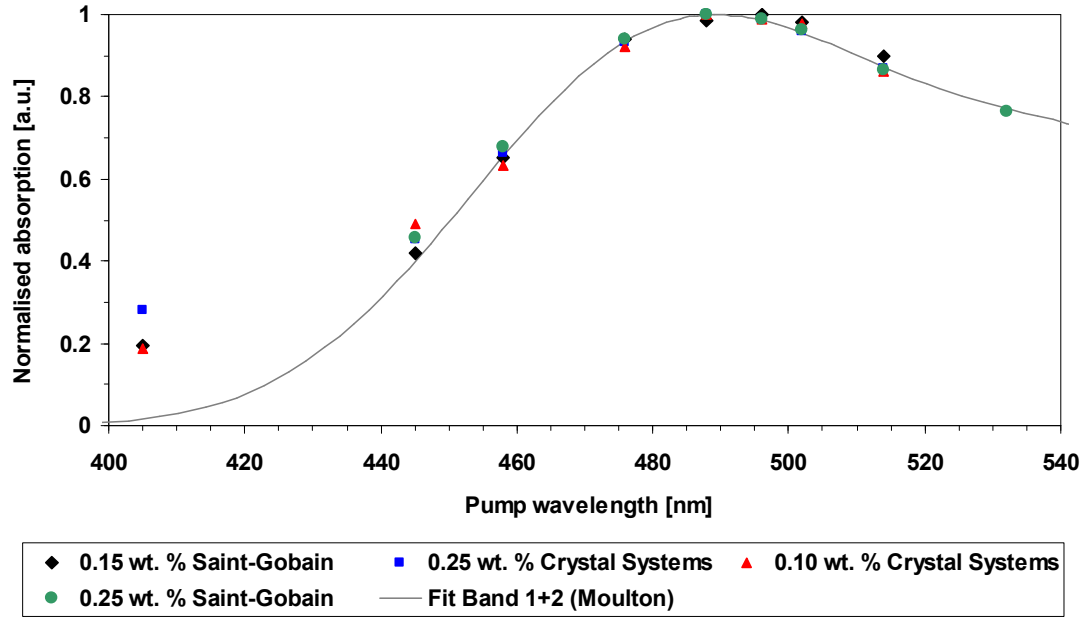

Fig. 4.10. Fit to the absorption data from measurements on the samples used in this work accounting for the Jahn-Teller splitting of the upper laser level. This shows a poor fit on the short wavelength side.

4.6 Conclusions

A deterioration of the Ti:sapphire laser performance over time results from a pump-induced loss for pump wavelengths of 458nm and below. This deterioration saturates after a few minutes to gives stable performance with reduced output powers. It is these stable results that are reported for continuous-wave and modelocked operation in chapters 2 and 3 respectively. Above some pump wavelength between 458 nm and 477 nm, this deterioration does not occur. The experimental work presented in this chapter indicates that the deterioration over time in laser performance results from a pump-induced increase in the crystal loss of about 1% per round trip, rather than a reduction in gain.

This deterioration is stable when the pump laser is switched off and the same level of performance is achieved when the pump laser is switched back on – thus although this effect reduces the efficiency of diode-pump Ti:sapphire lasers, it is not a fundamental bar to the use of such lasers in applications.

Besides the pump-induced loss, a reduction in the quantum efficiency of the optically excited fluorescence is observed at pump wavelengths below 458 nm. This will contribute significantly to the lower than expected performance observed from directly diode-laser-pumped Ti:sapphire lasers and would be consistent with pumping of another optical centre in addition to simply Ti^{3+}.

To my knowledge, this combination of pump-induced loss and reduction in quantum efficiency at shorter pump wavelengths has not yet been reported in detail. Hoffstädt made some observations of a pump-induced loss in flashlamp pumped Ti:sapphire lasers [10] which might be the result of the same effect. Hoffstädt tentatively attributed this loss to charge transfer interactions in Ti^{3+}-Ti^{4+} pairs and this suggestion is consistent with the analysis of the absorption spectrum in Ti:sapphire undertaken by Dr Peter Moulton and discussed in section 4.4, which suggests that not all of the absorption observed in Ti:sapphire below 460 nm can be explained by the Ti^{3+} ion alone. Nonetheless, considerable further research will be required to determine the mechanism at work here.

4.7 References

1. P. W. Roth, A. J. Maclean, D. Burns, and A. J. Kemp, "Directly diode-laser-pumped Ti:sapphire laser," Opt. Lett. **34**, 3334-3336 (2009).
2. D. Findlay and R. A. Clay, "The measurement of internal losses in 4-level lasers," Physics Letters **20**, 277-278 (1966).
3. J. A. Caird, S. A. Payne, P. R. Staver, A. J. Ramponi, L. L. Chase, and W. F. Krupke, "Quantum Electronic-Properties of the $Na_3Ga_2Li_3F_{12}:Cr^{3+}$ Laser," IEEE J. Quantum Electron. **24**, 1077-1099 (1988).
4. P. W. Roth, A. J. Maclean, D. Burns, and A. J. Kemp, "Direct diode-laser pumping of a mode-locked Ti:sapphire laser," Opt. Lett. **36**, 304-306 (2011).
5. A. J. Maclean, P. Roth, G. J. Valentine, A. J. Kemp, and D. Burns, "Direct Diode Laser Pumping of a Ti:Sapphire Laser," in *Advanced Solid-State Photonics*, OSA Technical Digest Series (CD) (Optical Society of America, 2009), WE2.
6. P. F. Moulton, "Ti-doped sapphire: tunable solid-state laser," OPN **8**, 9 (1982).
7. P. F. Moulton, "Spectroscopic and Laser Characteristics of $Ti:Al_2O_3$," J. Opt. Soc. Am. B-Opt. Phys. **3**, 125-133 (1986).
8. A. J. Maclean, P. W. Roth, D. Burns, A. J. Kemp, and P. F. Moulton, "Pump Induced Loss in Directly-Diode Laser Pumped Ti:Sapphire Lasers," in *Advanced Solid-State Photonics*, OSA Technical Digest Series (CD) (Optical Society of America, 2010), AWB16.
9. P. F. Moulton, (personal communication, 2009).
10. A. Hoffstadt, "Design and performance of a high-average-power flashlamp-pumped Ti:Sapphire laser and amplifier," IEEE J. Quantum Electron. **33**, 1850-1863 (1997).

5 Conclusions and Outlook

5 Conclusions and Outlook

5.1 Summary and conclusions

The subject matter of this thesis concerns the development and characterisation of directly diode-laser-pumped Ti:sapphire lasers. Ti:sapphire is one of the most versatile laser gain materials, most notably due to its exceptional spectral bandwidth which allows lasers to be widely tunable and capable of generating femtosecond pulses. Due to material properties that strongly favour high-brightness pump sources and the absence of high-power diode lasers in the blue-green region of the optical spectrum, Ti:sapphire was previously thought of as unsuitable for direct diode-laser pumping. By optimising laser resonator and pump optics design, the laser thresholds in continuous-wave and mode-locked operation were reduced to a level that permitted pumping with low-brightness gallium nitride diode lasers.

The design and characterisation of a number of cw Ti:sapphire lasers was described in chapter 2. As a benchmark for further development, a basic three-mirror resonator was built with a Ti:sapphire crystal of the sort that is typically used in commercial lasers and characterised with a conventional pump – a frequency-doubled Nd:YVO_4 laser – at 532 nm, resulting in Watt-level pump thresholds. This then represents the 'standard' performance associated with Ti:sapphire lasers.

Rate-equation-based modelling of laser performance was used to ascertain the crystal parameters and resonator design for a low-threshold Ti:sapphire laser suitable for pumping with GaN diode lasers. Calculations of the laser performance as a function of the GaN diode laser wavelength, beam quality and pump waist size were presented.

Based on the modelling results, a low-threshold, three-mirror Ti:sapphire laser with a highly doped, low parasitic loss crystal was built and characterised. Conventional pumping at 532 nm with thresholds as low as 106 mW and, for the first time, GaN diode laser pumping of a Ti:sapphire laser were demonstrated [1]. A maximum

output power of 19 mW was achieved with a single GaN diode laser delivering 1 W of pump power at 452 nm.

Refinements in the modelling and resonator design resulted in an improved low-threshold, three-mirror Ti:sapphire laser. Pump thresholds as low as 67 mW were demonstrated under conventional pumping. The maximum Ti:sapphire laser output power increased to 24 mW with a single GaN diode laser pump.

The design and characterisation of a mode-locked Ti:sapphire laser suitable for direct diode-laser pumping was described in chapter 3. The resonator parameters that the modelling indicated would result in optimised performance dictated the use of an asymmetric, Z-folded four-mirror resonator. In cw operation, a maximum output power of 40 mW was achieved by pumping with a single GaN diode laser. For conventional pumping at 532 nm, a threshold of only 60 mW and a slope efficiency of 15% were demonstrated with 0.5% output coupling [2]. Although the laser design was optimized for GaN diode-laser pumping, the performance when pumped at 532 nm was significantly better than the reported performance of low-threshold Ti:sapphire lasers optimised for conventional pumping. The cw threshold at 532 nm is, to my knowledge, the lowest yet reported for a Ti:sapphire laser.

By using an AlGaAs/GaAs saturable Bragg reflector, mode-locked operation of a directly diode-laser-pumped Ti:sapphire laser was demonstrated for the first time [2]. With a single GaN diode laser pump, pulses as short as 114 fs were generated. A maximum output power of 13 mW and a mode-locking threshold of 408 mW were achieved.

In order to increase the output power of the laser, a double-sided pumping configuration with two GaN diode lasers was subsequently employed. Cw output powers of more than 100 mW were obtained over a tuning range of 740 – 820 nm. In mode-locked operation a maximum output power increased to 101 mW at a pulse duration of 111 fs.

The Ti:sapphire laser performance under GaN diode laser pumping was generally lower than suggested by the modelling and a deterioration over time was observed. Chapter 4 presents the experimental work carried out to investigate this effect. Collinear pumping of a GaN diode laser with an argon-ion or a frequency-doubled Nd:YVO_4 laser showed that the laser performance deterioration over a period of minutes results from a pump-induced loss in the Ti:sapphire crystal for pump wavelengths of 458 nm and below. Resonator-based loss measurements quantified the pump-induced crystal loss to be on the order of 1% per resonator roundtrip. The laser characteristics discussed in previous paragraphs quote the lower but repeatable performance levels achieved once this loss settled to its steady state level. The lasers operated at this level from turn on for subsequent diode-laser pumped operation.

Besides the pump-induced loss, a significant reduction in the quantum efficiency of optically excited fluorescence was observed at pump wavelengths below 458 nm. Fluorescence and absorption measurements on a range of Ti:sapphire crystals strongly suggested absorption by non-laser active centres as the reason for the reduction in quantum efficiency at GaN diode laser wavelengths. It also is plausible that these centres are involved in the process causing the pump-induced loss.

In summary, direct diode-laser pumping of Ti:sapphire lasers offers a route to tunable and ultrashort pulse sources that are potentially less complex, more compact, and lower-cost than conventionally pumped systems. With the performance levels demonstrated in this thesis, such lasers would be attractive for many low-power applications including multi-photon microscopy, fluorescence-lifetime imaging and spectroscopy. GaN diode lasers offer much higher power to footprint ratios at significantly lower costs than conventional pump lasers. Directly diode-laser-pumped Ti:sapphire lasers therefore have the potential to open up new applications unsuited to lab-bound lasers or where the price and/or footprint of the current technology is prohibitive.

5.2 Outlook

The combination of pump-induced loss and reduction in quantum efficiency of optically excited fluorescence has not been reported before, to my knowledge. Hoffstädt [3] made some observations on flashlamp-pumped Ti:sapphire lasers that might be the result of pump-induced crystal loss. So far, the underlying mechanism has not been identified and considerable further research will be required. To this end, a tunable blue laser, e. g. the second harmonic generated from a Ti:sapphire laser, could be used to pump a Ti:sapphire crystal in order to determine the wavelength dependence of both effects more precisely. Instead of using laser resonator loss measurements to quantify the pump-induced crystal loss more accurate techniques like cavity ring-down spectroscopy could be employed, which would also be more convenient for the investigation of crystals of varying doping concentrations, figures of merit and growth methods.

The rate-equation-based modelling presented in chapters 2 and 3 did not account for the reduction in quantum efficiency of optically excited fluorescence. As described in chapter 4, a reduction in pump quantum efficiency or in fluorescence quantum efficiency would affect the laser performance differently. Modelling the laser performance implications of both effects would allow inferences to be drawn about the mechanism from measured performance data.

Such an improved model could be used to further optimise the performance of directly diode-laser-pumped Ti:sapphire lasers. Apart from achieving better laser performance, it would be helpful to study how critical some of the design parameters, for example the crystal figure of merit, are and to determine the performance cost of relaxing them. This is important as crystals with very high figures of merit are expensive and not widely available.

The pulse duration of the mode-locked diode-pumped Ti:sapphire laser could be reduced further by optimising the dispersion compensation. For passive mode locking with a saturable Bragg reflector, pulse durations well below 100 fs should be possible. Kerr-lens mode locking would allow the generation of even shorter pulses.

Based on the performance described in chapter 3, double-sided pumping should be sufficient to provide the pulse energies necessary for Kerr-lens mode locking. For example, Bartels et al. have demonstrated Kerr-lens mode locking of a conventionally pumped Ti:sapphire laser with intracavity pulse energies of only 4.5 nJ [4].

Of considerable practical importance would be the demonstration of a broadly tunable Ti:sapphire laser pumped by GaN diode lasers. This would only require broadband mirrors since the laser tuning range reported in chapter 3 was essentially limited by the mirror reflectivity. With a ring resonator, single-frequency operation could subsequently be demonstrated, which would prove the viability of directly diode-laser-pumped Ti:sapphire lasers for imaging and spectroscopy applications.

A highly compact, portable and battery-powered laser could be built to demonstrate the potential of directly diode-laser-pumped Ti:sapphire lasers for applications unsuited to lab-bound lasers. Hopkins et al. have demonstrated such a system based on Cr:LiSAF [5].

Higher output powers can be obtained by combining the output of several diode lasers. Pumping with a pair of polarization-coupled 1 W GaN diode lasers from either side of the crystal would provide up to 4 W of combined pump power. The performance measured in chapter 3 suggests that such a laser could generate roughly 250 mW of output power. With spectral and spatial beam combining the pump power can be increased even further.

The rapid progress in gallium nitride diode-laser technology towards higher output powers means that substantial performance improvements are possible over the next few years. The rapid development of this technology was driven by consumer electronics applications like optical data storage. There is now a considerable research effort underway to develop high-power diode-lasers with emission wavelengths in the green part of the optical spectrum [6, 7] driven again by commercial applications, e.g. mobile projectors. At the time of writing GaN diode

lasers with emission wavelengths of 483 – 493 nm and 60 mW of output power are commercially available (Nichia NDS4113) [8]. The pump thresholds measured under conventional pumping in chapters 2 and 3 suggest that no more than two of these diode lasers would be required to demonstrate laser oscillation with an optimised low-threshold Ti:sapphire laser. Diode lasers with emission wavelengths longer than 470 nm would eliminate the problems of pump-induced loss and reduced quantum efficiency. Should such diode lasers reach the Watt-level output powers of their shorter wavelengths siblings, then diode lasers might become the pump source of choice for the majority of Ti:sapphire lasers. The laser performance measured under argon-ion laser pumping in chapter 4 suggests that four 1 W diode laser pumps of this type would be sufficient to achieve one Watt of output power from a Ti:sapphire laser.

5.3 References

1. P. W. Roth, A. J. Maclean, D. Burns, and A. J. Kemp, "Directly diode-laser-pumped Ti:sapphire laser," Opt. Lett. **34**, 3334-3336 (2009).
2. P. W. Roth, A. J. Maclean, D. Burns, and A. J. Kemp, "Direct diode-laser pumping of a mode-locked Ti:sapphire laser," Opt. Lett. **36**, 304-306 (2011).
3. A. Hoffstädt, "Design and performance of a high-average-power flashlamp-pumped Ti:sapphire laser and amplifier," IEEE J. Quantum Electron. **33**, 1850-1863 (1997).
4. A. Bartels, T. Dekorsy, and H. Kurz, "Femtosecond Ti:sapphire ring laser with a 2-GHz repetition rate and its application in time-resolved spectroscopy," Opt. Lett. **24**, 996-998 (1999).
5. J. M. Hopkins, G. J. Valentine, B. Agate, A. J. Kemp, U. Keller, and W. Sibbett, "Highly compact and efficient femtosecond Cr : LiSAF lasers," IEEE J. Quantum Electron. **38**, 360-368 (2002).
6. K. Okamoto, "Nonpolar m-plane InGaN multiple quantum well laser diodes with a lasing wavelength of 499.8 nm," Appl. Phys. Lett. **94**, 071105 (2009).
7. D. Queren, "500 nm electrically driven InGaN based laser diodes," Appl. Phys. Lett. **94**, 081119 (2009).
8. "Laser Diode" (Nichia Corp.), retrieved 03 October, 2011, http://www.nichia.co.jp/en/product/laser_main.html.

Appendix

List of publications on diode-laser-pumped Ti:sapphire lasers

Journals

[1] P. W. Roth, A. J. Maclean, D. Burns, and A. J. Kemp, "Direct diode-laser pumping of a mode-locked Ti:sapphire laser," Opt. Lett. 36, 304-306 (2011).

[2] P. W. Roth, A. J. Maclean, D. Burns, and A. J. Kemp, "Directly diode-laser-pumped Ti:sapphire laser," Opt. Lett. 34, 3334-3336 (2009).

Conferences

[1] P. W. Roth, A. J. Maclean, D. Burns, and A. J. Kemp, "Modelocking of a Diode-Laser-Pumped Ti:Sapphire Laser," CMNN1, presented at the *Conference on Lasers and Electro-Optics*, San Jose, 2010.

[2] A. J. Maclean, P. W. Roth, D. Burns, A. J. Kemp, P. F. Moulton, "Pump Induced Loss in Directly-Diode Laser Pumped Ti:Sapphire Lasers", presented at *Advanced Solid-State Photonics*, San Diego, 2010.

[3] A. J. Kemp, P. W. Roth, A. J. Maclean, and D. Burns, "Directly diode-pumped Ti:sapphire Lasers (Invited)", presented at the *International Laser Physics Workshop*, Barcelona, 2009.

[4] P. W. Roth, A. J. Maclean, A. J. Kemp, and D. Burns, "A Directly Diode Laser Pumped Ti:sapphire Laser: Design, Demonstration and Power-scaling Challenges", CA7.6, presented at the *Conference on Lasers and Electro-Optics – Europe*, Munich, 2009.

[5] A. J. Maclean, P. Roth, G. J. Valentine, A. J. Kemp, and D. Burns, “Direct Diode Laser Pumping of a Ti:Sapphire Laser”, presented at *Advanced Solid-State Photonics*, Denver, 2009.